Opto-chemical biosensor development, and analytics for point-of-care applications

by

Souvik Kundu

A dissertation submitted to the graduate faculty

in partial fulfillment of the requirements for the degree of

DOCTOR OF PHILOSOPHY

Major: Electrical Engineering (Bioengineering)

Program of Study Committee:
Ratnesh Kumar, Major Professor
Long Que
Santosh Pandey
Carmen Gomes
Geetu Tuteja

The student author, whose presentation of the scholarship herein was approved by the program of study committee, is solely responsible for the content of this dissertation. The Graduate College will ensure this dissertation is globally accessible and will not permit alterations after a degree is conferred.

Iowa State University

Ames, Iowa

2023

DEDICATION

I dedicate this thesis with profound love and gratitude to my parents, sister and my beloved wife, who have been my unwavering pillars of support and inspiration throughout my academic journey.

My mother, Aparna Kundu, and my father, Ajit Kundu, both of you have been my pillars of strength and endless inspiration. Your dedication, sacrifices, and belief in my abilities have played a pivotal role in shaping my educational journey. Even during the most difficult times, your support and understanding have kept me motivated and focused. Your confidence in my abilities has given me the courage to pursue my academic goals. I am truly grateful for your guidance, as your words of wisdom have helped me navigate the ups and downs of this journey.

To my beloved wife, Dimpy, I deeply acknowledge and appreciate the sacrifices you have made, standing by my side and offering support while ensuring that I had the time and space to focus on my studies. Your ability to manage our home, care for our family, and provide a nurturing environment has allowed me to pursue my academic goals with a sense of peace and tranquility. Beyond academia, you have been my partner, my best friend, and my confidante. Your love, support, and understanding have served as an anchor, keeping me grounded throughout this journey.

To my beloved little sister, Moma, I cannot express enough gratitude for your support, enthusiasm, and love. This thesis stands as a testament to our strong bond and the positive impact you have had on my academic journey, both as a teacher and philosopher. I dedicate this achievement to you as a token of my deep appreciation for everything you have done for me since our childhood.

With all my love and gratitude, ***Souvik Kundu (Abhi)***

TABLE OF CONTENTS

Page

LIST OF TABLES

Page

LIST OF FIGURES

Page

ACKNOWLEDGMENTS

I would like to express my deepest gratitude and appreciation to the following individuals and organizations who have contributed to the successful completion of my thesis:

Institutional Support: I would like to acknowledge the Iowa State University for providing the necessary resources, facilities, and research grants that have supported this study. The institutional environment and opportunities have been instrumental in the successful completion of this research.

My Supervisor: I am sincerely grateful to my supervisor, Prof. Ratnesh Kumar, for his invaluable guidance, support, and patience throughout the entire research process. His expertise, constructive feedback, and continuous encouragement have been instrumental in shaping this thesis.

Committee Members and collaborators : I extend my heartfelt thanks to the committee members Prof. Long Que, ISU Prof. Carmen Gomes, ISU, Prof. Santosh Pandey, ISU and Prof. Geetu Tuteja, ISU for their expertise and guidance during my academic journey. Their intellectual contributions, insightful discussions, and valuable suggestions and evaluations have significantly enriched my research work. I am also thankful to Dr. E. Dale Able, UCLA for providing guidance on medical aspects and providing facilities for experiments on animal model for my research work. I am indebted to Prof. Shawana Tabassum , UT Tyler for guiding me in the initial period of my research work, providing valuable knowledge to conduct research on biosensors.

Parents : Mother, your unconditional love and nurturing nature have laid the foundation upon which I have built my aspirations. Your belief in my abilities has instilled in me the confidence to face any challenge that comes my way. I deeply appreciate your tireless efforts in creating an environment conducive to my studies, which have not gone unnoticed.

Father, your hard work, dedication, and determination have exemplified the value of perseverance and the importance of setting high standards for oneself. Your continuous encouragement and wise counsel have shaped my mindset and contributed to my growth as both a researcher and an individual. I am honored to have you as my role model.

Friends and Peers: I am thankful to my friends (Kushagra, Subhanwit, Krishna, Ramij, Soumya da, Anindya, Saunak, Amitangshu, Amit, Raghunandan) at ISU with whom I have spent numerous hours hanging out, playing and discussing stuffs besides research. I am also thankful to my peers Madhav, Bhuwan, Anupam, Balaji, Rahma for several research discussions and insights. I would also like to mention Sourav Koley, whose role has been instrumental in my life as he has always been a great friend and support since we met during our undergrad days.

ISU ISSO and ECpE Support Staffs: I would like to thank Leland Harker of ETG for helping me with custom designs and ideas for my experiments and designs. Vicky Thorland-Oster has been a great support during my study as she has provided all the necessary information for academic success and provided much needed TAs when I needed the most as a source of funding. Also, like to thank Katherine Worley, DSO who have helped me with all complex immigration questions related to my F1 status, which helped me to gain both 1 yr full time and 2 yrs part time CPT experience as a part of my study and also provided immense help in strategies regarding the OPT and STEM OPT applications and their respective timelines.

Lastly, I would like to acknowledge all the individuals who may not be directly mentioned but have contributed in various ways, both big and small, to the completion of this thesis. Your support, encouragement, and belief in my abilities have meant the world to me.

Souvik Kundu

ABSTRACT

Optical biosensors are highly sensitive devices that employ optical techniques and biological recognition elements to detect and measure specific analytes in real-time. Their real-time continuous monitoring, high sensitivity, and non-destructive sampling make them applicable in various fields, including medical diagnostics, environmental monitoring, and food safety. This thesis presents a brief survey on biosensors, focusing on the detection of sepsis biomarkers and continuous glucose monitoring in whole blood over extended periods. The proposed methods have been tested and validated using an animal model. Additionally, a machine learning-based approach for feature selection and data analytics is explored to predict diseases based on biomarker data from publicly available hospital database. Overall, this thesis summarizes the current state of biosensors, and sensor fabrication for in-vitro and in-vivo point-of-care applications and addresses limitations in continuous monitoring in whole blood, proposes innovative solutions with animal model validation, and presents a data analytics framework for disease prediction.

CHAPTER 1. GENERAL INTRODUCTION

This chapter narrates the organization, contents, and contribution of this thesis. The thesis discusses 4 aspects that are narrated in the next 4 chapters, followed by the conclusion and future work. This chapter also discusses the motivation behind the research, the socio-economic significance of this work, and the practical applications of optical biosensors.

1.1 Overview and Organization of the chapters

The research was based on the applications of optical sensors for sensing biomolecules critical for diagnosing and prognosis of diseases critical for patients in ICU/CCU. The research outcome is aimed at the development of point-of-care devices which can provide test results quickly and facilitate continuous bio-molecule monitoring. In Chapter 2 a survey has been reported on sepsis pathogenesis, related biomarkers, and sensing principles, and an extensive discussion on the comparison between different kinds of biosensors and their applications and limitations, which acts as a foundation for the development of improved biosensors for sepsis and glycemia detection. Both the projects narrated in chapters 3 and 4 provide detailed literature, motivation, fabrication, and results related to developing respective sensors to detect molecules related to sepsis and diabetes, respectively. Once the sensor senses the biomolecules in whole blood, it becomes necessary to analyze it and make appropriate and quick decisions based on the data. Chapter 5 discusses the application of data analytics in predicting diseases early and also assists physicians with their decisions. MIMIC-III database was used to predict sepsis based on different biomarker data present. Two feature selection algorithms were employed and 8 machine learning models were applied to study the efficiency of a set of physiological and physio-chemical biomarkers in the patient data and compare it with the traditional qSOFA-based sepsis evaluation based on sepsis-3-definition and recommendation. We have provided a methodology that shows a slightly

improved performance compared to the traditional qSOFA-based approach. Fig.1.1 illustrates

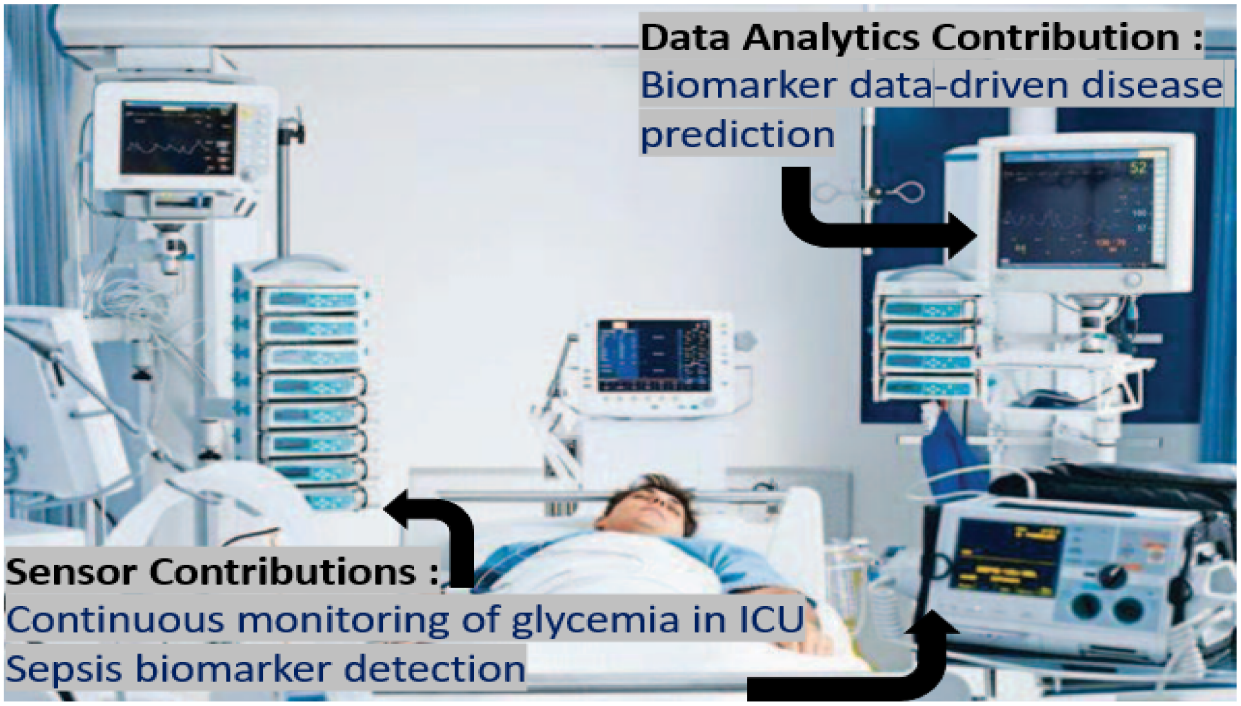

Figure 1.1 Contribution of the thesis. Image inspired from Uddin et al. (2017) Copyright IEEE

the contributions of this thesis which is primarily developing two opto-chemical plasmonic biosensors for in-vitro detection of sepsis biomarkers and in-vivo continuous monitoring of glucose and a proposed data analytics methodology to predict sepsis based on biomarker data. The thesis also narrates a proof-of-concept how the proposed sensing technology can be applied to an animal model for continuous biomarker monitoring for a prolonged time period.

1.2 Motivation

This thesis is intended to provide insights and a holistic overview of why biosensors are important in the present day, how doctors and healthcare personnel can be benefited from using them, and related data analytics complimenting them. This will ultimately pave the way for an intelligent patient monitoring system that can utilize sensor-based, networked networks to

autonomously monitor the health of the patients. For obtaining a patient's biological and physio-chemical data, different types of point-of-care biosensors can be used. The data can be processed in an IoT cloud where the relevant biological data can be sent for analytics. This can be computed in real-time using intelligent cloud computing technology and can instantaneously send push notifications to doctors, nurses, and hospital staff after analyzing sensor data to identify a patient's health condition. This helps doctors and nurses by allowing them to observe their related patients without having to visit them in person. With restricted access, patients' families can also gain from this system. So, the motivation was to contribute towards such biosensor development in first place and propose a data analytics framework to process such sensor reading in predicting diseases and help save millions of lives across the world.

1.3 Socio-Economic Importance of Biosensors

Biosensors have had a profound effect on our society, bringing about important socio-economic changes in various domains. These innovative devices, which combine biology and technology, can detect and analyze biological information, ranging from small molecules to physiological changes in living organisms. Their influence can be observed in healthcare, agriculture, environmental monitoring, and food safety. In the healthcare sector, biosensors have revolutionized diagnostics and patient monitoring. They enable early disease detection, personalized medicine, and the rapid identification of infectious diseases like COVID-19, sepsis, etc. By facilitating early intervention and tailored treatments, biosensors improve patient outcomes and reduce healthcare costs. In agriculture, biosensors optimize crop production and help address food security challenges Geballa-Koukoula et al. (2023).

Furthermore, biosensors contribute to economic growth by fostering innovation, entrepreneurship, and job creation. They encourage collaboration among scientists, engineers, and business professionals, which fuels the growth of the biosensor industry McGrath et al. (2013). Additionally, the application of biosensors in various sectors stimulates economic development and enhances competitiveness. However, challenges still exist regarding affordability,

accessibility, and ethical considerations. Ensuring that biosensor technologies are affordable and accessible to all, especially in low-resource settings, is crucial for promoting equitable healthcare and sustainable development. Addressing ethical concerns related to privacy, consent, and responsible use of biosensor data is also essential.

In summary, biosensors have had a significant socio-economic impact. They have improved healthcare, agriculture, environmental monitoring, and food safety, resulting in better outcomes, increased productivity, and sustainable practices. Biosensors empower individuals, industries, and governments to make informed decisions, driving positive socio-economic changes in our society.

1.4 Optical Biosensors and it's Applications

Optical biosensors Singh et al. (2023) Damborskỳ et al. (2016) have emerged as highly effective devices for continuous monitoring in a range of fields. These biosensors utilize a combination of optical techniques and biological recognition elements to detect and measure specific analytes in real-time. They offer several advantages, including real-time measurements, high sensitivity, specificity, and non-destructive sampling. The ability of optical biosensors to provide real-time measurements is a significant benefit. They employ optical techniques such as fluorescence, surface plasmon resonance (SPR), or interferometry to quickly and accurately detect analytes without the need for complex sample preparation. This real-time capability is particularly valuable in time-sensitive applications like medical diagnostics and environmental monitoring.

The high sensitivity of optical biosensors is another key advantage Kim et al. (2021). They can detect analytes at very low concentrations, often in the nanomolar or picomolar range. This sensitivity is achieved through signal amplification methods, enabling the precise detection of analytes and the continuous monitoring of subtle changes in analyte levels. Optical biosensors also demonstrate excellent specificity. By incorporating biological recognition elements like antibodies or enzymes, they can selectively detect the target analyte of interest. This specificity ensures accurate measurements and reduces the risk of false-positive or false-negative results. Moreover, the non-destructive nature of optical biosensors is beneficial for continuous monitoring.

Unlike traditional techniques that may require sample destruction or modification, optical biosensors enable repeated measurements without altering the sample. This feature is particularly advantageous when working with limited or valuable samples. The applications of optical biosensors for continuous monitoring are wide-ranging. They find utility in medical diagnostics for real-time monitoring of biomarkers, enabling early disease detection and personalized medicine. In environmental monitoring, optical biosensors continuously track pollutants in air, water, and soil, aiding in pollution control and resource management. Additionally, in food safety, these biosensors ensure the continuous monitoring of contaminants, contributing to the quality and safety of food products. In this thesis we will explore how optical biosensors can be used in the medical world for disease monitoring and detection.

In summary, optical biosensors offer significant benefits especially for continuous monitoring in various domains. Their real-time measurements, high sensitivity, specificity, and non-destructive sampling capabilities make them valuable tools for tracking dynamic changes in analyte levels. As technology advances and portable optical biosensors become more prevalent, their applications for continuous monitoring are expected to expand, leading to enhanced diagnostics, improved understanding, and effective management of complex systems.

1.5 References

Damborskỳ, P., Švitel, J., and Katrlík, J. (2016). Optical biosensors. *Essays in biochemistry*, 60(1):91–100.

Geballa-Koukoula, A., Ross, G., Bosman, A., Zhao, Y., Zhou, H., Nielen, M., Rafferty, K., Elliott, C., and Salentijn, G. I. (2023). Best practices and current implementation of emerging smartphone-based (bio) sensors-part 2: Development, validation, and social impact. *TrAC Trends in Analytical Chemistry*, 161:116986.

Kim, Y., Gonzales, J., and Zheng, Y. (2021). Sensitivity-enhancing strategies in optical biosensing. *Small*, 17(4):2004988.

McGrath, M. J., Scanaill, C. N., McGrath, M. J., and Scanaill, C. N. (2013). The data economy of biosensors. *Sensor Technologies: Healthcare, Wellness, and Environmental Applications*, pages 137–156.

Singh, A. K., Mittal, S., Das, M., Saharia, A., and Tiwari, M. (2023). Optical biosensors: A decade in review. *Alexandria Engineering Journal*, 67:673–691.

Uddin, M. S., Alam, J. B., and Banu, S. (2017). Real time patient monitoring system based on internet of things. In *2017 4th International conference on Advances in Electrical Engineering (ICAEE)*, pages 516–521. IEEE.

CHAPTER 2. A PERSPECTIVE ON SEPSIS PATHOGENESIS, BIOMARKERS , AND DIAGNOSIS : A CONCISE SURVEY

Souvik Kundu[1], Shawana Tabassum[1], and Ratnesh Kumar[1]

[1] Department of Electrical and Computer Engineering, Iowa State University, Ames, IA, 50010, USA

Modified from a manuscript published in *Medical Devices and Sensors, Wiley*

2.1 Abstract

Sepsis is a potentially fatal physiological state caused by an imbalance in the body's immune response to an infection, and is one of the most common causes for deaths in the non-coronary intensive care unit worldwide. In this article, the state-of-art on sepsis is presented in a manner that facilitates easy comprehension also for the non-medical researchers by introducing sepsis, it's causes, extent, and comparison of diagnostic techniques (conventional labeled as well as label-free detection). The article also provides a comprehensive discussion on sepsis biomarkers, to help researchers from multi-disciplinary domain in developing devices and ideas to compliment the existing sepsis diagnosis systems for quick and premature detection of the physiological condition and reduce mortality by means of early treatments.

2.2 Introduction

The word Sepsis originates from the Greek word [$\sigma\eta\psi\iota\varsigma$], which refers to bacterial decomposition of animal- or plant-based organic materials Geroulanos and Douka (2006). In addition to that, it was also mentioned by Homer's poems as 'sepo' [$\sigma\eta\pi\omega$], by which he meant 'I rotted'. Even during the 460-370 BC, Hippocrates, in order to describe 'dissolution of a structure', used the word 'sepidon' which is synonymous with modern day sepsis. Interestingly,

the term was also used by great philosophers and physicians like Aristotle and Galen with similar meaning and prevailed for over 2700 years Gül et al. (2017). However, it was not until the *ACCP/SCCM Consensus Conference* at Chicago in 1991 that the terms related to sepsis were standardized Bone et al. (1992). The conference aimed at providing general guidelines for future investigations related to sepsis, so that researchers could compare and improve various existing therapeutic protocols. They provided a definition of sepsis and systemic inflammatory response syndrome (SIRS) along with details of physiological parameters which can categorize sepsis and non-sepsis cases. In modern medical science, sepsis can be broadly defined as an unbalanced immune response of an organism to an infection that eventually ends up injuring its own organs or tissues. However, the definition of sepsis has changed over the years. Due to advancement in science and technology now it is possible to assess sepsis criterion based on patient's past health records data. Thus the definition was modified in 2001 and again on 2016 the latest definition of sepsis has been provided by a task force comprising of personnel from infectious diseases, Intensive Care Unit (ICU), and surgical and pulmonary specialists. They have published their recommendations in *The Third International Consensus Definitions for Sepsis and Septic Shock (Sepsis-3)*, where Sepsis is defined as a life-threatening organ dysfunction caused by a dysregulated host response to infection. Also, SIRS was substituted with a shortened sequential organ failure assessment score known as the quick Sequential Organ Failure Assessment (qSOFA) score . This comprises of two of the following three physiological conditions suffered by a patient: increased breathing rate, low blood pressure, and change in level of consciousness Singer et al. (2016). Based on historical records on the inception and expression of sepsis, Figure 2.1 illustrates the transformation of sepsis definition over a span of 24 years.

Sepsis starts with an inflammatory response to the presence or invasion of a microorganism. Several clinical symptoms arise with the progression of sepsis, including a rise in body temperature above 38.3°C (101°F) or a temperature drop below 36°C (96.8°F), a heart rate and respiratory rate of more than 90 beats/min and 20 breaths/min respectively, acute alternations in white blood cell (WBC) count, i.e., either greater than 12000 per cu. mm. or less than 4000 per

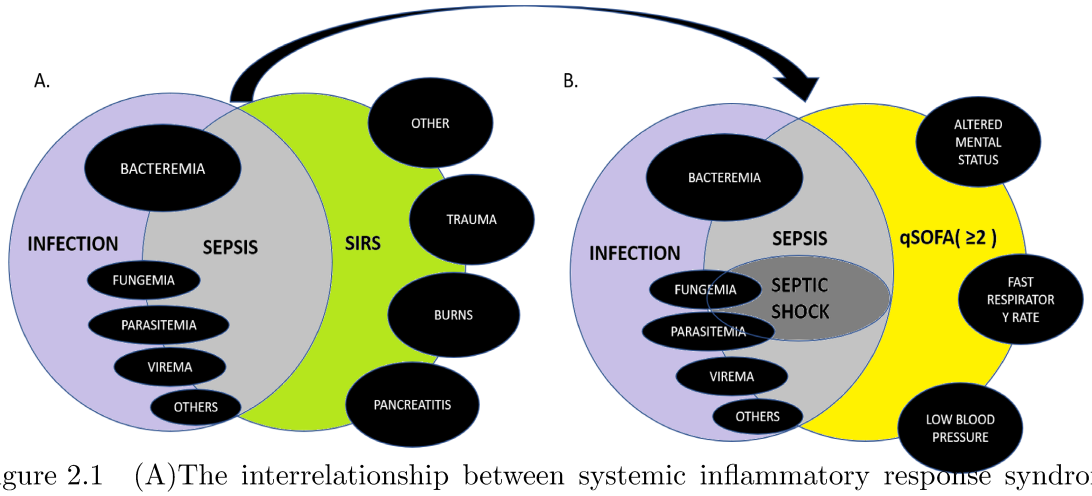

Figure 2.1 (A)The interrelationship between systemic inflammatory response syndrome (SIRS), sepsis, and infection Bone et al. (1992) (B) Modern definition of Sepsis-3

cu. mm [1]. Sepsis can progress toward severe sepsis resulting in multiple organ dysfunctions. Further on, a host can suffer from septic shock which is accompanied by hypotension despite adequate fluid resuscitation and perfusion abnormalities including lactic acidosis, oliguria, or an acute alteration in mental status Bone et al. (1992).

More than 1.7 million cases of sepsis are registered in the United States each year and approximately 270,000 result in death. Moreover, 1 in 3 deaths that occur in hospitals, is due to sepsis [2]. Sepsis occurs unpredictably and progresses alarmingly fast. Septic shock, a widespread inflammation all over the body ultimately leading to multiple organ failures and deaths, sets in if sepsis is not detected at an early stage. Therefore, understanding the symptoms and early diagnosis of sepsis is of utmost importance. Thompson et al. (2019) and Gyawali et al. (2019) have narrated a comprehensive review on sepsis, it's physio-pathogenesis, along with the current optimal approach in managing the physiological conditions in human relating to sepsis.

This review paper compliments the survey published by Kumar et al. (2019), Rello et al. (2017), Wentowski et al. (2019), Polat et al. (2017), Berg and Gerlach (2018) on recent advancement of sepsis, management and it's diagnosis methodologies. This article puts an extra layer on top of existing surveys which includes the recent advancements in sepsis diagnostic

[1] https://www.healthline.com/health/sepsissymptoms
[2] https://www.medicalnewstoday.com/articles/323023.php

techniques and methodologies explored in the year 2019. Along with that care has been taken to include the most popular sepsis diagnosis techniques over the years and they are grouped by their detection principle and depicted in form of Tables. Amendments to these techniques should lead to the fabrication of point-of-care devices which would result in early and quick diagnosis of sepsis and eventually save more lives in ICU by exercising proper antibiotics early on. The main focus of this survey paper is the review of causes of sepsis, molecular mechanisms underlying sepsis, and labeled and label-free sepsis diagnostic systems along with their advantages and limitations. Finally, the article ends with a discussion on the future prospects of diagnosis and treatment of sepsis.

2.3 Causes and effects of Sepsis

2.3.1 What underlies sepsis?

In the past years several research has been conducted to understand the root cause of sepsis, e.g., Schouten et al. (2008); Ward and Bosmann (2012); Hotchkiss et al. (2016). From prevalent research it is understood that the severity resulting from sepsis is not directly caused by invading microorganisms or pathogens, rather this clinical condition is caused by dysregulation of the host immune response that leads to multiple organ dysfunction, coagulopathy, and hypotension Schouten et al. (2008). This requires understanding of the interrelation between infection, inflammation, and coagulation as well as the difference between immune response during regular infection and during sepsis. In Opal and Esmon (2002) authors have claimed that when an external pathogen invades, an attempt is made by the host defense system to prevent the foreign organisms from spreading and multiplying inside the host body. This event is thus followed by an inflammatory response that activates the coagulation process and fibrin deposition. However, the exaggerated response of the immune system leads to a situation where severe coagulation leads to microvascular thrombosis and organ dysfunction also known as disseminated intravascular coagulation (DIC) Levi and Ten Cate (1999).

Essentially, this microvascular thrombosis is an adaptive response of the immune system when there is an infection that prevents the intruding pathogens present in the tissues from entering the systemic circulatory system. Thus, by clotting the path between the tissue and circulatory system temporarily, the immune system with the help of natural killer cells (a type of white blood cells) removes the pathogens or bacteria and repairs the damaged tissues. However, during acute infection the microvascular thrombosis becomes generalized, which results in organ failure and eventually death due to extensive tissue ischaemia (i.e. inadequate blood supply to an organ). This phenomenon is supported by studies on post-mortem of patients found positive with sepsis, as they demonstrate microvascular thrombosis in many organs including the lung, adrenals, liver, gut, kidney, and brain Dixon (2004). Researchers therefore have found a relation between inflammation and coagulatory response in the host system Esmon (2005), Levi et al. (2004), and have acknowledged the significance of endothelial activation for microvascular dysfunction, which is one of the hallmarks of sepsis Aird (2003), Bateman et al. (2003).

2.3.2 Compromise of immunity by sepsis

One aspect of immunity is the viable lymphocytes, a subtype of WBC, which mainly comprises of *natural killer* (NK) cells Freud et al. (2017), T-cells (thymus) Kumar et al. (2018), and B-cells (bone-marrow) Cooper (2015). NK cells are generally part of the innate or inborn immune system and are best known for killing the tumors and virally infected cells. On the other hand, T-cells are involved in cell-mediated immunity, i.e., they provide immunity by activating phagocytes, antigen-specific cytotoxic T-lymphocytes, and release multiple cytokines in response to a foreign organism (also called antigen). B-cells respond to pathogens by generating large amount of antibodies for neutralizing these foreign bodies, e.g., bacteria and viruses. These lymphocytes along with dendritic cells (DCs) Luckashenak and Eisenlohr (2013) can become dysfunctional during sepsis.

A recent study Boomer et al. (2011) infers that during sepsis there is a massive apoptosis of T- and B-cells which is accompanied by profound immunosuppression. An increased number of

T-suppressor cells is also noted. Sepsis can turn out to be lethal with the apoptosis of T- and B-cells followed by defective DCs, and marks the onset of immunosuppression. As a result of this defective innate immune system, the ability to engulf bacteria is greatly reduced, resulting in multi-organ failure (MOF) and finally death. Studies also reveal that sepsis can result in a huge buildup of reactive oxygen species (ROS) which causes redox imbalance in WBCs (leukocytes) and organs. This increased number of ROS and WBC imbalance gives rise to an inflammatory response called systemic immune response syndrome (SIRS), along with a sustained immune response and other immune activation states in endothelial cells and leukocytes, that ultimately causes MOF and death.The detailed analysis and pathways are narrated in several papers including Riedemann et al. (2002); Hotchkiss et al. (2001); Peck-Palmer et al. (2008); Budd (2002); Kasten et al. (2010); Hotchkiss et al. (2016).

2.4 Molecular mechanisms in sepsis pathogenesis

Any severe insult to the body including burns, pathogen attacks, or severe surgeries, triggers inflammatory responses by releasing one of the two types of molecular patterns into the bloodstream: damage-associated molecular patterns (DAMPs), when the body suffers from an injury, or pathogen-associated molecular patterns (PAMPs), when a pathogen invades the body Bone (1996). In order to understand the complex flow of events that accompanies sepsis, let us consider the example of bacterial infection. In this section, the flow of events, i.e., the immune response of the body that follows the inception of bacterial infection is narrated to facilitate easy grasp of the complex biological phenomenon. (The flow of events associated with the immune response of the body is nearly similar for most of the infections or injuries.)

Bacterial cell walls are composed of lipo-polysaccharides (LPSs) which are also known as endotoxin. These toxin molecular patterns that are present inside a bacterial cell are released when the cell disintegrates. These patterns are known as PAMPs and are received by *toll like receptors* (TLR) that resides on the host cell surface. TLRs belong to a class of proteins usually expressed on the leukocyte membranes including macrophages, dendritic cells and cells of

adaptive immunity (T- and B-lymphocytes), that recognize molecules derived from pathogens. This binding between LPS and TLR releases pro-inflammatory cytokines including tumor necrosis factor α (TNFα), interleukins (IL-1β, IL-6, IL-12), macrophage inflammatory protein-1α (MIP-1α), and human leukocyte antigen (HLA) that encodes the major histocompatibility complex (MHC) proteins in humans, as illustrated in Figure 2.3(a) Jaffer et al. (2010). Release of these cytokines is followed by a cascade of other inflammatory chemokines such as IL-8 and C–C motif ligand 2 (CCL2), also known as monocyte chemotactic protein-1 (MCP-1) Bone et al. (2015).

Figure 2.2 illustrates the immune response resulting from bacterial infection that initiates the following two processes:

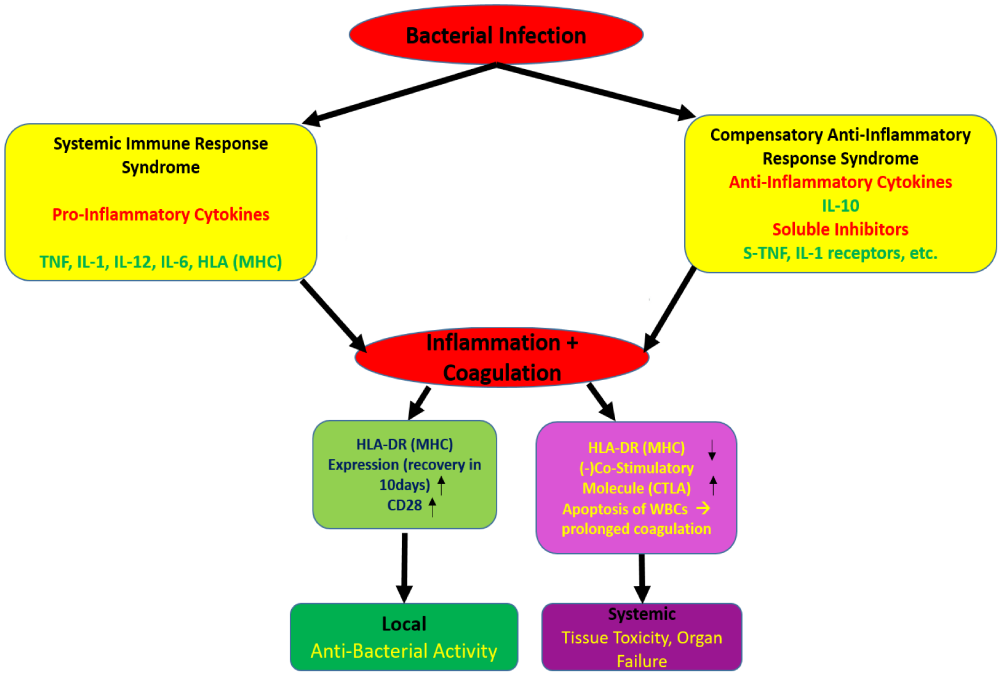

Figure 2.2 Flow of events during immune response in Sepsis and Non-Sepsis cases.

- recognition of multiple infection-derived microbial products Hotchkiss et al. (2016), and
- signalling the specific cell-surface receptors on cells (immune, epithelial, and endothelial), whose primary job is to continuously sample their local environment and do surveillance Takeuchi and Akira (2010).

C-reactive protein (CRP) is another protein, synthesized by the liver and found in blood plasma, whose circulating concentrations increase following IL-6 secretion by macrophages and T-cells Sproston and Ashworth (2018). Procalcitonin (PCT) is also produced by many cells in the body in response to both the infection and injuries. These phenomena are known as *systemic immune response syndrome* (SIRS) that leads to inflammation and coagulation.

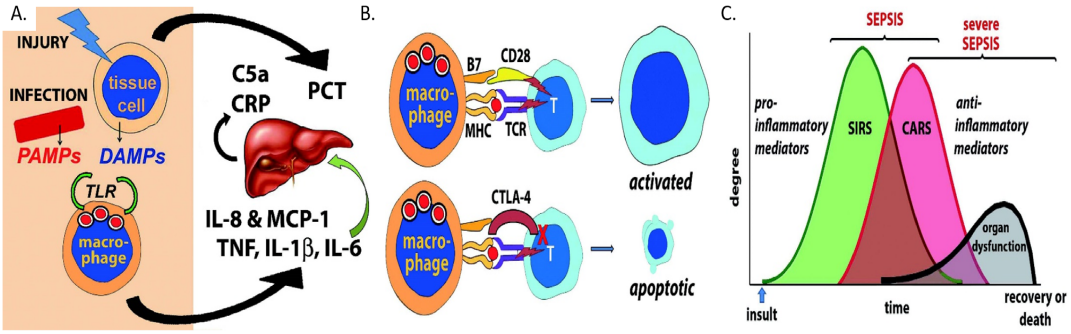

Figure 2.3 (A) Release of Biomarkers during Inflammation Process; (B) Activation and apoptosis of T-cells during non-sepsis and sepsis scenario respectively; (C) Balance and imbalance between SIRS and CARS during sepsis and severe sepsis Faix (2013).

Almost simultaneously, an anti-inflammatory response called *compensatory anti-inflammatory response syndrome* (CARS) is triggered in the body that strives to compensate the inflammatory process. This generates anti-inflammatory cytokines such as IL-4, IL-10, IL-11, and IL-13 Zhang and J. (2007). These cytokines inhibit pro-inflammatory cytokines synthesis. Hence, in general, with the invasion of any infection this complex dyad of inflammation and coagulation occurs with a balance between SIRS and CARS. The balance is disturbed when CARS does not kick in at the right time and instead of activation of T-cells by macrophages, apoptosis of T-cells occurs, as shown in Figure 2.2 and 2.3(b).

HLA-DR expression on macrophages is also reduced in patients suffering from severe sepsis. HLA-DR is an MHC class II cell surface receptor that resides on antigen presenting cells i.e. macrophages, B-cells, and dendritic cells. The prime role of HLA-DR is to present peptide antigens, originating from the bacterial cells, to T-cell receptors (TCRs) residing on T-cells. This eventually produces antibodies against the peptide antigen. However, in the event of severe sepsis,

reduced expression of HLA-DR is also accompanied by an increased expression of the negative co-stimulatory molecule CTLA-4 (cytotoxic T lymphocyte-associated antigen-4) Roger et al. (2009) as well as another molecule associated with apoptosis of T-cells called PD-1 (programmed cell death) Zhang et al. (2011). Generally, T-cells express a positive co-stimulatory molecule called CD28. Along with the TCRs, it recognizes peptide antigens presented by macrophages, which activates the T-cell. However, reduced expression of CD28 and enhanced expression of the alternative ligand CTLA-4 (also called CD152) leads to apoptosis of T-cells Kessel et al. (2009). When there is a lack of T-cells, the production of antibodies against the bacterial peptide antigen is reduced, thus delaying the elimination of bacterial infection. This leads to prolonged coagulation (one which tries to prevent the migration of infection to various organs of the body), and eventually due to this delayed coagulation, there is an insufficient supply of blood and nutrients to the organs which leads to organ failure and tissue toxicity. This becomes the cause of fatality in sepsis patients.

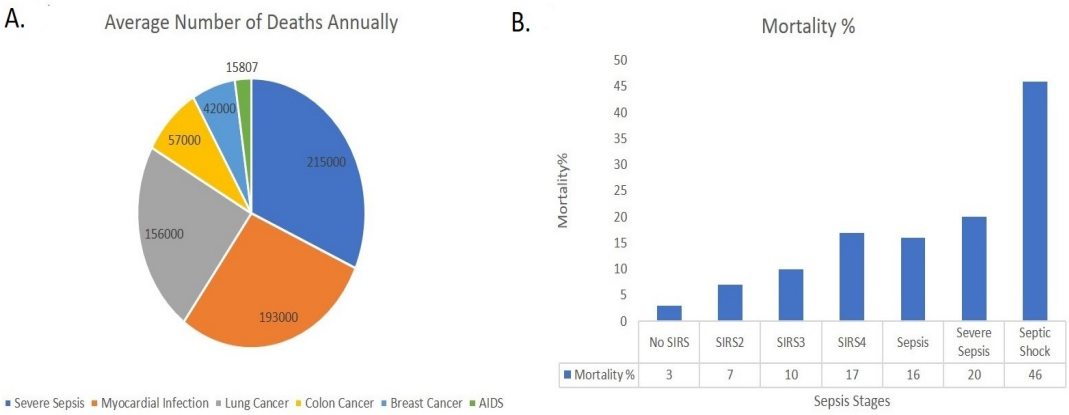

Figure 2.4 (A) Deaths from sepsis vs other diseases (https://www.cdc.gov/); (B) Rise in mortality with an increase in the number of systemic inflammatory response syndrome symptoms.

2.5 Impact Statistics of Sepsis

In order to appreciate the impact of sepsis worldwide, we hereby present a statistical representation of the scenario. Among the reported cases, there are over 31.5 million people who develop sepsis each year worldwide. Among those, 19.4 million suffer from severe sepsis and about

5.3 million people die Fleischmann et al. (2016). Further, it has been estimated that there are about 3 million cases of sepsis in neonates and 1.2 million in children per year globally, with mortality rates between 11-19% Fleischmann-Struzek et al. (2018). Due to puerperal sepsis, about 75,000 women die every year around the globe van Dillen et al. (2010). With mortality rates between 28-50% Gaieski et al. (2013), sepsis is clearly lethal; it also is remarkably expensive to treat. It is considered as one of the most exorbitant conditions to treat in the hospitals and clinics in the US, wherein the average cost for treating 3.1 million population sums up to US $4 billion per year Lagu et al. (2012); Gaieski et al. (2013). The estimated number of deaths in the US due to sepsis is higher than the combined deaths from prostate cancer, AIDS and breast cancer Adhikari et al. (2010).

A statistical overview and comparison among infectious diseases and mortality rates is illustrated in Figure 2.4. Underlying these stern numbers, a key factor is the absence of an accurate, prompt and point-of-care (POC) sepsis diagnostic method Daniels (2011). Early detection of the onset of sepsis is critical since for every hour of delay in exercising an appropriate antimicrobial medication to the patients results in roughly 7.6% decrease in survival rate. Mortality rates for each hour of antibiotic delay is shown in Figure 2.5 Linnér et al. (2013). The surviving patients who get discharged still suffer from a continuing risk of mortality Hotchkiss et al. (2000).

Figure 2.5 Relation between mortality rate and time to adequate antibiotics Linnér et al. (2013).

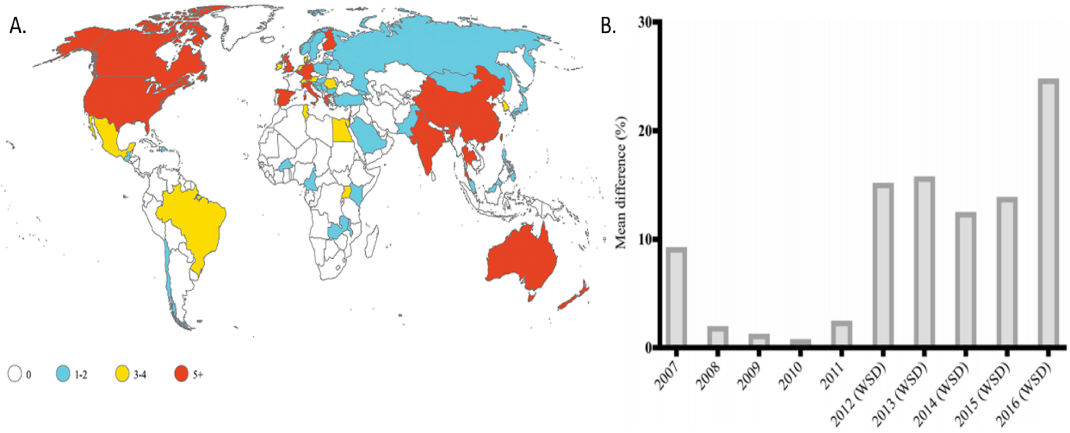

Figure 2.6 (A) Sepsis trials are predominantly conducted in high-income countries Rudd et al. (2018); (B) Rise in awareness world-wide Savelkoel et al. (2018).

These warrant an urgent need for an early detection of sepsis Kumar et al. (2006). In addition, a general awareness also needs to be instilled into the people and authorities. With this perspective, World Sepsis Day is observed across the globe since 2012 on 13^{th} September every year. Statistical analysis of Google search data on sepsis worldwide depicts a considerable amount of rising awareness regarding sepsis among the world population as illustrated in Figure 2.6(b). However, since the treatment of sepsis is considerably expensive, majority of sepsis trials registered at *ClinicalTrials.gov* (the US clinical trials registry, which is the largest in the world) and *anzctr.org.au* (the Australian New Zealand Clinical Trials Registry) belong to high-income countries as shown in Figure 2.6(a) Rudd et al. (2018). Therefore, clinicians and engineers are striving towards developing novel techniques and devices for fast and accurate diagnosis of sepsis.

2.6 Traditional Sepsis Diagnostics

Diagnosis of sepsis by traditional methods includes blood, urine, cerebro spinal fluid (CSF), and bronchial fluid culture. Generally, CRP or leukocyte count acts as an indicator or clinical sign for sepsis. Blood cultures are done in continuous-monitoring blood culture systems (CMBCS) and follow a set of pre-approved guidelines Wayne (2007).

Fully automated systems are prevalent for incubating the blood samples along with detection and analysis of CO_2 released and O_2 exhausted during the culture process. The sensing is

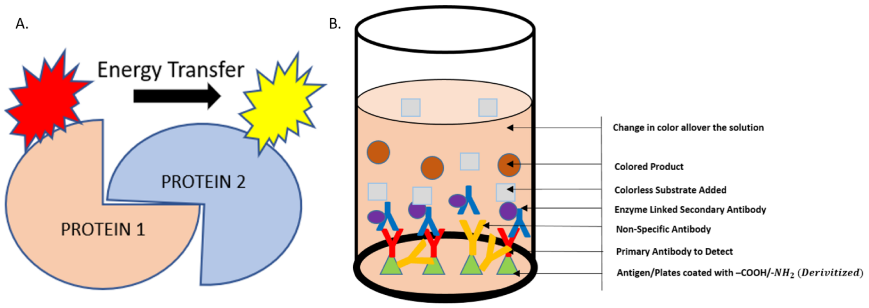

Figure 2.7 Conventional labeled detection technology: (A) FRET; (B) ELISA.

generally done using fluorescent sensors, which are popularly known as labeled sensing techniques Lakowicz (1999). Figure 2.7 illustrates two such common labeled techniques known as fluorescence resonance energy transfer (FRET) Ranjan et al. (2017) and enzyme-linked immunosorbent assay (ELISA) Voller et al. (1978) for detecting biomarker proteins. In addition to the labeled sensing techniques, there are several other techniques to estimate the concentration of gases released–calorimetric analysis Jin et al. (2016), automated growth detection techniques, and hybrid techniques including - lysis centrifugation-intrinsic fluorescence method (LC-IF), intrinsic fluorescence method for fast and direct identification of pathogens in blood cultures Walsh et al. (2013). There are some relatively new detection schemes that include - Multiplexed polymerase chain reaction (PCR) + hybridization or microarray, PCR + Mass Spectroscopy, Broad Spectrum PCR. These are primarily exercised on whole blood. Also, specialized techniques are employed nowadays for identification and susceptibility testing of positive blood culture. Use of techniques such as matrix-associated laser desorption ionisation-time of flight (MALDI-TOF), Molecular point-of-care test (POCT), and their combination or Multiplexed PCR along with mass spectroscopy are employed to increase the accuracy in the quantification of the pathogens. Most recent research published in late 2019 by Trung et al. (2019) bolsters the findings on PCR's supremacy over conventional blood culture based gold standard. They have demonstrated that their Sepsis@Quick test is much faster in detecting poly-microbial infections and multiple number of pathogens at a time.

Table 2.1 summarizes the conventional techniques for sepsis detection that rely mostly on pathogen detection (20 techniques are reported) Oeschger et al. (2019) and Reddy et al. (2018). A schematic diagram comparing the conventional and recent diagnostic methods for sepsis is depicted in Figure 2.8 Cohen et al. (2015). These methods involving analysis of blood culture is currently the *gold standard* for detecting any infectious disease such as sepsis. However, there are several limitations associated with the traditional diagnostic methods Mancini et al. (2010) which are briefly discussed in the next section.

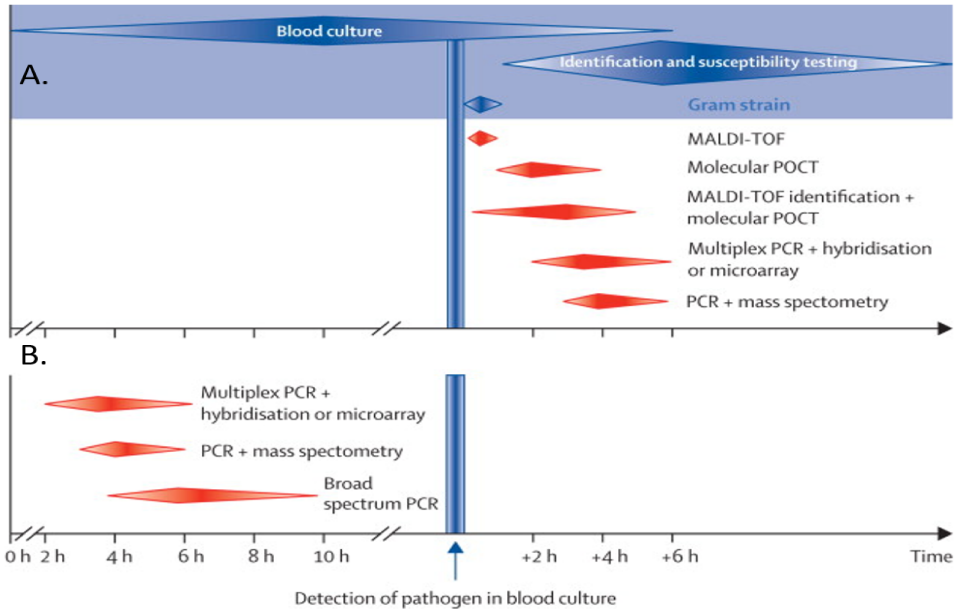

Figure 2.8 Time scale for the diagnosis of infections in bloodstream, with conventional and new technologies marked in blue and red respectively: (A) with positive blood cultures; (B) with whole blood. Blue vertical line represents the time at which blood cultures become positive Cohen et al. (2015). *Reprinted with permission from Elsevier.*

2.6.1 Limitations of Traditional Sepsis Diagnosis Systems

The limitations associated with traditional sepsis diagnosis systems are listed below:

- *Prolonged testing time:* Blood Culture tests take about 24 to 72 hours to confirm the prevalence of infection, pathogen invasion and anti-microbial susceptibilities Beekmann et al.

(2003); Campbell et al. (2003), and by the time a positive result arrives, the patient may have started suffering from severe sepsis or septic shock along with multiple organ failure.

- *Miss-classification due to non-specificity:* The anomalous counts for leukocytes or CRP may be misleading as that might be an outcome of some other clinical conditions or diseases rather than sepsis, thereby increasing the false-negative rate Angus and Van der Poll (2013).

- *Blood volume required for culture:* Studies reported at Bouza et al. (2007); Connell et al. (2007) confirm that the diagnostic yield improves with increase in extracted blood volume. Moreover, insufficient blood volume often yields in false-negative results. However, extracting large volume of blood from neonates and other pediatric patients with certain critical clinical conditions, is not always possible. This can be a bottleneck of traditional blood culture methodologies.

- *Existence of slow-growing pathogens:* Some pathogens multiply and express themselves slowly and this results in low microbial activities in the culture media, which reduces the signal to noise ratio Fenollar and Raoult (2007). The situation gets further deteriorated if the patients had received an anti-microbial therapy before.

- *Timeliness of sample testing:* Blood culture bottles need to be loaded into an automated instrument for measuring microbial activities Sautter et al. (2006); Schwetz et al. (2007). Ideally, to reduce false-negative results and minimize the detection time, the samples need to be loaded immediately, which puts additional constraints on accuracy.

It is evident that several diagnostic dilemma prevail in traditional blood-culture based sepsis diagnosis, and hence less limiting sepsis diagnostic methods are of paramount significance.

2.7 Biomarker-based Label-free Sepsis Diagnosis

The limitations of the traditional diagnosis discussed in the previous section motivate intervention of several interdisciplinary techniques. In the past decades, many novel techniques

Table 2.1 Traditional sepsis diagnosis techniques

Device	Company	Detection Method	Sample	Time-to-detect	Diagnosis	FDA Approved	POC
EPOC	Siemens	Blood gas (Analyzer)	Whole blood	1min	qSOFA	Yes	Semi
i-STAT	Abbott	Immuno Analyzers	Whole blood	30min	Circulating proteins	Yes	Yes
SeptiFast	Roche	PCR	Whole blood	6 hrs	Identify Pathogens	Yes	No
FAST-ID BSI Panel	Qvella	PCR	Whole blood	1 hr	Identify Pathogens	Yes	No
Microbiology - Septi-Chek	Becton Dickinson	Blood culture	Whole blood	38 hrs	Identify Pathogens	Yes	No
Oxoid signal	ThermoFisher Scientific	Blood culture	Whole blood	24 hrs	Identify Pathogens	Yes	No
QuickFISH	AdvanDx	Fluorescence	Positive blood culture	1.5 hrs	Identify Pathogens	Yes	No
Accllix	LeukoDx	Fluorescence/ Flow Cytometry	Positive blood culture	1-2 hrs	Cell Antigen Expression	No	No
SepsiTest	Molzym	PCR/ DNA Amplification	Whole blood	1-2 hrs	Identify Pathogens	Yes	No
AST	ImpeDx	Microfluidics/ Electrochemical	Positive blood culture	1-5 days	Identify Pathogens	Yes	No
hemoFISH	Miacom diagnostics	Fluorescence	Positive blood culture	0.5 hr	Identify Pathogens	Yes	No
Verigene	Luminex	PCR	Positive blood culture	3.5 hrs	Identify Pathogens	No	No
FilmArray	Biofire diagnostics	PCR	Positive blood culture	1 hr	Identify Pathogens	No	No
HYPLEX	BAG	PCR	Positive blood culture	3 hrs	Identify Pathogens	No	No
ACCU-PROBE	Gen-probe	Chemi-luminescent	Positive blood culture	3 hrs	Identify Pathogens	No	No
PLEX-ID BAC	Abbott	PCR	Positive blood culture	6 hrs	Identify Pathogens	No	No
Staph SR	Becton Dickinson	PCR	Positive blood culture	3 hrs	Identify Pathogens	Yes	No
StaphPlex	Qiagen	PCR	Positive blood culture	5 hrs	Identify Pathogens	No	No
MALDI-TOF	bioMérieux	Matrix assisted laser desorption	Positive blood culture	2 hrs	Identify Pathogens	No	No
Magicplex	Seegene	PCR	Whole blood	3.5 hrs	Identify Pathogens	No	No

have been developed with the aim to mitigate the existing limitations and achieve lower limits of detection. Some detection techniques focused on detecting the sepsis biomarker or a combination of biomarkers rather than directly detecting the pathogens, while some others studied the motion or motility of various blood components in a sepsis patient and compared those against a healthy subject. Biomarkers are measurable substances, the concentration of which increases or decreases in response to diseases, infections, or other environmental factors. The level of a specific biomarker or a combination of biomarkers gives an indication of the presence of a medical condition or disease. A large number of sepsis related biomarkers has been reported in literature. However, the accuracy and effectiveness of biomarker-based sepsis detection can not be evaluated until and unless the results are compared to some standards. In Liu et al. (2016) the authors conducted a systematic review and meta-analysis in order to evaluate the biomarkers reported in the last two decades by retrieving information from journals including PubMed and Embase. They identified seven most common sepsis biomarkers - PCT, CRP, IL-6, soluble triggering receptor expressed on myeloid cells-1, prepsin, lipopolysaccharide (LPS) binding protein, and CD64. Although, concentration of biomarkers correlates well with the severity of sepsis, due to the lack of specificity of biomarkers and different early inflammatory responses for different patients, distinguishing sepsis from other similar type of non-sepsis clinical conditions is critical. According to Pierrakos and Vincent (2010), approximately 178 sepsis biomarkers have been identified. But no biomarker shows sufficient sensitivity and specificity to sepsis Nobre et al. (2008) with one exception of PCT Rowland et al. (2015); de Jong et al. (2016). Hence, a combination of biomarkers can lead to better specificity and sensitivity Vincent and Beumier (2013). Table 2.2 lists the three major sepsis related biomarkers IL-6, PCT, and CRP, and their clinically important concentrations Reinhart et al. (2012).

Table 2.2 Key biomarker concentrations relevant for sepsis detection

Biomarker	Concentration in Blood (normal)[pg/mL]	Concentration in Blood (Sepsis)[pg/mL]
CRP	<3	>3
PCT	<10	10-10000
IL-6	<1	1-5000

In the following sub-section, we discuss some existing 'label-free' sepsis detection schemes which ultimately may lead to a POC (point-of-care) solution to sepsis detection.

2.7.1 Electrochemical Approach

Electrical transducers are widely used due to their high sensitivity, simplicity and amenability to inexpensive miniaturization. The increasing need for a patient-centered, efficient and inexpensive diagnostic system has resulted in the emergence and development of POC sepsis diagnostic systems. Min et al. (2018a) reported the development of a POC platform, termed IBS (integrated biosensor for sepsis) for rapid and reliable sepsis identification. A portable platform comprising of a disposable kit (to capture sepsis biomarker interleukin-3 (IL-3) on magnetic beads and label it for subsequent electrochemical measurements), an electrical detection system (to measure electrical current for IL-3 quantification), a microcontroller unit for signal processing and a bluetooth module for wireless communication, all packaged into a single monolithic device, outperformed the conventional enzyme-linked immunosorbent assays (ELISA) by providing >5 times faster response, >10 times more sensitivity and an order of magnitude larger dynamic detection range. Further, using human clinical samples ($n = 62$), sensitivity and specificity of 91.3% and 82.4% were achieved, respectively. In addition, survival analysis on patients suffering from septic shock, confirmed the significance of IL-3 as in indicator of organ failures. The total cost of the device was broken down to about $50 for the IBS reader and $5 per test for the reagent use. A scale-up production is expected to further reduce these prices, thus providing IBS competitive cost-advantages over ELISA ($11) or lateral flow strips ($10-$20).

The limitations in differentiating sepsis from other noninfectious causes of SIRS are overcome through multiplexed detection of multiple biomarkers that results in improved diagnosis. In this regard, Panneer Selvam and Prasad (2017a) reported the first-of-its-kind electrochemical impedance spectroscopy (EIS) based nanochannel system built with a nanoporous nylon membrane integrated onto microelectrodes. The covalent binding of biomarkers onto the electrode surface formed an electrical double layer which was transduced as impedance changes and

recorded via EIS. The sensor was demonstrated to detect three sepsis biomarkers, PCT, LPS and lipoteichoic acid (LTA) in pooled human serum as well as in human whole-blood samples with LODs of 0.1 ng ml^{-1}, 1 μg ml^{-1}, and 1 μg ml^{-1} respectively.

Other electrochemical sensors using highly-oriented pyrolytic graphite Mahe et al. (2014), host-guest nanonet electrode Shen et al. (2015), and enzyme-conjugated acrylic microspheres and gold nanoparticles composite coated onto a carbon-paste screen printed electrode Mansor et al. (2018) were also developed for sepsis biomarker detection as illustrated in Figure 2.9. Most recent development in electrochemical detection of sepsis in the year 2019 is the fabrication of needle shaped microelectrodes which can detect the levels of IL-6 Russell et al. (2019a), a sepsis biomarker. Figure 2.9(a) depicts the packaged device along with the needle shaped electrode structure and fabrication steps. Hannah et al. (2019) have also proposed an electrochemical detection method using screen printed electrodes, which provides a rapid test for anti-microbial susceptibility. Figure 2.9(b) illustrates the schematic of the detection system.

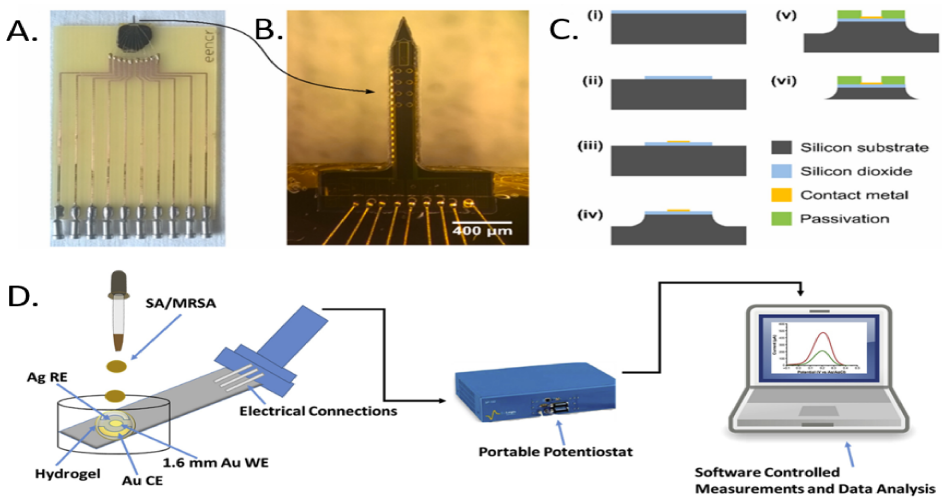

Figure 2.9 Electrochemical sensing : (A) Packaged Device (B) Micro-needle (C)Fabrication Steps Russell et al. (2019a) (D) Rapid Detection using Screen Printed Electrodes Hannah et al. (2019)

A comparative summary of 7 electrochemical sensors for sepsis diagnosis, detailing the samples they use, the biomarkers they target, the interfaces they utilize, their linearity and LOD, and their references, is presented in Table 2.3.

2.7.2 Optical Approach

Driven by the need to conduct in-situ measurements of sepsis, optical detection has proved to be an appealing platform. Zubiate et al. (2017) developed a high sensitive CRP measurement technique utilizing the lossy mode resonance (LMR) of optical fibers. LMR corresponds to the coupling of core mode of the fiber to a lossy mode in a thin-film. Arregui et al. (2014) also developed a similar fiber optic sensor utilizing LMR. The experimental setup is illustrated in Figure 2.10(A). A side polished D-shaped fiber was coated by a thin indium tin-oxide film and subsequently functionalized with layers of CRP-selective aptamers. The shifts in LMR wavelength were tracked in response to different concentrations of CRP solutions ranging from 0.0625 mgL^{-1} to 1 mgL^{-1}. The fabricated sensor could detect the minimum CRP concentrations of 0.0625 mgL^{-1} which is far below the clinical threshold value of 1 mgL^{-1}, demonstrating its potential in clinical diagnosis of sepsis.

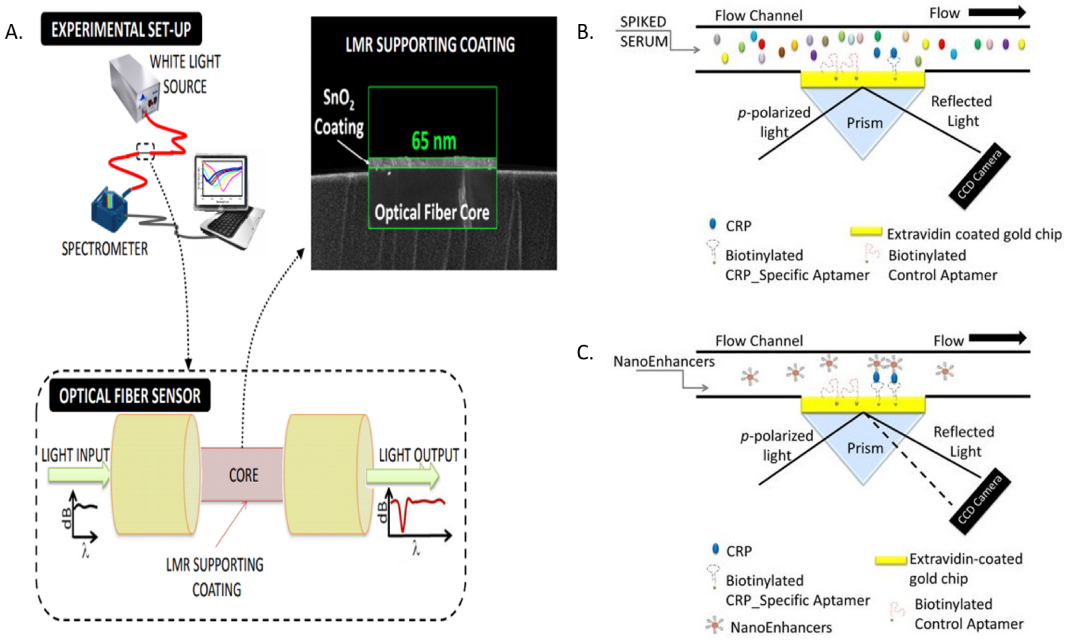

Figure 2.10 (A) Optical Fiber Sensor Arregui et al. (2014) and Detection of CRP using SPR technology: (B) without nano enhancers; (C) with nano enhancers Vance and Sandros (2014).

Table 2.3 Survey on electrochemical sensors for sepsis diagnosis

Principle	Sample	Biomarker	Interface	Linearity & LOD	Reference
Microelectrode	Buffer	Interlukin-6 (IL-6)	needle shaped micro-electrode	20-100pg/mL	Russell et al. (2019a)
Chrono-amperometry	Human Blood	IL-3	Antibodies, oxidizing enzyme (HRP)/ mediators	10 pg/mL	Min et al. (2018b)
Amperometric	Human Serum/ Blood	Secretory Phospholipase Group 2-IIA (Enzyme)	Enz. Conj. acrylic μspheres and Au NP coated on (SPE)	0.01–100 ng/mL, 5 x 10−3 ng/mL	Mansor et al. (2018)
Electrochemical Impedance Spectroscopy (EIS)	Human Serum/ Blood	PCT, LPS and lipoteichoic acid (LTA)	nanoporous nylon membrane integrated onto microelectrodes	0.1ng/ml, 1μ g/ml, 1μ g/ml	Panneer Selvam and Prasad (2017b)
Electrochemical Immunosensor	Buffer	PCT	Cu/Mn Double-Doped CeO2 Nanocomposites	0.03pg/ml	Yang et al. (2017)
Multiplexed EC Sensor	Infected Blood	Medium specific to bacterial species	AuNPs on SPE	290 CFU/mL	Gao et al. (2017)
Electrochemical Immunosensor	Human Serum/ Blood	TNF	Microarray ELISA	60pg/mL	Arya and Estrela (2017)

Surface plasmon resonance (SPR) is another promising label-free technique for selectively identifying sepsis. In Vance and Sandros (2014), an SPR system was developed to detect ultra-low concentrations of the CRP biomarker in blood. In this work, a sandwich assay was implemented by introducing aptamer-modified quantum dots (QDs), which could measure 7 zeptomole (at 5 fg/mL) of CRP in spiked human serum. Figure 2.10 (B) and (C) illustrate the set up. Wang et al. (2017) coated a thin gold film on the exposed region of the fiber core to excite the surface plasmon polaritons at the interface between the gold coating and the dielectric overlayer.

Afterwards, the SPR sensor was modified with a polydopamine, followed by the immobilization of anti-CRP monoclonal antibodies. The shifts in the SPR dip appearing at the output signal were measured and the sensitivity was observed to be 1.17nm μg $^{-1}$ mL. The

Table 2.4 Survey on optical sensors for sepsis diagnosis

Principle	**Sample**	**Biomarker**	**Interface**	**Linearity & LOD**	**Reference**
Nano-Plasmonic	Buffer	*E. coli (bacteria)*	Bioprinted Microarray Based Lens free Interferometer	Single bacterial cell in 40 min	Dey et al. (2018)
Optical Fiber (LMR)	Blood Plasma	CRP	Core-Cladding Interface	0.0625 - 1 mg/L	Zubiate et al. (2017)
Plasmonic (Nano-particles)	Buffer	CRP	Digital Biomarker detection in Microarray (NP enhanced gold nano-hole arrays)	27pg/mL	Belushkin et al. (2018)
Fiber Based Immunosensor	Buffer	IL-6	fluorescent magnetic nanoparticle	0.1 pg/mL	Zhang et al. (2018a)
SPR	Human Serum	Folic Acid Proteins	Graphene + Folic acid	5−500 fM 5fM	He et al. (2016)
SPR	Buffer	PCT	KOH treated gold-coated SPR chip	4.2 ng/mL	Vashist et al. (2012)
Fluorescence [FRET]	Buffer	Folate Receptor Proteins	Ag nanoclusters coated DNA /SWCNTs	0.1−3 ng/mL 33pg/mL	He et al. (2017)
Total Internal Reflection Fluorescence (TIRF)	Serum and Plasma	PCT, IL-6	microarray based multiparameter immunofluorescence assays	IL-6: 0.27 ng/mL in serum 0.77 ng/mL in plasma PCT: 0.37ng/mL in serum 1 ng/mL in plasma	Rascher et al. (2014)

optimum binding time between the anti-CRP and CRP was observed to be 60 mins which is far less than the conventional schemes. A point-of-care application for PCT quantification was proposed by Rascher et al. (2014), that worked on the principle of total internal reflection (TIRF). A comparative summary of 9 optical sensors for sepsis diagnosis, detailing the samples they use, the biomarkers they target, the interfaces they utilize, their linearity and LOD, and their references, is presented in Table 2.4.

2.7.3 Microfluidics Based Approach

Ellett et al. (2018) reported a novel sepsis diagnostic procedure where the motility of neutrophils present in blood was measured in a microfluidic assay. This device, as illustrated in Figure 2.11, required only a drop of diluted whole blood for diagnosis. Five motility parameters were studied and a hybrid score was calculated to estimate the prevalence of sepsis. Supervised machine learning algorithms were also applied to narrow down the total number of control parameters which increased the efficiency of the overall diagnosis process. The motility of neutrophils collected from sepsis patients exhibited higher motility compared to neutrophils collected from a healthy human. The complete detection process took about 6 hrs to complete which may be viewed as a limiting factor. Recently, researchers from MIT Wu and Voldman (2019) have developed a novel point-of-care microfluidic chip to detect sepsis in about 30 min. This biochip detects levels of IL-6, which is a sepsis biomarker from blood. The novelty lies in the fact that the detection is possible using only micro-liters of blood rather than conventional milliliters and can replace bulky devices with similar detection performance.

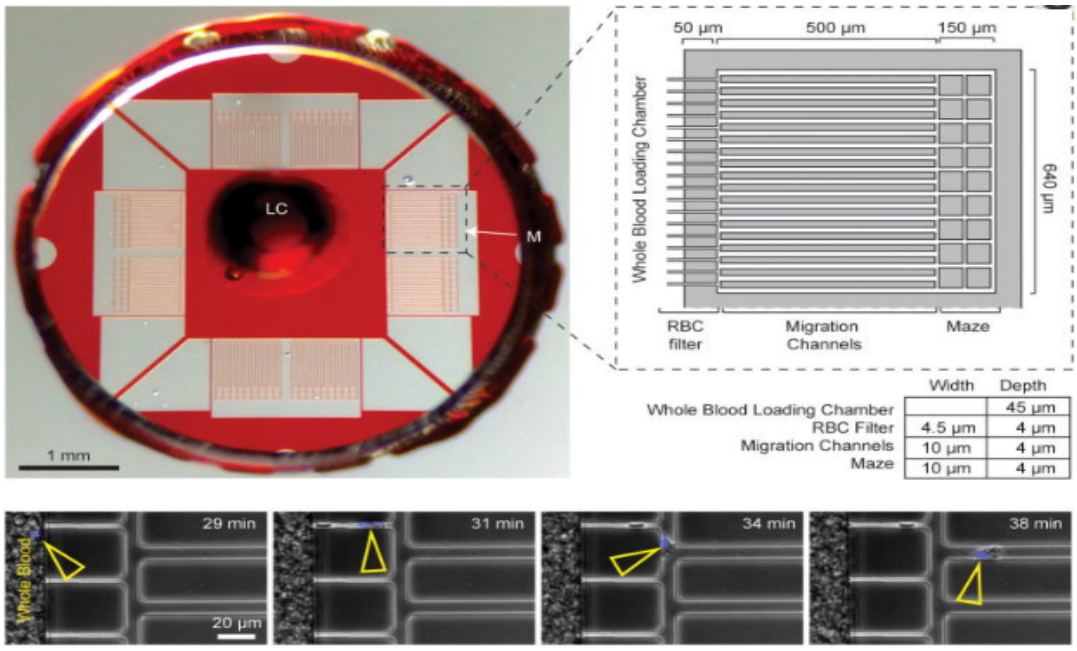

Figure 2.11 Microfluidic device to estimate neutrophil motility from a drop of blood Ellett et al. (2018) *Reprinted with permission from Springer Nature.*

Table 2.5 Survey on microfluidic and lab-on-chip sensors for sepsis diagnosis

Detection Principle	Sample	Biomarker	Interface	Linearity & LOD	Reference
Micro-fluidic	Drop of Blood	Neutrophils	N/A	N/A	Ellett et al. (2018)
Micro-fluidic	Blood	nCD64	cell counts	619 +/- 340 cells/ chip	Zhang et al. (2018b)
PoC Microfluidic Biochip	Blood	nCD64	cell counts	102 in 10uL of Blood	Hassan et al. (2017)
Lab on a Chip (Micro-fluidic)	Buffer	IL-3	magneto-electrochemical sensing	10pg/mL	Min et al. (2018b)

A comparative summary of 4 sepsis sensors realized on a microfluidics platform, detailing the samples they use, the biomarkers they target, the interfaces they utilize, their linearity and LOD, and their references, is presented in Table 2.5.

2.7.4 Field-Effect Transistor Based Approach

Field-effect transistors have been gaining more attention for infectious disease detection because of their low voltage operation (<1V), inherent gain amplification, biocompatibility and miniaturization Torsi et al. (2013). Seshadri et al. (2018a) developed a electrolyte-gated organic field-effect transistor (EGOFET) for label-free detection of PCT biomarker. The corresponding schematic diagram and actual implementation are depicted in Figure 2.12 (A) and (B) respectively. Monoclonal antibodies were immobilized on the surface of a poly-3-hexylthiophene (P3HT) organic semiconductor (OSC) that formed the transistor electronic channel. The antibody immobilization and analyte-receptor binding events induced distinct changes in the transistor figures of merit, namely, threshold voltage, drain current, and carrier mobility. The antibody functionalized to the OSC channel induced alterations in transfer path of charge carrier which translated into changes in carrier mobility. On the other hand, the net negative charge on the target PCT acted as traps for holes induced in the OSC, eventually reducing the drain current and shifting the device threshold voltage. The reported EGOFET could detect PCT concentrations, ranging from 0.8 pM to 4.7 nM with a detection limit of 2.2 pM. Similar FET based label free sensing using aptamer and carbon nano tubes has also been explored to detect IgE by Khung and Narducci (2013). Figure 2.12(C) illustrates a generalized scheme for fabrication

of such sensors, where underlying detection principle is similar to EGOFET discussed earlier. Recently Macchia et al. (2019) has developed similar organic transistor for detection of c-reactive proteins at it's physical limits, which is of course an improvement over existing Organic FETs.

A combined comparative summary of 2 sepsis sensors realized on a FET platform, along with the other two approaches discussed in the following, detailing the samples they use, the biomarkers they target, the interfaces they utilize, their linearity and LOD, and their references, is presented in Table 2.6.

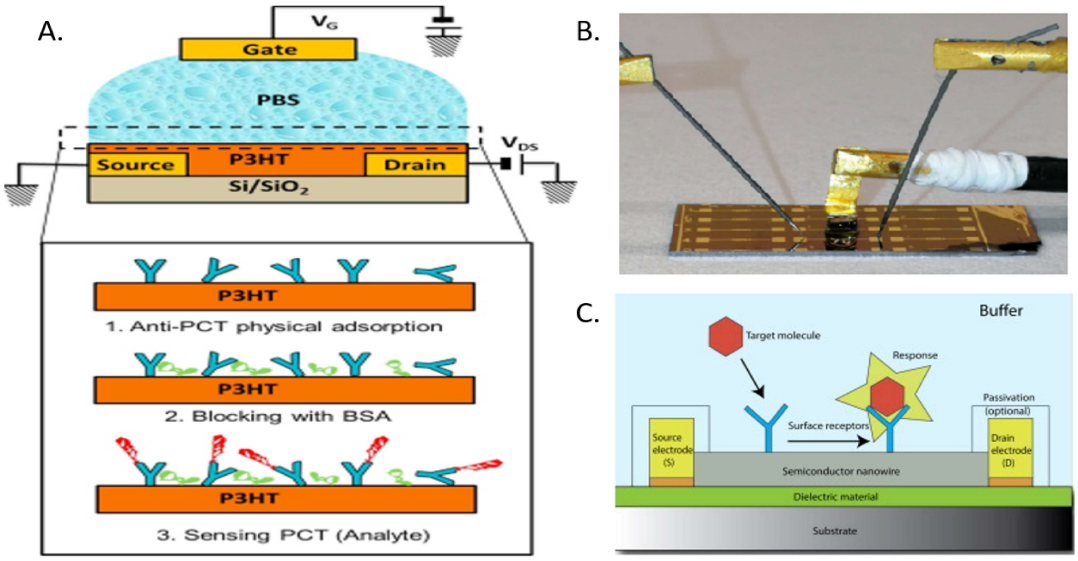

Figure 2.12 (A) Electrolyte Gated Organic FET Schematic and (B) Implementation Seshadri et al. (2018a). *Reprinted with permission from Elsevier.*(C) Schematic of a nano-wire/aptamer FET based label free detection of IgE biosensor Khung and Narducci (2013)

2.7.5 Machine Learning Based Approach

With the advent of data analytics and machine learning (ML) algorithms, researchers now have another way of predicting sepsis by using a set of observations from past diagnosis and tests. For instance, Logistic Regression (LR), Support Vector Machines (SVM), and Logistic Model Trees (LMT) were used to predict the onset of sepsis from the vital signs and blood samples of adult patients at the ICU Wang et al. (2018a). Wang et al. (2018b) used a 'random forest-improved fruit-fly optimization algorithm-kernel' based learning machine to effectively

diagnose the sepsis. The model employed random forest algorithm that enhanced the diagnosis accuracy. It was concluded that there was an increase in the levels of acetic acid, and a decrease in linoleic acid and cholesterol levels in sepsis patients.

Sepsis is prevalent in newborns which makes its early detection extremely important. In Hu et al. (2018) three physiological attributes Lehman et al. (2018) were utilized to predict sepsis which included: heart rate, respiratory rate, and blood oxygen saturation. The experienced pediatricians at the NICU of Monash Children Hospital utilized these variables to predict the onset of sepsis in preterm infants. Machine Learning algorithms including Multi-layer Neural Network (NN), Logistic Regression (LR), Support vector machines (SVM) with Gaussian kernel, and ensemble learning models including, Random Forest (RF) and Gradient Boosting Decision Tree (GBDT) were used, and from the results it was evident that RF and GBDT outperformed LR, SVM, and NN. Authors also claimed that the method could accurately predict the onset of sepsis 24 hours in advance. This provides clinicians ample opportunities to restrict the infection before it begins to cause harm to the newborn.

Now-a-days hospitals are employing Artificial Intelligence (AI) to monitor the onset of sepsis. Duke University Hospital has officially launched Sepsis Watch, that identifies incipient sepsis cases and raises an alarm Strickland (2018). Several other deep learning (convolutional - long short term memory) Lin et al. (2018); Saqib et al. (2018) based prediction algorithms are also presented in literature that predict sepsis with high efficiency. Recent Temporal Patterns (RTPs) used in conjunction with SVM classifier outperforms some other state-of-the-art machine learning techniques Khoshnevisan et al. (2018). Also, cloud based systems have been proposed that work in conjunction with ML and AI. For example, GE Healthcare and Roche Diagnostics have partnered together[3] to provide a cloud based digital analytical tool to utilize the pentabytes of patient data that is generated by hospitals yearly. Also, Faisal et al. (2019) have developed a computer model which defines a new score called computer-aided National Early Warning Score (cNEWS) which they claim to be more accurate than conventional qSOFA score and also easily

[3]https://www.gehealthcare.com/article/a-bot-for-sepsis-and-cancer-care-in-the-cloud

integrable with existing analytics in hospitals. These data provides a clear picture about an overall involvement of machine learning and data analytics tools in healthcare.

2.7.6 Miscellaneous Approaches

In addition to the above-mentioned techniques, there are other diagnostic schemes for cost-effective, timely, and real-time detection of infections. Recently, for easy tunability properties of the porous silicon (PSi) (e.g. pore morphology, photonic properties, biocompatibility and surface chemistry), biosensors based on PSi are gaining popularity . Over years, the initial drawbacks on sensitivity caused due to limited diffusion of biomolecules inside PSi nanopores have been overcome: The technique reported in Mariani et al. (2016), depicts a 10,000 fold increased sensitivity while detecting 3.0 nM concentration of sepsis biomarker protein TNFα with an enhanced signal to noise ratio of 10.6. Arshavsky-Graham et al. (2017) reported a proof of concept on enhancing the sensitivity by means of on-chip protein pre-concentration using electrokinetic isotachophoresis (ITP) on porous silicon (PSi) biosensor. The detection was based on Reflective Interferometric Fourier transform spectroscopy (RIFTS) with a LoD of 7.5 nM. Similar PSi based interferometric highly sensitive label-free detection of sepsis biomarker TNFα was also reported in Mariani et al. (2017), where Interferogram Average over Wavelength (IAW) reflectance spectroscopy was used as the detection principle, and concentrations ranging from 3 to 390 nM were detected. In Terracciano et al. (2019), authors have presented the recent progress in the development of PSi optical aptasensors for bioengineering and biomedical applications, also dicussing various PSi functionalization strategies along with techniques to improve the device performance in terms of sensitivity, response time, and limit of detection (LOD).

Voltammetric diagnosis Ly et al. (2018) of *E. Coli* done on blood plasma infected by sepsis, is another scheme in use. In Henne et al. (2006), researchers developed a gold-coated quartz crystal microbalance biosensor for the detection of folate binding protein (FBP), which is a biomarker for sepsis. A LOD of 30 nM was achieved for the sensor. Figure 2.13 (A) and (B) depict the working principle of this acoustic biosensor for the detection of FBP. Figure 2.13 (C) illustrates a

generalized response curve for the change in frequency with respect to protein binding. It depicts that the oscillation frequency decreases with the increase in specific protein bindings on the sensor surface. Isansys has developed patient status engine (PSE), which is a wearable sensor patch that can continuously monitor a patient's vital signs and help predict the onset of sepsis in real time by analyzing the physiological changes in the readings. Recently colorimetric detection of change in motion of multifunctional janus particle was used by Russell et al. (2019b) to detect procalcitonin (PCT) biomarker related to sepsis from whole blood.

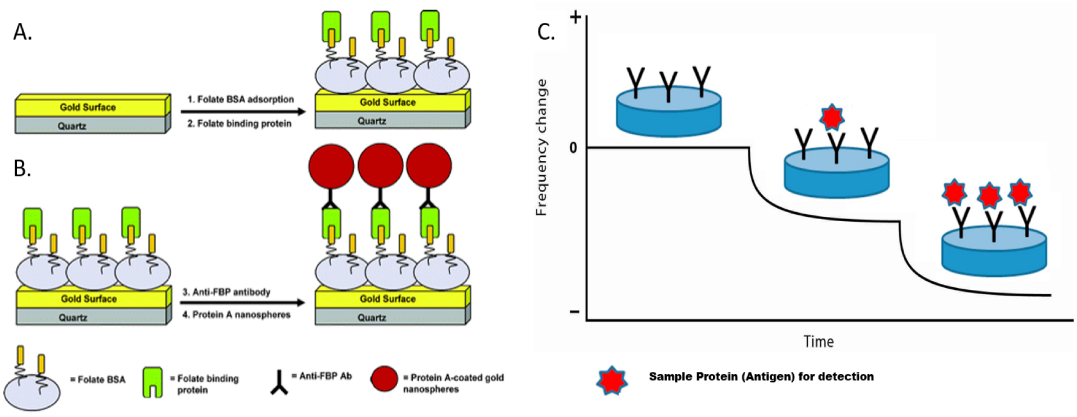

Figure 2.13 Acoustic Biosensor (A) Functionalization of the sensor surface (B) Protein detection using QCM Henne et al. (2006). *Reprinted with permission from ACS.* (C) Generalized schematic of change in frequency with respect to protein binding on the sensor surface.

A combined comparative summary of 5 sepsis sensing techniques realized using the last three approaches discussed above, detailing the samples they use, the biomarkers they target, the interfaces they utilize, their linearity and LOD, and their references, is presented in Table 2.6.

2.8 Concluding remarks and outlook

In this survey we have provided a clear perspective on the current status of sepsis that is one of the most challenging medical disorders, with a discussion on its mechanism of action. In addition, a review of existing literature on sepsis diagnosis technologies and the areas wherein a fast and robust point of care sepsis detection system can be designed, is also over-viewed.

Table 2.6 Survey on FET, Mass, and Machine Learning based sensors for sepsis diagnosis

Principle	Sample	Biomarker	Interface	Linearity & LOD	Reference
Organic FET	Saliva	CRP	millimeter-sized transistor (SiMoT)	590 zM	Macchia et al. (2019)
Colorimetry	Whole Blood	PCT	poly-3-janus transducers	0.4ng/mL	Russell et al. (2019b)
Machine Learning Based	N/A	N/A	Prediction from variation of physiological data analysis of historic data available on sepsis	N/A	Hu et al. (2018) Lehman et al. (2018) Strickland (2018) Lin et al. (2018) Saqib et al. (2018) Khoshnevisan et al. (2018)
Electrolyte Gated OFET	Buffer	PCT	poly-3- hexylthiophene (P3HT) / Antibody (anti-PCT)	2.2pM	Seshadri et al. (2018b)Mulla et al. (2015)
Field Effect Transistor	Buffer	CRP	CMOS Technology	0.1ng/mL	Sohn and Kim (2008) Park et al. (2010)
Quartz Crystal Microbalance - D300 QCM unit	Human Serum	Folate Binding Proteins	Au+ folate / BSA+ anti-FBP	50pM − 2μM	Henne et al. (2006)

There has been a great advancement in the diagnosis of sepsis, especially in methods that do not require blood culture, such as PCR, MALDI-TOF, and ELISA based technology. These technologies have facilitated a great deal of velocity in which the infections along with their anti-microbial activity patterns are identified. However, challenges continue to persist and unless the clinicians can detect sepsis at its onset, the infected blood samples cannot be obtained from patients which results in retardation in diagnosis and delay in exercising antibiotics. Thus, there is an urgent need for point of care devices that can detect sepsis within minutes from the onset of sepsis. From the existing literature review narrated in this paper, it is evident that point of care biochips can be fabricated with the capability of detecting multiple sepsis biomarkers at a time. Thus, label-free biomarker detection can eventually pave the way for future automatic diagnosis of sepsis in intensive care units and thereby contribute significantly to the reduction in sepsis fatality worldwide.

In addition to the measurement issues, the occurrence of sepsis depends on a combination of system factors: hosts, pathogens, and health-care systems, as illustrated by the venn diagram in Figure 2.14. These factors are inter-related and hence their interplay can be a crucial factor. The factors can be social and demographic which include: diet, lifestyle, economic status, sex, race. Even access to health-care system is very critical in determining the prevalence, extent, and

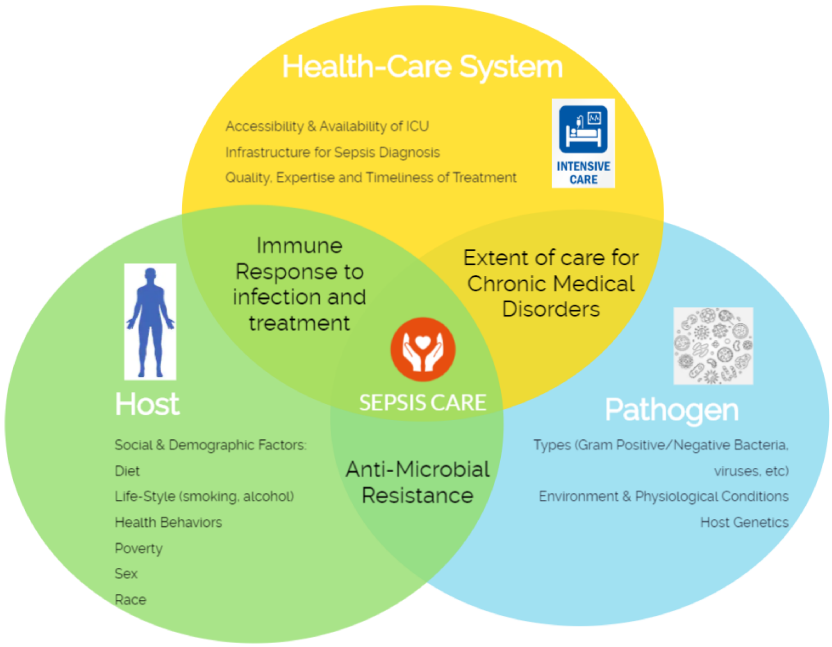

Figure 2.14 Determining factors for the incidence of sepsis. (Figure inspired from Cohen et al. (2015))

subsequent survival of a patient during the septic shock or severe sepsis. Also, clinical data are only available in high-income rate countries thereby limiting the correct statistical characterization of the diagnosis and its treatment results.

2.9 References

Adhikari, N. K., Fowler, R. A., Bhagwanjee, S., and Rubenfeld, G. D. (2010). Critical care and the global burden of critical illness in adults. *The Lancet*, 376(9749):1339–1346.

Aird, W. C. (2003). The role of the endothelium in severe sepsis and multiple organ dysfunction syndrome. *Blood*, 101(10):3765–3777.

Angus, D. C. and Van der Poll, T. (2013). Severe sepsis and septic shock. *N Engl J Med*, 369:840–851.

Arregui, F. J., Del Villar, I., Corres, J. M., Goicoechea, J., Zamarreño, C. R., Elosua, C., Hernaez, M., Rivero, P. J., Socorro, A. B., Urrutia, A., et al. (2014). Fiber-optic lossy mode resonance sensors. *Procedia Engineering*, 87:3–8.

Arshavsky-Graham, S., Massad-Ivanir, N., Paratore, F., Scheper, T., Bercovici, M., and Segal, E. (2017). On chip protein pre-concentration for enhancing the sensitivity of porous silicon biosensors. *ACS sensors*, 2(12):1767–1773.

Arya, S. K. and Estrela, P. (2017). Electrochemical immunosensor for tumor necrosis factor-alpha detection in undiluted serum. *Methods*, 116:125–131.

Bateman, R. M., Sharpe, M. D., and Ellis, C. G. (2003). Bench-to-bedside review: microvascular dysfunction in sepsis–hemodynamics, oxygen transport, and nitric oxide. *Critical care*, 7(5):359.

Beekmann, S., Diekema, D., Chapin, K., and Doern, G. (2003). Effects of rapid detection of bloodstream infections on length of hospitalization and hospital charges. *Journal of clinical microbiology*, 41(7):3119–3125.

Belushkin, A., Yesilkoy, F., and Altug, H. (2018). Nanoparticle-enhanced plasmonic biosensor for digital biomarker detection in a microarray. *ACS nano*, 12(5):4453–4461.

Berg, D. and Gerlach, H. (2018). Recent advances in understanding and managing sepsis. *F1000Research*, 7.

Bone, H. E., Hoelscher, G. L., Ingram, J. A., Bethea, S., Cox, M., and N., H. J. E. (2015). Proinflammatory cytokines modulate the chemokine ccl2 (mcp-1) in human annulus cells in vitro: Ccl2 expression and production. *Experimental and Molecular Pathology*, 98(1):102–105.

Bone, R. C. (1996). Immunologic dissonance: a continuing evolution in our understanding of the systemic inflammatory response syndrome (sirs) and the multiple organ dysfunction syndrome (mods). *Annals Internal Med.*, 125:680–687.

Bone, R. C., Balk, R. A., Cerra, F. B., Dellinger, R. P., Fein, A. M., Knaus, W. A., Schein, R. M., and Sibbald, W. J. (1992). Definitions for sepsis and organ failure and guidelines for the use of innovative therapies in sepsis. *Chest*, 101(6):1644–1655.

Boomer, J. S., To, K., Chang, K. C., Takasu, O., Osborne, D. F., Walton, A. H., Bricker, T. L., Jarman, S. D., Kreisel, D., Krupnick, A. S., et al. (2011). Immunosuppression in patients who die of sepsis and multiple organ failure. *Jama*, 306(23):2594–2605.

Bouza, E., Sousa, D., Rodríguez-Créixems, M., Lechuz, J. G., and Munoz, P. (2007). Is the volume of blood cultured still a significant factor in the diagnosis of bloodstream infections? *Journal of clinical microbiology*, 45(9):2765–2769.

Budd, R. C. (2002). Death receptors couple to both cell proliferation and apoptosis. *The Journal of clinical investigation*, 109(4):437–442.

Campbell, S. G., Marrie, T. J., Anstey, R., Dickinson, G., Ackroyd-Stolarz, S., capital Study Investigators, et al. (2003). The contribution of blood cultures to the clinical management of adult patients admitted to the hospital with community-acquired pneumonia: a prospective observational study. *Chest*, 123(4):1142–1150.

Cohen, J., Vincent, J.-L., Adhikari, N. K., Machado, F. R., Angus, D. C., Calandra, T., Jaton, K., Giulieri, S., Delaloye, J., Opal, S., et al. (2015). Sepsis: a roadmap for future research. *The Lancet infectious diseases*, 15(5):581–614.

Connell, T. G., Rele, M., Cowley, D., Buttery, J. P., and Curtis, N. (2007). How reliable is a negative blood culture result? volume of blood submitted for culture in routine practice in a children's hospital. *Pediatrics*, 119(5):891–896.

Cooper, M. D. (2015). The early history of b cells. *Nature Reviews Immunology*, 15(3):191.

Daniels, R. (2011). Surviving the first hours in sepsis: getting the basics right (an intensivist's perspective). *Journal of Antimicrobial Chemotherapy*, 66(suppl_2):ii11–ii23.

de Jong, E., van Oers, J. A., Beishuizen, A., Vos, P., Vermeijden, W. J., Haas, L. E., Loef, B. G., Dormans, T., van Melsen, G. C., Kluiters, Y. C., et al. (2016). Efficacy and safety of procalcitonin guidance in reducing the duration of antibiotic treatment in critically ill patients: a randomised, controlled, open-label trial. *The Lancet Infectious Diseases*, 16(7):819–827.

Dey, P., Fabri-Faja, N., Calvo-Lozano, O., Terborg, R. A., Belushkin, A., Yesilkoy, F., Fabrega, A., Ruiz-Rodriguez, J. C., Ferrer, R., Gonzalez-Lopez, J. J., et al. (2018). Label-free bacteria quantification in blood plasma by a bioprinted microarray based interferometric point-of-care device. *ACS sensors*, 4(1):52–60.

Dixon, B. (2004). The role of microvascular thrombosis in sepsis. *Anaesthesia and intensive care*, 32(5):619–629.

Ellett, F., Jorgensen, J., Marand, A. L., Liu, Y. M., Martinez, M. M., Sein, V., Butler, K. L., Lee, J., and Irimia, D. (2018). Diagnosis of sepsis from a drop of blood by measurement of spontaneous neutrophil motility in a microfluidic assay. *Nature Biomedical Engineering*, 2(4):207.

Esmon, C. T. (2005). The interactions between inflammation and coagulation. *British journal of haematology*, 131(4):417–430.

Faisal, M., Richardson, D., Scally, A. J., Howes, R., Beatson, K., Speed, K., and Mohammed, M. A. (2019). Computer-aided national early warning score to predict the risk of sepsis following emergency medical admission to hospital: a model development and external validation study. *CMAJ*, 191(14):E382–E389.

Faix, J. D. (2013). Biomarkers of sepsis. *Critical reviews in clinical laboratory sciences*, 50(1):23–36.

Fenollar, F. and Raoult, D. (2007). Molecular diagnosis of bloodstream infections caused by non-cultivable bacteria. *International journal of antimicrobial agents*, 30:7–15.

Fleischmann, C., Scherag, A., Adhikari, N. K., Hartog, C. S., Tsaganos, T., Schlattmann, P., Angus, D. C., and Reinhart, K. (2016). Assessment of global incidence and mortality of hospital-treated sepsis. current estimates and limitations. *American journal of respiratory and critical care medicine*, 193(3):259–272.

Fleischmann-Struzek, C., Goldfarb, D. M., Schlattmann, P., Schlapbach, L. J., Reinhart, K., and Kissoon, N. (2018). The global burden of paediatric and neonatal sepsis: a systematic review. *The Lancet Respiratory Medicine*, 6(3):223–230.

Freud, A. G., Mundy-Bosse, B. L., Yu, J., and Caligiuri, M. A. (2017). The broad spectrum of human natural killer cell diversity. *Immunity*, 47(5):820–833.

Gaieski, D. F., Edwards, J. M., Kallan, M. J., and Carr, B. G. (2013). Benchmarking the incidence and mortality of severe sepsis in the united states. *Critical care medicine*, 41(5):1167–1174.

Gao, J., Jeffries, L., Mach, K. E., Craft, D. W., Thomas, N. J., Gau, V., Liao, J. C., and Wong, P. K. (2017). A multiplex electrochemical biosensor for bloodstream infection diagnosis. *SLAS TECHNOLOGY: Translating Life Sciences Innovation*, 22(4):466–474.

Geroulanos, S. and Douka, E. T. (2006). Historical perspective of the word "sepsis". *Intensive care medicine*, 32(12):2077–2077.

Gül, F., Arslantaş, M. K., Cinel, İ., and Kumar, A. (2017). Changing definitions of sepsis. *Turkish journal of anaesthesiology and reanimation*, 45(3):129.

Gyawali, B., Ramakrishna, K., and Dhamoon, A. S. (2019). Sepsis: The evolution in definition, pathophysiology, and management. *SAGE open medicine*, 7:2050312119835043.

Hannah, S., Addington, E., Alcorn, D., Shu, W., Hoskisson, P. A., and Corrigan, D. K. (2019). Rapid antibiotic susceptibility testing using low-cost, commercially available screen-printed electrodes. *Biosensors and Bioelectronics*, 145:111696.

Hassan, U., Ghonge, T., Reddy Jr, B., Patel, M., Rappleye, M., Taneja, I., Tanna, A., Healey, R., Manusry, N., Price, Z., et al. (2017). A point-of-care microfluidic biochip for quantification of cd64 expression from whole blood for sepsis stratification. *Nature communications*, 8(1):1–12.

He, L., Pagneux, Q., Larroulet, I., Serrano, A. Y., Pesquera, A., Zurutuza, A., Mandler, D., Boukherroub, R., and Szunerits, S. (2017). Label-free femtomolar cancer biomarker detection in human serum using graphene-coated surface plasmon resonance chips. *Biosensors and Bioelectronics*, 89:606–611.

He, L., Wang, Q., Mandler, D., Li, M., Boukherroub, R., and Szunerits, S. (2016). Detection of folic acid protein in human serum using reduced graphene oxide electrodes modified by folic-acid. *Biosensors and Bioelectronics*, 75:389–395.

Henne, W. A., Doorneweerd, D. D., Lee, J., Low, P. S., and Savran, C. (2006). Detection of folate binding protein with enhanced sensitivity using a functionalized quartz crystal microbalance sensor. *Analytical chemistry*, 78(14):4880–4884.

Hotchkiss, R., Chang, K., Swanson, P., Tinsley, K., Hui, J., Klender, P., Xanthoudakis, S., Roy, S., Black, C., Grimm, E., et al. (2000). Caspase inhibitors improve survival in sepsis: a critical role of the lymphocyte. *Nature immunology*, 1(6):496.

Hotchkiss, R. S., Moldawer, L. L., Opal, S. M., Reinhart, K., Turnbull, I. R., and Vincent, J.-L. (2016). Sepsis and septic shock. *Nature reviews Disease primers*, 2:16045.

Hotchkiss, R. S., Tinsley, K. W., Swanson, P. E., Schmieg, R. E., Hui, J. J., Chang, K. C., Osborne, D. F., Freeman, B. D., Cobb, J. P., Buchman, T. G., et al. (2001). Sepsis-induced apoptosis causes progressive profound depletion of b and cd4+ t lymphocytes in humans. *The Journal of Immunology*, 166(11):6952–6963.

Hu, Y., Lee, V. C., and Tan, K. (2018). Prediction of clinicians' treatment in preterm infants with suspected late-onset sepsis—an ml approach. In *2018 13th IEEE Conference on Industrial Electronics and Applications (ICIEA)*, pages 1177–1182. IEEE.

Jaffer, U., Wade, R. G., and Gourlay, T. (2010). Cytokines in the systemic inflammatory response syndrome: a review. *HSR Proceedings in Intensive Care and Cardiovascular Anesthesia*, 2:161–175.

Jin, Y.-J., Moon, B.-C., and Kwak, G. (2016). Colorimetric fluorescence response to carbon dioxide using charge transfer dye and molecular rotor dye in smart solvent system. *Dyes and Pigments*, 132:270–273.

Kasten, K. R., Prakash, P. S., Unsinger, J., Goetzman, H. S., England, L. G., Cave, C. M., Seitz, A. P., Mazuski, C. N., Zhou, T. T., Morre, M., et al. (2010). Interleukin-7 (il-7) treatment accelerates neutrophil recruitment through $\gamma\delta$ t-cell il-17 production in a murine model of sepsis. *Infection and immunity*, 78(11):4714–4722.

Kessel, A., Bamberger, E., Masalha, M., and Toubi, E. (2009). The role of t regulatory cells in human sepsis. *Journal of autoimmunity*, 32(3-4):211–215.

Khoshnevisan, F., Ivy, J., Capan, M., Arnold, R., Huddleston, J., and Chi, M. (2018). Recent temporal pattern mining for septic shock early prediction. In *2018 IEEE International Conference on Healthcare Informatics (ICHI)*, pages 229–240.

Khung, Y. L. and Narducci, D. (2013). Synergizing nucleic acid aptamers with 1-dimensional nanostructures as label-free field-effect transistor biosensors. *Biosensors and Bioelectronics*, 50:278–293.

Kumar, A., Roberts, D., Wood, K. E., Light, B., Parrillo, J. E., Sharma, S., Suppes, R., Feinstein, D., Zanotti, S., Taiberg, L., et al. (2006). Duration of hypotension before initiation of effective antimicrobial therapy is the critical determinant of survival in human septic shock. *Critical care medicine*, 34(6):1589–1596.

Kumar, B. V., Connors, T. J., and Farber, D. L. (2018). Human t cell development, localization, and function throughout life. *Immunity*, 48(2):202–213.

Kumar, S., Tripathy, S., Jyoti, A., and Singh, S. G. (2019). Recent advances in biosensors for diagnosis and detection of sepsis: A comprehensive review. *Biosensors and Bioelectronics*, 124:205–215.

Lagu, T., Rothberg, M. B., Shieh, M.-S., Pekow, P. S., Steingrub, J. S., and Lindenauer, P. K. (2012). Hospitalizations, costs, and outcomes of severe sepsis in the united states 2003 to 2007. *Critical care medicine*, 40(3):754–761.

Lakowicz, J. R. (1999). Fluorescence sensing. In *Principles of fluorescence spectroscopy*, pages 531–572. Springer.

Lehman, L. H., Mark, R. G., and Nemati, S. (2018). A model-based machine learning approach to probing autonomic regulation from nonstationary vital-sign time series. *IEEE Journal of Biomedical and Health Informatics*, 22(1):56–66.

Levi, M. and Ten Cate, H. (1999). Disseminated intravascular coagulation. *New England Journal of Medicine*, 341(8):586–592.

Levi, M., van der Poll, T., and Buller, H. R. (2004). Bidirectional relation between inflammation and coagulation. *Circulation*, 109(22):2698–2704.

Lin, C., Zhangy, Y., Ivy, J., Capan, M., Arnold, R., Huddleston, J. M., and Chi, M. (2018). Early diagnosis and prediction of sepsis shock by combining static and dynamic information using convolutional-lstm. In *2018 IEEE International Conference on Healthcare Informatics (ICHI)*, pages 219–228.

Linnér, A., Sundén-Cullberg, J., Johansson, L., Hjelmqvist, H., Norrby-Teglund, A., and Treutiger, C. J. (2013). Short-and long-term mortality in severe sepsis/septic shock in a setting with low antibiotic resistance: a prospective observational study in a swedish university hospital. *Frontiers in public health*, 1:51.

Liu, Y., Hou, J.-h., Li, Q., Chen, K.-j., Wang, S.-N., and Wang, J.-m. (2016). Biomarkers for diagnosis of sepsis in patients with systemic inflammatory response syndrome: a systematic review and meta-analysis. *Springerplus*, 5(1):2091.

Luckashenak, N. and Eisenlohr, L. C. (2013). Dendritic cells: Antigen processing and presentation. In *Cancer Immunotherapy (Second Edition)*, pages 55–70. Elsevier.

Ly, S. Y., Kim, Y. C., Hong, H. J., Kim, J., and Lee, K. (2018). Rapid voltammetric diagnosis of escherichia coli contamination in non-treated human blood plasma of healthy and sepsis-infected patients. *Korea*, 139:743.

Macchia, E., Manoli, K., Holzer, B., Di Franco, C., Picca, R. A., Cioffi, N., Scamarcio, G., Palazzo, G., and Torsi, L. (2019). Selective single-molecule analytical detection of c-reactive protein in saliva with an organic transistor. *Analytical and bioanalytical chemistry*, 411(19):4899–4908.

Mahe, L. S. A., Green, S. J., Winlove, C. P., and Jenkins, A. T. A. (2014). Pyrene-wired antibodies on highly oriented pyrolytic graphite as a label-free impedance biosensor for the sepsis biomarker procalcitonin. *J. Solid State Electrochem.*, 18:3245–3249.

Mancini, N., Carletti, S., Ghidoli, N., Cichero, P., Burioni, R., and Clementi, M. (2010). The era of molecular and other non-culture-based methods in diagnosis of sepsis. *Clinical microbiology reviews*, 23(1):235–251.

Mansor, N. N. N., Leong, T. T., Safitri, E., Futra, D., Ahmad, N. S., Nasuruddin, D. N., Itnin, A., Zaini, I. Z., Arifin, K. T., Heng, L. Y., and Hassan, N. I. (2018). An amperometric biosensor for the determination of bacterial sepsis biomarker, secretory phospholipase group 2-iia using a tri-enzyme system. *Sensors*, 18:686.

Mariani, S., Pino, L., Strambini, L. M., Tedeschi, L., and Barillaro, G. (2016). 10 000-fold improvement in protein detection using nanostructured porous silicon interferometric aptasensors. *ACS sensors*, 1(12):1471–1479.

Mariani, S., Strambini, L., Tedeschi, L., and Barillaro, G. (2017). Porous silicon interferometers for high-sensitivity label-free detection of biomolecules. In *2017 IEEE SENSORS*, pages 1–3. IEEE.

Min, J., Nothing, M., Coble, B., Zheng, H., Park, J., Im, H., Weber, G. F., Castro, C. M., Swirski, F. K., Weissleder, R., et al. (2018a). Integrated biosensor for rapid and point-of-care sepsis diagnosis. *Acs Nano*, 12(4):3378–3384.

Min, J., Nothing, M., Coble, B., Zheng, H., Park, J., Im, H., Weber, G. F., Castro, C. M., Swirski, F. K., Weissleder, R., et al. (2018b). Integrated biosensor for rapid and point-of-care sepsis diagnosis. *ACS nano*, 12(4):3378–3384.

Mulla, M., Seshadri, P., Torsi, L., Manoli, K., Mallardi, A., Ditaranto, N., Santacroce, M., Di Franco, C., Scamarcio, G., and Magliulo, M. (2015). Uv crosslinked poly (acrylic acid): a simple method to bio-functionalize electrolyte-gated ofet biosensors. *Journal of Materials Chemistry B*, 3(25):5049–5057.

Nobre, V., Harbarth, S., Graf, J.-D., Rohner, P., Pugin, J., et al. (2008). Use of procalcitonin to shorten antibiotic treatment duration in septic patients: a randomized trial. *American journal of respiratory and critical care medicine*, 177(5):498.

Oeschger, T., McCloskey, D., Kopparthy, V., Singh, A., and Erickson, D. (2019). Point of care technologies for sepsis diagnosis and treatment. *Lab on a Chip*, 19(5):728–737.

Opal, S. M. and Esmon, C. T. (2002). Bench-to-bedside review: functional relationships between coagulation and the innate immune response and their respective roles in the pathogenesis of sepsis. *Critical Care*, 7(1):23.

Panneer Selvam, A. and Prasad, S. (2017a). Companion and point-of-care sensor system for rapid multiplexed detection of a panel of infectious disease markers. *SLAS TECHNOLOGY: Translating Life Sciences Innovation*, 22(3):338–347.

Panneer Selvam, A. and Prasad, S. (2017b). Companion and point-of-care sensor system for rapid multiplexed detection of a panel of infectious disease markers. *SLAS TECHNOLOGY: Translating Life Sciences Innovation*, 22(3):338–347.

Park, H.-J., Kim, S. K., Park, K., Yi, S. Y., Chung, J. W., Chung, B. H., and Kim, M. (2010). Monitoring of c-reactive protein using ion sensitive field effect transistor biosensor. *Sensor Letters*, 8(2):233–237.

Peck-Palmer, O. M., Unsinger, J., Chang, K. C., Davis, C. G., McDunn, J. E., and Hotchkiss, R. S. (2008). Deletion of myd88 markedly attenuates sepsis-induced t and b lymphocyte apoptosis but worsens survival. *Journal of leukocyte biology*, 83(4):1009–1018.

Pierrakos, C. and Vincent, J.-L. (2010). Sepsis biomarkers: a review. *Critical care*, 14(1):R15.

Polat, G., Ugan, R. A., Cadirci, E., and Halici, Z. (2017). Sepsis and septic shock: current treatment strategies and new approaches. *The Eurasian journal of medicine*, 49(1):53.

Ranjan, R., Esimbekova, E. N., and Kratasyuk, V. A. (2017). Rapid biosensing tools for cancer biomarkers. *Biosensors and Bioelectronics*, 87:918–930.

Rascher, D., Geerlof, A., Kremmer, E., Kramer, P., Schmid, M., Hartmann, A., and Rieger, M. (2014). Total internal reflection (tirf)-based quantification of procalcitonin for sepsis diagnosis–a point-of-care testing application. *Biosensors and Bioelectronics*, 59:251–258.

Reddy, B., Hassan, U., Seymour, C., Angus, D., Isbell, T., White, K., Weir, W., Yeh, L., Vincent, A., and Bashir, R. (2018). Point-of-care sensors for the management of sepsis. *Nature biomedical engineering*, 2(9):640.

Reinhart, K., Bauer, M., Riedemann, N. C., and Hartog, C. S. (2012). New approaches to sepsis: molecular diagnostics and biomarkers. *Clinical microbiology reviews*, 25(4):609–634.

Rello, J., Valenzuela-Sanchez, F., Ruiz-Rodriguez, M., and Moyano, S. (2017). Sepsis: a review of advances in management. *Advances in therapy*, 34(11):2393–2411.

Riedemann, N. C., Guo, R.-F., Laudes, I. J., Keller, K., Sarma, V. J., Padgaonkar, V., and WARD, P. A. (2002). C5a receptor and thymocyte apoptosis in sepsis. *The FASEB Journal*, 16(8):887–888.

Roger, P.-M., Hyvernat, H., Breittmayer, J.-P., Dunais, B., Dellamonica, J., Bernardin, G., and Bernard, A. (2009). Enhanced t-cell apoptosis in human septic shock is associated with alteration of the costimulatory pathway. *European journal of clinical microbiology & infectious diseases*, 28(6):575–584.

Rowland, T., Hilliard, H., and Barlow, G. (2015). Procalcitonin: potential role in diagnosis and management of sepsis. In *Advances in clinical chemistry*, volume 68, pages 71–86. Elsevier.

Rudd, K. E., Kissoon, N., Limmathurotsakul, D., Bory, S., Mutahunga, B., Seymour, C. W., Angus, D. C., and West, T. E. (2018). The global burden of sepsis: barriers and potential solutions. *Critical Care*, 22(1):232.

Russell, C., Ward, A. C., Vezza, V., Hoskisson, P., Alcorn, D., Steenson, D. P., and Corrigan, D. K. (2019a). Development of a needle shaped microelectrode for electrochemical detection of the sepsis biomarker interleukin-6 (il-6) in real time. *Biosensors and Bioelectronics*, 126:806–814.

Russell, S. M., Alba-Patiño, A., Borges, M., and de la Rica, R. (2019b). Multifunctional motion-to-color janus transducers for the rapid detection of sepsis biomarkers in whole blood. *Biosensors and Bioelectronics*, 140:111346.

Saqib, M., Sha, Y., and Wang, M. D. (2018). Early prediction of sepsis in emr records using traditional ml techniques and deep learning lstm networks. In *2018 40th Annual International Conference of the IEEE Engineering in Medicine and Biology Society (EMBC)*, pages 4038–4041.

Sautter, R., Bills, A., Lang, D., Ruschell, G., Heiter, B., and Bourbeau, P. (2006). Effects of delayed-entry conditions on the recovery and detection of microorganisms from bact/alert and bactec blood culture bottles. *Journal of clinical microbiology*, 44(4):1245–1249.

Savelkoel, J., Claushuis, T. A., van Engelen, T. S., Scheres, L. J., and Wiersinga, W. J. (2018). Global impact of world sepsis day on digital awareness of sepsis: an evaluation using google trends. *Critical Care*, 22(1):61.

Schouten, M., Wiersinga, W. J., Levi, M., and Van Der Poll, T. (2008). Inflammation, endothelium, and coagulation in sepsis. *Journal of leukocyte biology*, 83(3):536–545.

Schwetz, I., Hinrichs, G., Reisinger, E., Krejs, G., Olschewski, H., and Krause, R. (2007). Delayed processing of blood samples influences time to positivity of blood cultures and results of gram stain-acridine orange leukocyte cytospin test. *Journal of clinical microbiology*, 45(8):2691–2694.

Seshadri, P., Manoli, K., Marra, N. S., Anthes, U., Wierzchowiec, P., Bonrad, K., Franco, C. D., and Torsi, L. (2018a). Low-picomolar, label-free procalcitonin analytical detection with an electrolyte-gated organic field-effect transistor based electronic immunosensor. *Biosens. Bioelectron.*, 104:113–119.

Seshadri, P., Manoli, K., Schneiderhan-Marra, N., Anthes, U., Wierzchowiec, P., Bonrad, K., Di Franco, C., and Torsi, L. (2018b). Low-picomolar, label-free procalcitonin analytical detection with an electrolyte-gated organic field-effect transistor based electronic immunosensor. *Biosensors and Bioelectronics*, 104:113–119.

Shen, W. J., Zhuo, Y., Chai, Y. Q., Yang, Z. H., Han, J., and Yuan, R. (2015). Enzyme-free electrochemical immunosensor based on host−guest nanonets catalyzing amplification for procalcitonin detection. *ACS Appl. Mater. Interfaces*, 7:4127–4134.

Singer, M., Deutschman, C. S., Seymour, C. W., Shankar-Hari, M., Annane, D., Bauer, M., Bellomo, R., Bernard, G. R., Chiche, J.-D., Coopersmith, C. M., et al. (2016). The third international consensus definitions for sepsis and septic shock (sepsis-3). *Jama*, 315(8):801–810.

Sohn, Y.-S. and Kim, Y. (2008). Field-effect-transistor type c-reactive protein sensor using cysteine-tagged protein g. *Electronics Letters*, 44(16):955–956.

Sproston, N. R. and Ashworth, J. J. (2018). Role of c-reactive protein at sites of inflammation and infection. *Front. Immunol.*, 9:754.

Strickland, E. (2018). Hospitals fight sepsis with ai: By predicting cases, sepsis watch could save lives - [news]. *IEEE Spectrum*, 55(11):9–10.

Takeuchi, O. and Akira, S. (2010). Pattern recognition receptors and inflammation. *Cell*, 140(6):805–820.

Terracciano, M., Rea, I., Borbone, N., Moretta, R., Oliviero, G., Piccialli, G., and De Stefano, L. (2019). Porous silicon-based aptasensors: The next generation of label-free devices for health monitoring. *Molecules*, 24(12):2216.

Thompson, K., Venkatesh, B., and Finfer, S. (2019). Sepsis and septic shock: current approaches to management. *Internal medicine journal*, 49(2):160–170.

Torsi, L., Magliulo, M., Manoli, K., and Palazzo, G. (2013). Organic field-effect transistor sensors: a tutorial review. *Chem. Soc. Rev.*, 42:8612–8628.

Trung, N. T., Thau, N. S., Bang, M. H., et al. (2019). Pcr-based sepsis@ quick test is superior in comparison with blood culture for identification of sepsis-causative pathogens. *Scientific reports*, 9(1):1–7.

van Dillen, J., Zwart, J., Schutte, J., and van Roosmalen, J. (2010). Maternal sepsis: epidemiology, etiology and outcome. *Current opinion in infectious diseases*, 23(3):249–254.

Vance, S. A. and Sandros, M. G. (2014). Zeptomole detection of c-reactive protein in serum by a nanoparticle amplified surface plasmon resonance imaging aptasensor. *Scientific reports*, 4:5129.

Vashist, S. K., Saraswat, M., and Holthšfer, H. (2012). Comparative study of the developed chemiluminescent, elisa and spr immunoassay formats for the highly sensitive detection of human albumin. *Procedia Chemistry*, 6:184–193.

Vincent, J.-L. and Beumier, M. (2013). Diagnostic and prognostic markers in sepsis. *Expert review of anti-infective therapy*, 11(3):265–275.

Voller, A., Bartlett, A., and Bidwell, D. (1978). Enzyme immunoassays with special reference to elisa techniques. *Journal of clinical pathology*, 31(6):507–520.

Walsh, J. D., Hyman, J. M., Borzhemskaya, L., Bowen, A., McKellar, C., Ullery, M., Mathias, E., Ronsick, C., Link, J., Wilson, M., et al. (2013). Rapid intrinsic fluorescence method for direct identification of pathogens in blood cultures. *MBio*, 4(6):e00865–13.

Wang, R. Z., Sun, C. H., Schroeder, P. H., Ameko, M. K., Moore, C. C., and Barnes, L. E. (2018a). Predictive models of sepsis in adult icu patients. In *2018 IEEE International Conference on Healthcare Informatics (ICHI)*, pages 390–391. IEEE.

Wang, W., Mai, Z., Chen, Y., Wang, J., Li, L., Su, Q., Li, X., and Hong, X. (2017). A label-free fiber optic spr biosensor for specific detection of c-reactive protein. *Sci. Rep.*, 7:16904.

Wang, X., Wang, Z., Weng, J., Wen, C., Chen, H., and Wang, X. (2018b). A new effective machine learning framework for sepsis diagnosis. *IEEE Access*, 6:48300–48310.

Ward, P. A. and Bosmann, M. (2012). A historical perspective on sepsis. *The American journal of pathology*, 181(1):2–7.

Wayne, P. (2007). Principles and procedures for blood cultures; approved guideline, clsi document m47-a. *Clinical and Laboratory Standards Institute (CLSI)*.

Wentowski, C., Mewada, N., and Nielsen, N. D. (2019). Sepsis in 2018: a review. *Anaesthesia & Intensive Care Medicine*, 20(1):6–13.

Wu, D. and Voldman, J. (2019). An integrated and automated electronic system for point-of-care protein testing. In *2019 41st Annual International Conference of the IEEE Engineering in Medicine and Biology Society (EMBC)*, pages 1571–1574. IEEE.

Yang, Z.-H., Ren, S., Zhuo, Y., Yuan, R., and Chai, Y.-Q. (2017). Cu/mn double-doped ceo2 nanocomposites as signal tags and signal amplifiers for sensitive electrochemical detection of procalcitonin. *Analytical chemistry*, 89(24):13349–13356.

Zhang, J. M. and J., A. (2007). Cytokines, inflammation and pain. *Int. Anesthesiol. Clin.*, 45(2):27–37.

Zhang, K., Liu, G., and Goldys, E. M. (2018a). Robust immunosensing system based on biotin-streptavidin coupling for spatially localized femtogram ml- 1 level detection of interleukin-6. *Biosensors and Bioelectronics*, 102:80–86.

Zhang, Y., Li, J., Lou, J., Zhou, Y., Bo, L., Zhu, J., Zhu, K., Wan, X., Cai, Z., and Deng, X. (2011). Upregulation of programmed death-1 on t cells and programmed death ligand-1 on monocytes in septic shock patients. *Critical care*, 15(1):R70.

Zhang, Y., Li, W., Zhou, Y., Johnson, A., Venable, A., Hassan, A., Griswold, J., and Pappas, D. (2018b). Detection of sepsis in patient blood samples using cd64 expression in a microfluidic cell separation device. *Analyst*, 143(1):241–249.

Zubiate, P., Zamarreno, C. R., Sanchez, P., Matias, I. R., and Arregui, F. J. (2017). High sensitive and selective c-reactive protein detection by means of lossy mode resonance based optical fiber devices. *Biosens. Bioelectron.*, 93:176–181.

CHAPTER 3. PLASMONIC POINT-OF-CARE DEVICE FOR SEPSIS BIO-MARKER DETECTION

Souvik Kundu[1], Shawana Tabassum[1], and Ratnesh Kumar[1]

[1] Department of Electrical and Computer Engineering, Iowa State University, Ames, IA, 50010, USA

Modified from a manuscript published in *IEEE Sensors Journal*

3.1 Abstract

The need for point-of-care (POC) devices for detecting the onset of sepsis has become critical since sepsis is one of the most prevalent causes of deaths worldwide in non-coronary intensive care units at the hospitals. Every one hour delay in exercising proper medication can lead to an exponential rise in mortality. Motivated by this, we propose a POC device for sepsis biomarker detection, which will complement traditional blood culture-based techniques for easy and quicker diagnosis and monitoring of sepsis state. The working principle of the device is based on amalgamation of surface plasmon resonance (SPR) technology with microfluidics. The sensing chip consists of a gold and graphene oxide coated patterned array of periodic nanoposts to detect target biomarker molecules in a limited sample volume. The nanoposts are functionalized with specific receptor molecules that serve as a nanostructured plasmonic crystal for SPR-based bio-sensing via the excitation of surface plasmon polaritons. The sensitivity of the device to one of the known sepsis biomarkers, Pro-calcitonin (PCT), was found to be 0.0125 a.u./ pg ml^{-1} in the range of 0 pg/ml to 10^2 pg/ml and 0.0395 a.u./ pg ml^{-1} in the range of 10^3 pg/ml to 10^5 pg/ml, and a LOD of 6.32 pg/ml. The sensor chip provides an opportunity to dynamically measure antigen-antibody bindings and the soft-lithography based sensor manufacturing technology provides high reproducibility of the sensor response to PCT molecules even at a

picomolar level. The microfluidics-based platform provides potential for future integration with other microfluidic devices viz. plasma separator for separating the PCT-sized molecules to enable blood sample measurements.

3.2 Introduction

There are more than 31.5 million people who suffer from sepsis every year around the world. Among them, 19.4 million develop severe sepsis and about 5.3 million people die Fleischmann et al. (2016). Further, it has been estimated that there are about 3 million sepsis cases in newborn babies and 1.2 million in children per year globally, with mortality rates between 11% and 19% Fleischmann-Struzek et al. (2018). As stated by Daniels (2011), the cause of these grim numbers is due to the lack of an prompt, accurate and point-of-care (POC) sepsis diagnosis method.

A concise discussion on the sepsis pathogenesis, impact, diagnosis and a review of state of the art diagnostic techniques and its limitations can be found in Kundu et al. (2020). Traditional sepsis testing involves blood, bronchial fluid, cerebrospinal fluid (CSF) and urine culture. Due to typical prolonged blood culture turnaround time of around 24-72 hrs (from specimen collection to actionable test results), septic patients may progress toward septic shock along with multi organ dysfunction (MoD) Beekmann et al. (2003). Each hour of delay in exercising an appropriate anti-microbial medicine to the patients results in 7.6% decline in the survival rate of a patient Linnér et al. (2013). Also, statistically the diagnostic accuracy of the traditional blood culture based methodologies improve with higher volume of extracted patient blood Bouza et al. (2007). However, for critical care patients, extraction of sufficient amount of blood for testing is often not possible which is another challenge for conventional blood-culture based diagnosis of sepsis. Measurements of leukocytes or C-reactive proteins (CRP) are also conducted to identify an infection. However, elevated leukocytes or CRP may also correspond to clinical conditions other than sepsis Angus and Van der Poll (2013). Thus, there is an urgent need for rapid and bedside monitoring of sepsis with limited blood volume.

Several label-free detection techniques have been employed for sepsis biomarker detection ranging from electrochemical Russell et al. (2019), opticalDey et al. (2018), field effect transistor-based Macchia et al. (2019), acousticOhlsson et al. (2018), and microfluidic-based Ellett et al. (2018). Although electrochemical sensors provides higher sensitivity, but generally these sensors provide little information on binding kinetics of protein-protein interactions on the sensor surface Im et al. (2012). This limitation can be overcome by our microfluidic plasmonic sensor, as proposed in this work. It allows us to quantify the protein–protein binding affinity by studying binding kinetics represented by the sensorgram, which helps in designing and implementing a better target antibody for a given antigenJoe et al. (2007). Among various biomarkers including CRP and interlukin-6, procalcitonin (PCT) is most commonly used biomarker for identifying bacterial sepsis Reinhart et al. (2012). The concentration of PCT in normal human being is less than 10pg/ml and the concentration can rise from 10 to 10,000 pg/ml during sepsis condition. Therefore, we have used our microfluidics plasmonic biochip for detecting PCT in a buffer solution in the above concentration range, and have demonstrated the application of our sensor for measuring the sepsis biomarker PCT.

Point-of-Care solution to biomarker detection/diagnosis in blood samples can be broken up into two steps: Extraction of plasma from blood (which removes the larger molecules such as red blood cells, white blood cells and platelets from blood), and detection/diagnosis of the analyte biomarkers in plasma. There already exist several POC approaches to extract plasma from blood Dixon et al. (2020); Yang et al. (2006), and here we provide POC approach for detecting/diagnosis sepsis biomarker in blood plasma and spiked buffer analyte solution (a common practice as for example also in the works of Neugebauer et al. (2014); Shenoy (2019); Fabri-Faja et al. (2019)). It will be possible to integrate the plasma extraction step with our proposed biochip, and the current work focuses on providing a proof-of-concept for POC sepsis biomarker PCT detection. Accordingly, in this paper we have provided:

- Detailed fabrication process for the microfluidic plasmonic biosenosr chip;

- Analysis of mode of surface plasmon resonance of the sensor, and estimation of sensitivity w.r.t. the changes in surrounding refractive indices;
- SPR measurements with PCT protein at different flow rates and demonstration of the real-time monitoring of the kinetics of protein-protein binding at the sensor surface;
- Exposition of the specificity of our sensor to PCT, with negligible rate of change of sensor response to non-specific proteins in human plasma;
- Comparison of performance of the proposed sensor w.r.t. the sensors reported in literature for the PCT detection.

3.3 Plasmonic Sensor Working Principle

An electromagnetic wave impinging on a metal-dielectric interface gives rise to collective oscillations of free electrons, which leads to the formation of surface waves called surface plasmon polaritons (SPP) Ghaemi et al. (1998). However, electromagnetic radiation by itself can not attain SPP resonance due to absence of momentum match between the incident radiation and that of surface plasmons (SP). For a resonance to occur, the component of the wave vector of the incident radiation along the interface should equal the wave vector of the SP. Thus in order to attain SPP resonance several configurations have been employed Raether (1988) viz. Kretschmann configuration, Otto configuration, waveguide SPR, and grating coupling.

3.3.1 Grating Coupled Surface Plasmon Resonance

In our work, we have employed grating coupling configuration for the momentum matching using a 2-D array of nanoposts having diameter, pitch, and depth of 250 nm, 500 nm, and 210 nm respectively.

Fig. 3.1 depicts the generation of SPP wave vector, $\vec{k}_{spp}$, by the in-plane wave vector of the incident radiation, $\vec{k}_p$, and the Grating momentum wave vector, $\vec{G}_{m,n}$, as in (3.1):

$$\vec{k}_{spp} = \vec{k}_p + \vec{G}_{m,n}. \tag{3.1}$$

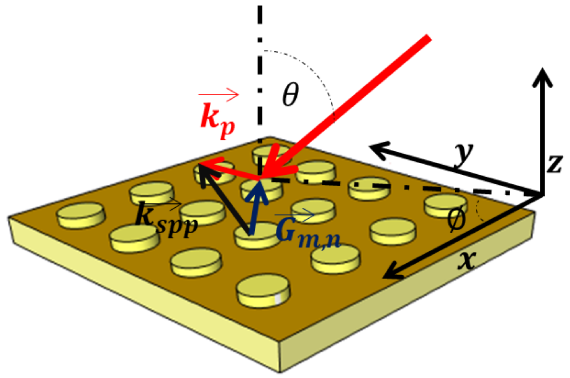

Figure 3.1 Nano-post induced SPP excitation: Schematic illustration of the nanopost array on which incident light with in-plane wavevector $\vec{k}_p$ couples to the Grating momentum vector $\vec{G}_{m,n}$ supported by the structure resulting in the (m,n) Bloch-SPP mode being excited and propagating in the direction of $\vec{k}_{spp}$ Sarid and Challener (2010).

The grating wave-vector is defined by (3.2), where Λ denotes the pitch of the square lattice of the nanopost array (lattice constant), and the order of SPP is given by (m,n).

$$\vec{G}_{m,n} = m\frac{2\pi}{\Lambda}\hat{x} + n\frac{2\pi}{\Lambda}\hat{y}. \tag{3.2}$$

The in-plane wave vector of incident radiation is given by (3.3), where θ is the angle of incidence and ϕ is the azimuthal angle, illustrated in Fig. 3.1:

$$\vec{k}_p = m\frac{2\pi}{\lambda}\sin(\theta)\cos(\phi)\hat{x} + n\frac{2\pi}{\lambda}\sin(\theta)\sin(\phi)\hat{y}. \tag{3.3}$$

$\vec{k}_{spp}$ is the wave vector of the generated surface wave that propagates along the metal-dielectric interface. $\vec{k}_{spp}$ is a function of dielectric permittivity of both metal (ϵ_m) and dielectric (ϵ_d) and is given by

$$\vec{k}_{spp} = \frac{2\pi}{\lambda}\sqrt{\frac{\epsilon_d\epsilon_m}{\epsilon_d+\epsilon_m}}.$$

Combining (3.1)-(3.3), at resonant wavelength, $\lambda = \lambda_{spp_{m,n}}$, corresponding to mode (m,n) of SPP, the condition in (3.4) must be satisfied:

$$\frac{2\pi}{\lambda}\sqrt{\frac{\epsilon_d\epsilon_m}{\epsilon_d+\epsilon_m}} = |m\frac{2\pi}{\lambda}\sin(\theta)\cos(\phi)\hat{x} + n\frac{2\pi}{\lambda}\sin(\theta)\sin(\phi)\hat{y} + m\frac{2\pi}{\Lambda}\hat{x} + n\frac{2\pi}{\Lambda}\hat{y}| \tag{3.4}$$

(3.4) can be rewritten by evaluating the magnitude of the right hand side to find the resonant wavelength as given by (3.5):

$$\frac{2\pi}{\lambda}\sqrt{\frac{\epsilon_d\epsilon_m}{\epsilon_d+\epsilon_m}} = 2\pi\sqrt{\left(\frac{m}{\Lambda}+\frac{\sin(\theta)\cos(\phi)}{\lambda}\right)^2+\left(\frac{n}{\Lambda}+\frac{\sin(\theta)\sin(\phi)}{\lambda}\right)^2}. \tag{3.5}$$

For our experimental set up, the incident radiation was taken to be normal to the x-y plane, hence by setting $\theta = 0^\circ$ and squaring both sides of (3.5), we obtain the simplified form (3.6) for the resonant wavelength corresponding to our sensor structure's SPP excitation mode.

$$\lambda_{spp_{m,n}} = \frac{\Lambda}{\sqrt{m^2+n^2}}\sqrt{\frac{\epsilon_d\epsilon_m}{\epsilon_d+\epsilon_m}}. \tag{3.6}$$

3.3.2 Working Principle of the Proposed Sensor

Any changes in the dielectric permitivity that occurs in the surrounding medium, results in a change in the surface plasmon coupling condition due to a change in permittivity at the metal-dielectric interface. The surface plasmon waves that are excited at the metal-dielectric interface, propagate along the surface, and respond to changes in surrounding electrical permitivity caused by capture of analyte on the surface (in our case Procalcitonin (PCT), a sepsis biomarker). The changes in permittivity can be detected in three different ways: (a) measuring changes in coupling angle at a fixed resonant wavelength, (b) measuring changes in coupling λ at a fixed angle, or (c) measuring change in intensity of transmitted/reflected light at fixed wavelength and angle. In this work, we used (c), i.e., measured shifts in the reflected light intensity at the resonance wavelength of our sensor structure and at normal incidence.

3.4 Sensor Fabrication and Functionalization

Fig. 3.2 depicts the fabricated portable, plasmonic biochip at the POC for quantification of PCT protein. The buffer solution spiked with the PCT protein is injected through the inlet and the solution reaches the sensor surface through a microfluidic channel. The sensor surface is a grating structure of pitch 500 nm containing nanoposts (height 210 nm, diameter 250 nm) coated with gold, graphene oxide (GO), and functionalized with anti-PCT, resulting in SPR resonance in

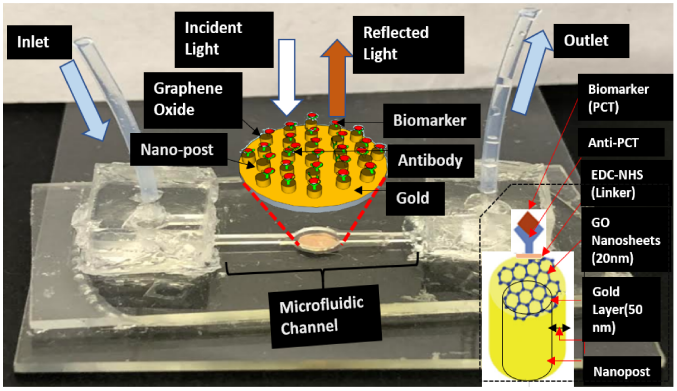

Figure 3.2 Fabricated Sepsis Microfluidic Biochip

visible range as desired (at 637 nm). The nanoposts are first coated with gold of thickness 50 nm. Next, in order to functionalize the gold nanopost sensor surface with anti-PCT protein, graphene oxide is deposited. For this the gold nanopost array was drop coated with a 20 nm thick layer of GO nanosheets. Graphene oxide consists of covalently attached oxygen-containing functional groups such as hydroxyl, epoxy, carbonyl and carboxyl groups that allow binding with anti-PCT. The periodic GO-Au nanopost array was next functionalized with anti-PCT molecules via EDC-NHS coupling chemistry Ali et al. (2017). A schematic diagram of the nanopost along with all layers is illustrated in the inset of Fig. 3.2. Light is shone on the grated sensor surface from a white light source and the reflected light is detected by a spectrometer. It is worth mentioning here that the thickness of the gold layer was chosen to maximize the quality factor Q of the resonance. (The resonant wavelength itself is a function of the pitch of the nanoposts and permittivities of gold vs. nanoposts, but is unaffected by its depth.) The quality factor of resonance is defined as the ratio of the stored energy to the energy dissipated. At an optimal thickness, the energy lost by the collision among the oscillatory plasmons is minimized, thereby maximizing the overall quality factor. This is confirmed in Uddin et al. (2017) where the sharpness of resonance is studied as the metal (Au) layer thickness is varied. The lowest value of the the reflection minima is achieved at around 50 nm gold layer thickness. Accordingly, we have chosen the gold layer of 50nm thickness. The reflected light carries information on the binding kinetics of biomolecular interactions at the surface of the biosensor. A continuous flow rate for a

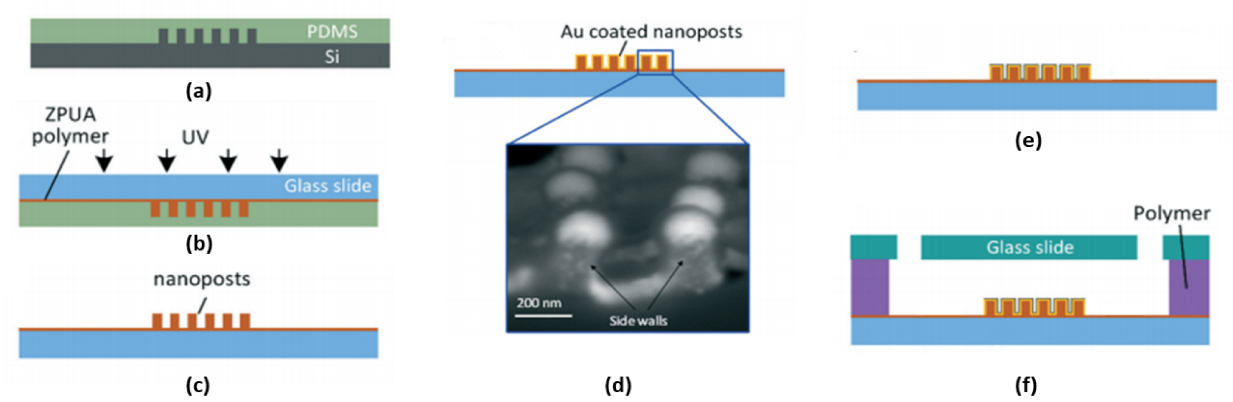

Figure 3.3 Fabrication steps: (a)–(f) Step-wise representation for the fabrication of sepsis biosensor. The SEM image for the gold coating on the sidewalls of nanoposts is given by inset of (d)

given amount of time is maintained using a syringe pump and the remaining protein solution is collected at the outlet via a vial.

3.4.1 Sensor Fabrication

A soft lithography based replica nanomolding technique is employed to fabricate the sensor. In order to form the grating structure, an array of polymeric nanoposts was created followed by graphene oxide deposition and immobilization of anti-PCT molecules, followed by the formation of microfluidic channel, inlet, and outlet ports. Fig. 3.3(a)-(e) illustrates the detailed fabrication steps.

First, a silicon (Si) master mold was fabricated using electron-beam lithography and reactive ion etching is done after that. Salinization was done for approximately twenty minutes with the help of (tridecafluoro-1,1,2,2-tetrahydrooctyl)-1-trichlorosilane. We employed a two-step process for polydimethylsiloxane (PDMS) mold preparation from the Si master mold. Firstly, we have mixed poly (7– 8% vinylmethyl-siloxane)-(dimethylsiloxane), (1,3,5,7-tetravinyl1,3,5,7-tetramethylcyclotetrasiloxane), platinum catalyst xylene and poly (25–30% methylhydro-siloxane)-(dimethylsiloxane) at a weight ratio of $3.4 : 0.1 : 0.05 : 1$ to prepare a hard-PDMS (h-PDMS) precursor solution. Next, mixture was degassed for about ten

minutes to remove air bubbles. After that, the hard-PDMS solution was spun-coated on the Si surface of master mold at 1000 rpm for 40 s. It was then subsequently cured for ten minutes at 70°C. Next, to make a soft-PDMS (s-PDMS) pre-polymer solution, Sylgard 184 monomer and it's curing agent were mixed at the weight ratio of 10 : 1 followed by degassing for about 30 min. Then the s-PDMS solution was poured over cured h-PDMS and the combination was cured for 2 hrs at 65°C as shown in Fig. 3.3(a). Finally, the cured PDMS mold was peeled off from the Si master mold and thus a complimentary nanohole structure was formed on the PDMS mold. The above two step process of mold preparation is significant because generally the pre-polymer solution of s-PDMS has a higher viscosity which makes it hard for the solution to enter the nanostructures fully at the surface of the Si mold. However, one can argue that if we increase the weight ratio of the monomer to curing agent, it can decrease the viscosity, but in that case the cured PDMS structure would be difficult to peel off from the Si mold without damage. The h-PDMS precursor solution is relatively less viscos than s-PDMS and therefore conforms well along with the nano-structured surface of the Si mold. Hence h-PDMS helps in better conformation and the s-PDMS facilitates easy peeling off the PDMS mold from the Si mold.

In order to transfer the nanostructures from the PDMS mold to a glass substrate, an ultra-violet (UV) curable ZPUA precursor solution procured from Gelest, Inc. was drop cast over the PDMS mold and then the PDMS mold was placed over a glass slide. For curing the ZPUA, the combination of glass and mould was exposed for 5 min to a UV light of intensity 3.3 mW cm^{-2} to form the periodic array of ZPUA nanoposts as shown in Fig. 3.3(b) and (c). Finally, a 5 nm thick titanium layer was deposited by e-beam evaporation to provide good adhesion to the continuing thickness build up of the 80 nm thick gold layer deposited next on the ZPUA nanoposts array, as illustrated in Fig. 3.3(d). Next the sample substrates were mounted on a rotating and tilting substrate holder for improving the sidewall gold deposition coverage on the nanoposts. This sidewall coverage of gold on the nanoposts was confirmed from the scanning electron microscopic (SEM) image (Fig. 3.3(d)).

An *in situ* liquid phase polymerization processDong et al. (2006) was performed for the integration of the SPR sensor inside a microfluidic channel, that is made of a photo-patternable polymerBeebe et al. (2000). In this step, to make an air cavity, 400 μm thick sticky polymer spacers were placed in between a 1 mm thick glass slide and the substrate with the nanoposts. On the glass slide two 1 mm diameter holes were drilled using milling machine with diamond drill bit of 1 mm diameter to form the inlet and outlet of the microfluidic channel. Next, a photo-patternable polymer solution was prepared by mixing isobornyl acrylate (IBA), crosslinker tetraethylene glycol dimethacrylate, and photoinitiator−2,2−dimethoxy−2−phenylacetophenone at a weight ratio of 31.66 : 1.66 : 1. The solution was flown into the air cavity by means of a pipette through one of the drilled holes. Next, to prevent the channel from polymerization, a photomask was positioned over the glass slide and subsequently the device was exposed for about 60s to a UV light of intensity 12 mW cm^{-2}. Finally unpolymerized polymer solution was removed by washing with ethanol for few minutes. The final microfluidic biochip formed is shown in Fig. 3.2 and the schematic is illustrated in Fig. 3.3(f).

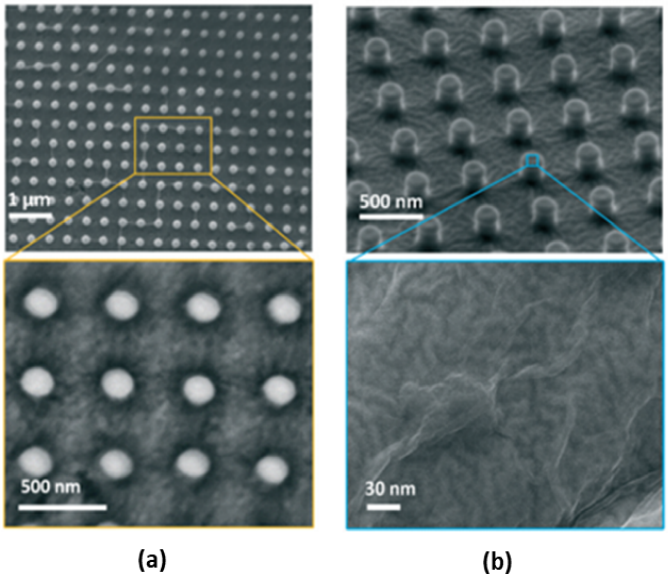

Figure 3.4 SEM Characterization (a) The Gold(Au) nanoposts array (b) Graphene Oxide(GO) coated Gold(Au) nanopost array

3.4.2 Sensor Functionalization

In order to immobilize the anti-PCT protein on the surface of the gold nanopost array, layers of graphene oxide (GO) and ligands were deposited by flowing them over the Au nanopost array. Colloidal solution of concentration 0.1 mg/mL was made using DI water followed by sonication to form single-layer graphene oxide nanosheets. 20 μL of the GO solution was introduced inside the microfluidic channel via the inlet. The GO solution is flown over the nanopost and kept at room temperature for 2 hr for drying. The GO nanosheets thus gets conforms to the shape of the nanoposts underneath it and this was confirmed from the SEM image of the fabricated GO/Au nanopost array illustrated in Fig. 3.4(b). At GO nanosheets, since there are ample functional groups viz. carboxylic and carbonyl etc., the GO layer serves as covalent binding site for the anti-PCT proteins. The covalent linkage was formed using EDC–NHS coupling chemistry Ali et al. (2017). To immobilize the ligands, a solution of 1 : 1 volume ratio containing 1 mg/mL anti-PCT and EDC–NHS (EDC : 0.2 M; NHS : 0.05 M) was made. The surface of GO–Au nanoposts was covered by introducing 200 μL of the solution containing anti-PCT, EDC and NHS. The set up was kept inside a humid chamber for 12 hr at $4°C$. During this time, EDC reacts covalently with carboxyl groups present at the GO nanosheets forming an intermediate O-acylisourea. In the meantime another intermediate amine reactive stable NHS ester is produced by NHS that facilitates the association between the primary amines of anti-PCT by forming C–N covalent bonds. In order to prevent non-specific bindings and block the sites devoid of anti-PCT over the sensor surface, 2 mg/mL of bovine serum albumin (BSA) solution was introduced inside the channel. Finally the sensor surface is washed with the phosphate-buffered saline solution (PBS) of pH = 7.4 Ali et al. (2018).

3.4.3 SPR Characterization and Simulation

Fig. 3.5(a) illustrates the simulation and experimental data comparison. After fabricating the nanopost array on the substrate, it was embedded in a microfluidic channel and the resonance was measured at 607 nm as shown by the green waveform. After coating a layer of graphene oxide

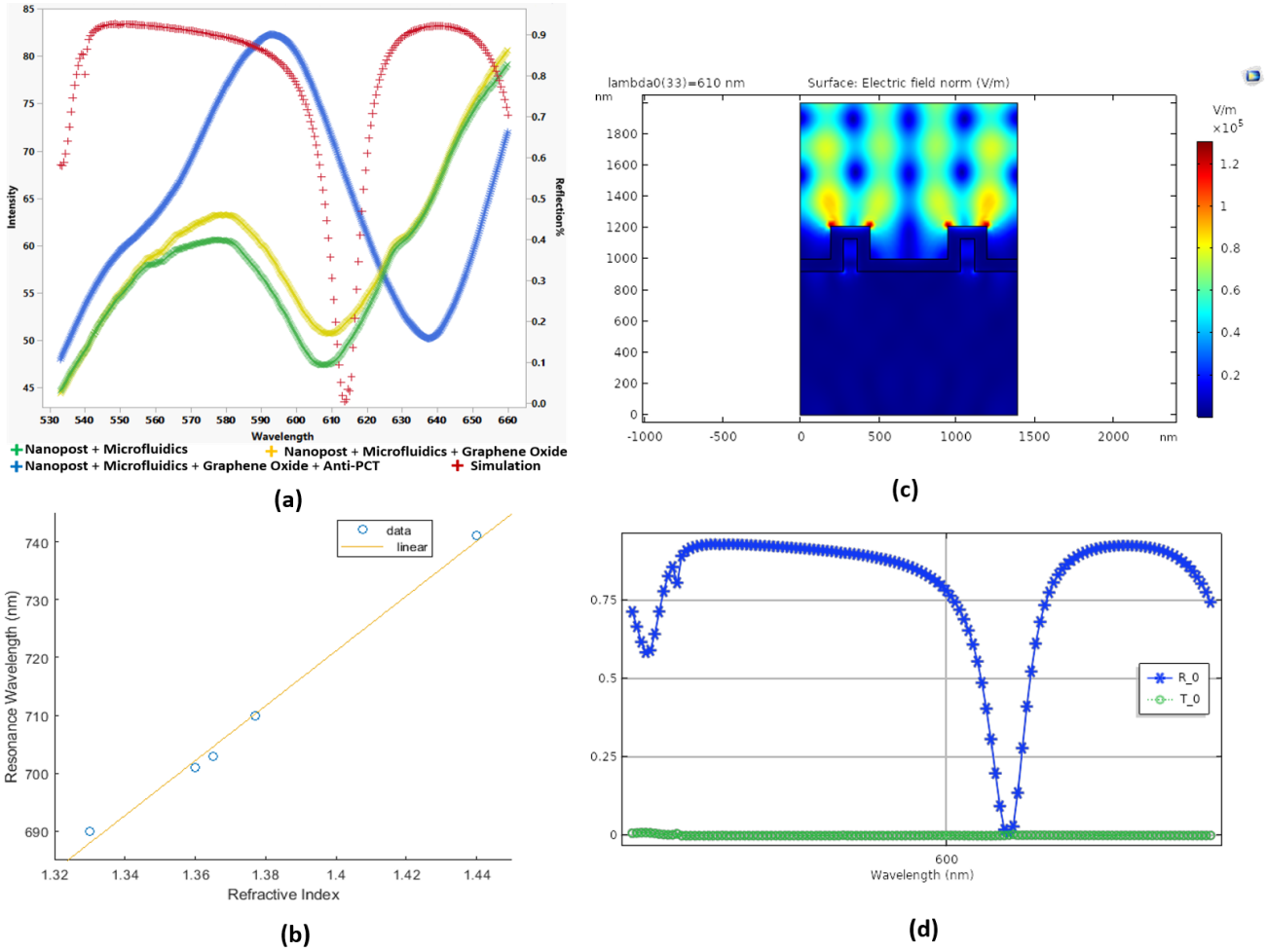

Figure 3.5 Sensor Characterization (a) The resonance wavelength for the nanopost array embedded in a microfluidic channel is obtained at 607 nm. Red shift of 1 nm in SPR responses is depicted when Au nanoposts are coated with graphene oxide. After immobilization of anti-PCT over GO-Au nanoposts, the resonance red shifts to 637 nm. COMSOL simulation, depicts that the resonance dip is obtained at a wavelength of 614 nm prior to GO/anti-PCT functionalization and at 635 nm after functionalization. (b) Bulk RI sensitivity of the sensor w.r.t. different refractive index solutions (c) FEM simulation of the nanopost array using COMSOL Multiphysics 5.5. applying periodic boundary conditions at the boundaries in parallel to the light propagation direction. (d) Reflection spectrum of the simulated structure.

on nanopost the resonant wavelength got shifted slightly by 1 nm (yellow waveform). Finally, after functionalizing the sensor with anti-PCT the resonance wavelength red shifted to 637 nm (shown by blue waveform).

COMSOL simulation, on the other hand, depicts that the resonance dip occurs at a wavelength of 614 nm prior to GO/anti-PCT functionalization, and at 635 nm after functionalization. The COMSOL-based FEM simulation was performed using the COMSOL Multiphysics 5.5. software as shown in Fig.3.5 (c) and (d). In this simulation, periodic boundary conditions were applied at the boundaries in parallel to the light propagation direction. The top and bottom of the computation regions were placed with two perfectly matched layers (PMLs) so that all the scattered electromagnetic waves from the nanopost arrays were absorbed at the PMLs. In addition, the refractive index of the PMLs was set at the same value as of the surrounding media to simulate an infinitely thick substrate. Note since our analyte solution contains PCT which is a protein, the refractive index of the analyte solution was selected as 1.33 for simulation purpose.

The bulk index sensitivity of the fabricated gold nanoposts array was measured to be 470 nm per RIU by flowing water, acetone, ethanol, isopropyl alcohol, and chloroform with refractive indices 1.33, 1.36, 1.365, 1.377, and 1.44 respectively over the sensor surface illustrated in Fig. 3.5(b).

The main characteristics of the sensor is its resonance wavelength and the associated quality factor. An imperfection in sensor would affect both parameters, but it is only the quality factor that affects the sensor performance. As long as the resonance wavelength falls within the visible spectrum, its exact value is immaterial to sensor performance. In this sense, the sensor performance is unaffected by the pitch or depth of the nanoposts as long as the resonant wavelength remains within the realm of visible spectrum. The only things that can affect the quality factor (and hence the sensor performance) is the gold layer thickness, as discussed earlier in section-3.4 which is optimized at thickness of 50 nm. A variation in that thickness will lead to lowering of sensor sensitivity. Further the thickness of functionalization Layers (GO, EDC-NHS,

Anti-PCT) affect the reflectance minimum Usman et al. (2019), that in turn affects the limit of detection of the sensor.

3.5 Experimental Setup and Sample Preparation

The experimental set up, illustrated in Fig. 3.6, consists of the fabricated microfluidic sensor chip (inset of Fig. 3.6), the optical source and detector module, a syringe pump to flow the sepsis biomarker (PCT), collecting vial at the output and a PC for real time data acquisition and analysis.

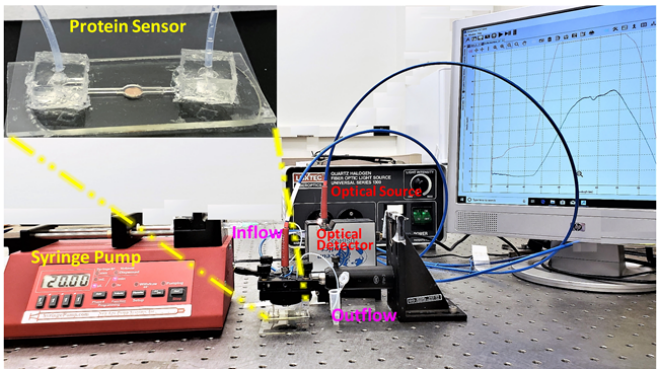

Figure 3.6 Experimental Setup

3.5.1 Instruments

For optical measurements, a white light source of power 150 watt quartz halogen lamp (Luxtec Fiber Optics, Plainsboro, NJ) was connected to a bifurcated optical fiber (BIF 400-VIS-NIR, Ocean Optics). A collimator (F220SMA-A from Thorlabs) was used to illuminate the nanoposts area inside the channel at normal incidence. The reflected light from the sensor surface was collected and measured by a UV/VIS spectrometer (USB-4000, Ocean Optics) attached to the other end of the bifurcated fiber. A syringe pump was used to inject the PCT solutions through the inlet of the microfluidic channel.

3.5.2 Chemicals and Sample Preparation

Materials used in sensor are ZUPA (Gelest, Inc.) nanoposts (pitch of 500 nm, height of 210 nm, and width of 250 nm), gold layer (50 nm thick), GO layer (20 nm thick), and anti-PCT layer (2 nm thick). Their refractive indices are: 1.470, 0.17689+ i3.47 (at 637nm), 1.9 , 1.33 respectively. Lyophilized form of Procalcitonin (PCT), prepared at a 10 mM sodium phosphate buffer and pH of 7.5, was procured from Millipore Sigma. The vial containing the PCT was centrifuged prior to use. Then it was reconstituted in sterile H_2O to a concentration of 0.1 mg/ml. This formed the stock solution which was further diluted to form different concentrations of PCT ranging from 10^5 pg/ml to 10 pg/ml. Deionized (DI) water (resistivity > 18.2 MΩ-cm), used in our experiments was produced using a purification system from Millipore, Billerica, MA, USA. N-Ethyl N-(3-dimethylaminopropyl carbodiimide) (EDC) and N-hydroxysuccinimide (NHS) were obtained from Sigma Aldrich, MO, USA.

3.6 Results and Discussions

3.6.1 Effect of flow rate on analyte capture

The specific capture of protein molecules depends not only on the sensor characteristics, but also on the flow rate. Increasing the flow rate reduces the protein capture time and imparts different amount of shear stress on the molecules, whereas decreasing the flow rate has reverse effect. Fig. 3.7(a) shows the effect of the flow rate (controlled by a syringe pump) on the specific absorption. When the flow rate was low, for instance 10 μL/min, the sensor surface required longer time (∼30 min) to saturate, resulting in a low protein capture rate, as was measured in terms of rate of change of intensity to be 0.04 min^{-1} (Fig. 3.7(a)). However, when the flow rate was raised to 20 μL/min, the sensor saturation took place within ∼10 min, giving rise to higher rate of change of sensor response of ∼0.15 min^{-1}. An even higher flow rate, namely, 40 μL/min, imparted higher shear stress on the molecules resulting in poor sensor response, and an even lower capture rate of ∼0.03 min^{-1}. Thus, a flow rate of 20 μL/min was found to be optimal and

selected for the sensing purpose. Fig. 3.7(b) shows the sensor response to non-specific absorption at this selected flow rate of 20 μL/min, when using BSA as the blocking agent.

We have evaluated the matrix effect and provided the sensor's response for 0, 10^4, and 10^6 pg/ml PCT prepared in buffer and plasma, as shown in Fig. 7(b). All three in-plasma readings are lower compared to the in-buffer readings. At 0 pg/ml, the sensor response is reduced by a factor of 2.33 for in-plasma w.r.t. in-buffer. There are reductions by factors of 2.64 and 2.4 at in 10^4 pg/ml and 10^6 pg/ml concentrations respectively. Thus the reduction in sensor's response in plasma is itself a concave curve (as can be seen in Fig. 7(b)), and this also gets addressed during calibration.

Lyophilized plasma sample prepared from pooled human blood was obtained from Sigma Aldrich (USA). No traces of PCT were found in the plasma as confirmed using the Synapt G2-Si H-Class UPLC Mass Spectrometer from Waters. The plasma was diluted with 1xPBS (pH = 7.4) buffer to prepare two different concentrations, 10^4 and 10^6 pg/ml. Both the plasma concentrations resulted in much lower sensor response as compared to the response due to PCT, thus further justifying the selection of 20 μL/min for our experiments.

3.6.2 Transient Response and Sensor Calibration Curve

As can be seen in Fig. 3.8, a reflection dip was found at the resonance wavelength of ∼637 nm when the anti-PCT conjugated GO-Au nanoposts array was excited by the normal incident light. At this resonance wavelength of 637 nm the intensity measurements at various PCT concentrations were performed because the maximum intensity variation to the concentration change is realized at the resonance, justifying the design of an Au-coated nano-patterned sensor surface in the first place.

Fig. 8 depicts the reflection spectra of the SPR sensor for 5 different concentrations of PCT (10 pg/ml, 10^2 pg/ml, 10^3 pg/ml, 10^4 pg/ml, and 10^5 pg/ml) in the 1xPBS solution (pH = 7.4) in the visible region of the light spectrum from 630 nm to 645 nm. We specifically examine the five PCT concentrations around the resonant wavelength of 637 nm. As the PCT concentration

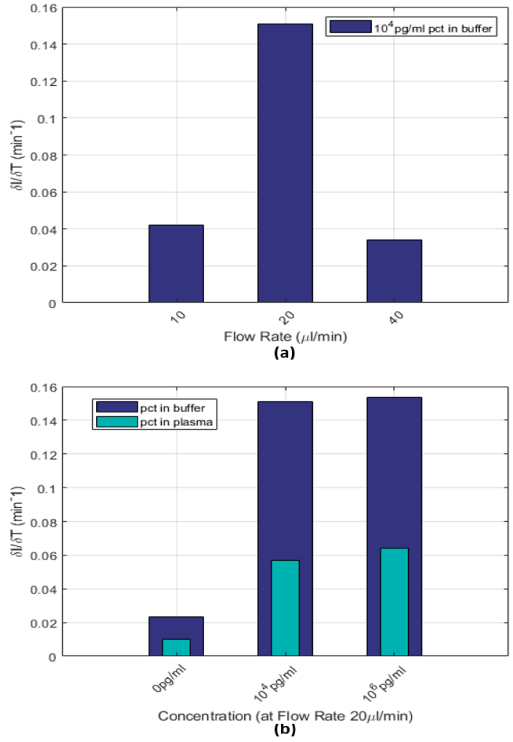

Figure 3.7 Effect of flow rate on analyte capture and non-specifics (a) The flow rate of 20 μl min^{-1} provides maximum rate of change of sensor response to the protein PCT. (b) At the flow rate of 20 μl min^{-1} sensor response to protein PCT in buffer versus in plasma. The observed reduction in response in plasma gets addressed through calibration.

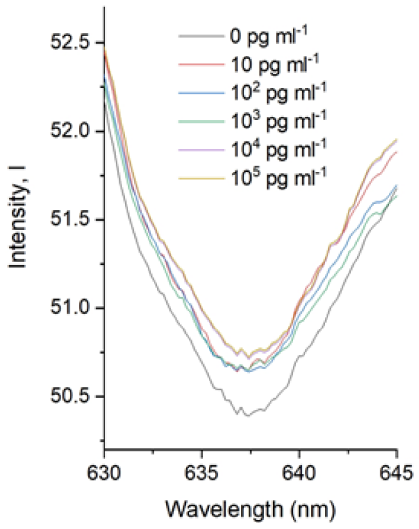

Figure 3.8 SPR Spectrum at six different PCT concentrations

increased from 0 pg/ml to 10 pg/ml, 10^2 pg/ml, 10^3 pg/ml, 10^4 pg/ml, and 10^5 pg/ml, the reflected light intensity increased by 0.23, 0.25, 0.26, 0.32 and 0.339, respectively. Each concentration of PCT solution was flown through the sensor surface for ∼2 min at a flow rate of 20 μL/min, and intensity spectra were recorded.

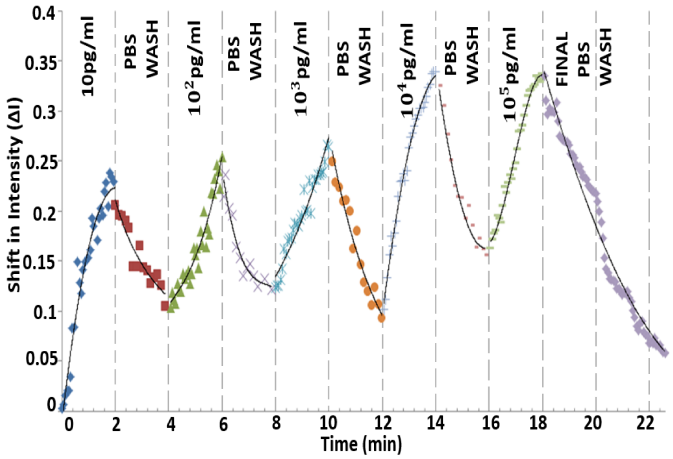

Figure 3.9 Transient response for PCT molecules detection at the concentrations of 0 pg/ml, 10 pg/ml, 10^2 pg/ml, 10^3 pg/ml, 10^4 pg/ml and 10^5 pg/ml, depicting the association and dissociation phases for binding (antigen-antibody) interactions in the spiked 1xPBS solution of pH 7.4.

Fig. 3.9 demonstrates the ability of the sensor to optically track the binding kinetics as the PCT concentration increased from 0 pg/ml to 10 pg/ml, 10^2 pg/ml, 10^3 pg/ml, 10^4 pg/ml, and 10^5 pg/ml in the PBS solution. For this, the sensor surface was initially covered by the PBS solution, and then, the 10 pg/ml PCT solution was flown through the microfluidic channel for 2 min. This association phase induced an intensity rise by 0.23. Next, in the dissociation phase, sensor surface was washed with the PBS to remove the unbound or loosely bound PCT proteins from the nanopost surface, that resulted in intensity drop by 0.13. The association and dissociation phases were further repeated for the remaining concentrations of PCT. For each association phase, PCT solution was flown at a rate of 20 μL/min through the sensor surface for ∼2 min, and without saturating the sensor surface. As the PCT concentration increased from 0 pg/ml to 10 pg/ml, 10^2 pg/ml, 10^3 pg/ml, 10^4 pg/ml, and 10^5 pg/ml, the reflection intensity increased by 0.24, 0.25, 0.26, 0.33 and 0.34, respectively, matching the results of Fig. 8 of the

Table 3.1 Comparison of optical techniques to detect sepsis biomarkers (PCT,CRP,sTREM-1)

Principle	Sample	Biomarker	Interface	Sensitivity	Limit of Detection	References
Plasmonic (nanoparticles)	Buffer	CRP	Microarray (Nano Particle enhanced gold nanohole arrays)	0.1 a.u./pg.ml^{-1}	27 pg/ml	Altug et. al. Belushkin et al. (2018)
Fiber Optic Evanescent Wave Excitation (FOEW)	Blood Plasma	PCT	Fiber optic nano-gold linked immunosorbent assay	0.024 a.u./pg.ml^{-1}	0.095 pg/ml	Chiang et. al. Chiang et al. (2020)
Surface Plasmon Resonance (SPR)	Buffer, Simulated Blood Plasma	PCT	Molecular imprinted polymer surface	1.78 a.u./pg.ml^{-1}	9900 pg/ml	Denizli et al. Sener et al. (2013)
Surface-Enhanced Raman Scattering (SERS)	Serum	PCT CRP sTREM 1	Au Coated MNPs	PCT (1.08 a.u./pM) CRP (4.62 a.u./pM) sTREM-1(1.69 a.u./pM)	0.028 pg/ml (PCT) 0.0073 pg/ml(CRP) 0.00046 pg/ml(sTREM1)	Nguyen et al. Nguyen et al. (2016)
Localized Surface Plasmon Resonance (LSPR)	Blood	PCT	Au Nanopillars	0.05 a.u./ pg.ml^{-1}	500 pg/ml	Deng et al. Sun et al. (2020)
Surface Plasmon Resonance (SPR)	Buffer	PCT	Au Nanopost Array, Microfluidic	0.0643 a.u./ pg.ml^{-1} at low conc. 0.0224 a.u./ pg.ml^{-1} at higher conc.	1.22 pg/ml	This work

static setting. Finally, Fig. 3.10 shows the calibration curve that we generated from the measurement plot of Fig. 3.9, demonstrating how we used the measured data to perform the calibration between the logarithmic PCT concentrations and the SPR response for the 6 measured concentrations. The response is shifted toward the higher detected intensity with increase in concentration, that results from the specific binding of the PCT molecules over 2 min window each, and increase in the refractive index at the sensor surface. The calibration curve fitted, as illustrated in Fig. 3.10, is chosen to be a montonically increasing power series (to guarantee 1-1 mapping and thereby allowing inversion for calibration, and one that also supports a higher reading for a higher concentration): $y = 0.207\ x^{0.2628} + 0.02296$, having $R^2 = 0.96$. At a lower concentration (0 pg/ml to 10^2 pg/ml), the sensitivity is around 0.0125 shift in intensity per pg/ml change in concentration of PCT, whereas at a higher concentration (10^3 pg/ml to 10^5 pg/ml) the sensitivity is around 0.0395 shift in intensity per pg/ml change in concentration of PCT. The Limit of Detection (LOD) is calculated from the fitted polynomial of the calibration curve as, $\frac{3\sigma}{\text{sensitivity}}(\text{at low conc.}) = 3 \times 0.02634/0.0125 = 6.32$ pg/ml. The coefficient of variation(CV%) values at concentrations 0 pg/ml, 10 pg/ml, 10^2 pg/ml, 10^3 pg/ml, 10^4 pg/ml, 10^5 pg/ml are $3.03\%, 8.6\%, 12\%, 7.6\%, 12.1\%, 2.9\%$ respectively.

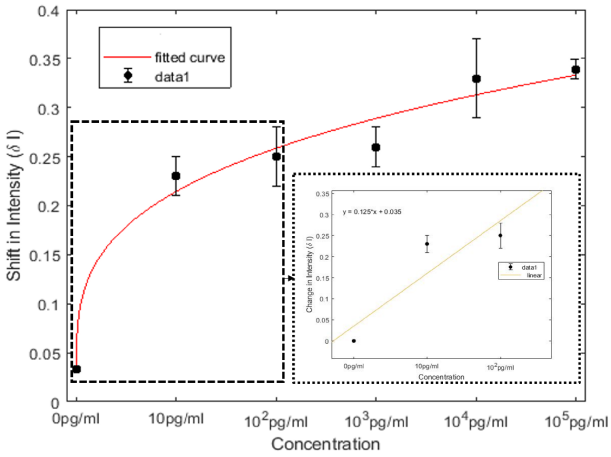

Figure 3.10 Calibration Curve: SPR intensity shifts as a function of PCT concentrations in spiked PBS buffer; generated from the measurement plot in Fig. 3.9

3.6.3 Performance Comparison

We compare the performance of our sensor with the other state of the art optical detection techniques for detecting sepsis biomarkers like PCT, CRP, sTREM-1, as enumerated in Table 3.1. The sensitivity column has been reported based on the calibration curves provided by the authors in their respective works. While are sensor sensitivity is lower, it is still adequate for measurement and calibration, and more importantly, it can measure over a much wider range, namely, 10 pg/ml to 10^5 pg/ml and that too in a POC setting. With regards to LOD, our fabricated POC sensor can detect up to 6.32 pg/ml of PCT concentration in buffer, which is one of the lowest LODs. While Chiang et al. (2020) and Nguyen et al. (2016) provide a slightly lower LOD, our sensor provides a portable and point-of-care solution, requiring little overhead of interfaced external devices or circuits for an integrated system. Further since our biosensor is microfluidics based, it can be easily integrated to render the measured protein in other samples, viz. blood, serum, etc.

The achieved sensitivity and LOD of our biosensor are thus remarkable for POC setting, and stand out in comparison to other reported techniques where biomarkers were also spiked in a buffered solution. This validates that our sensor serves as a good proof-of-principle plasmonic microfluidic biochip for POC sepsis biomarker detection.

3.7 Conclusion

To summarize the work, we have developed a novel microfluidic plasmonic device for real-time and label-free detection of a sepsis biomarker for POC application. The label-free detection of PCT reduces the detection time as compared to conventional labeled detection methodologies, and also portable biochip design makes it suitable for eventual POC application by integration with optics for excitation and measurement. Since our methodology involves detection of variations in intensity of the visible light reflected from the sensor surface, inexpensive source and detector can be integrated in a package to make the device portable and serve as a POC instrument for sepsis biomarker quantification. Future work will involve multiplexed detection of other sepsis biomarkers in a single chip, and design and fabrication of an integrated POC sensing system.

3.8 References

Ali, M. A., Mondal, K., Wang, Y., Jiang, H., Mahal, N. K., Castellano, M. J., Sharma, A., and Dong, L. (2017). In situ integration of graphene foam–titanium nitride based bio-scaffolds and microfluidic structures for soil nutrient sensors. *Lab on a Chip*, 17(2):274–285.

Ali, M. A., Tabassum, S., Wang, Q., Wang, Y., Kumar, R., and Dong, L. (2018). Integrated dual-modality microfluidic sensor for biomarker detection using lithographic plasmonic crystal. *Lab on a Chip*, 18(5):803–817.

Angus, D. C. and Van der Poll, T. (2013). Severe sepsis and septic shock. *N Engl J Med*, 369:840–851.

Beebe, D. J., Moore, J. S., Yu, Q., Liu, R. H., Kraft, M. L., Jo, B. H., and Devadoss, C. (2000). Microfluidic tectonics: a comprehensive construction platform for microfluidic systems. *Proceedings of the National Academy of Sciences*, 97(25):13488–13493.

Beekmann, S., Diekema, D., Chapin, K., and Doern, G. (2003). Effects of rapid detection of bloodstream infections on length of hospitalization and hospital charges. *Journal of clinical microbiology*, 41(7):3119–3125.

Belushkin, A., Yesilkoy, F., and Altug, H. (2018). Nanoparticle-enhanced plasmonic biosensor for digital biomarker detection in a microarray. *ACS nano*, 12(5):4453–4461.

Bouza, E., Sousa, D., Rodríguez-Créixems, M., Lechuz, J. G., and Munoz, P. (2007). Is the volume of blood cultured still a significant factor in the diagnosis of bloodstream infections? *Journal of clinical microbiology*, 45(9):2765–2769.

Chiang, C.-Y., Huang, T.-T., Wang, C.-H., Huang, C.-J., Tsai, T.-H., Yu, S.-N., Chen, Y.-T., Hong, S.-W., Hsu, C.-W., Chang, T.-C., et al. (2020). Fiber optic nanogold-linked immunosorbent assay for rapid detection of procalcitonin at femtomolar concentration level. *Biosensors and Bioelectronics*, 151:111871.

Daniels, R. (2011). Surviving the first hours in sepsis: getting the basics right (an intensivist's perspective). *Journal of Antimicrobial Chemotherapy*, 66(suppl_2):ii11–ii23.

Dey, P., Fabri-Faja, N., Calvo-Lozano, O., Terborg, R. A., Belushkin, A., Yesilkoy, F., Fabrega, A., Ruiz-Rodriguez, J. C., Ferrer, R., Gonzalez-Lopez, J. J., et al. (2018). Label-free bacteria quantification in blood plasma by a bioprinted microarray based interferometric point-of-care device. *ACS sensors*, 4(1):52–60.

Dixon, C., Lamanna, J., and Wheeler, A. R. (2020). Direct loading of blood for plasma separation and diagnostic assays on a digital microfluidic device. *Lab on a Chip*, 20(10):1845–1855.

Dong, L., Agarwal, A. K., Beebe, D. J., and Jiang, H. (2006). Adaptive liquid microlenses activated by stimuli-responsive hydrogels. *Nature*, 442(7102):551–554.

Ellett, F., Jorgensen, J., Marand, A. L., Liu, Y. M., Martinez, M. M., Sein, V., Butler, K. L., Lee, J., and Irimia, D. (2018). Diagnosis of sepsis from a drop of blood by measurement of spontaneous neutrophil motility in a microfluidic assay. *Nature Biomedical Engineering*, 2(4):207.

Fabri-Faja, N., Calvo-Lozano, O., Dey, P., Terborg, R. A., Estevez, M.-C., Belushkin, A., Yesilköy, F., Duempelmann, L., Altug, H., Pruneri, V., et al. (2019). Early sepsis diagnosis via protein and mirna biomarkers using a novel point-of-care photonic biosensor. *Analytica chimica acta*, 1077:232–242.

Fleischmann, C., Scherag, A., Adhikari, N. K., Hartog, C. S., Tsaganos, T., Schlattmann, P., Angus, D. C., and Reinhart, K. (2016). Assessment of global incidence and mortality of hospital-treated sepsis. current estimates and limitations. *American journal of respiratory and critical care medicine*, 193(3):259–272.

Fleischmann-Struzek, C., Goldfarb, D. M., Schlattmann, P., Schlapbach, L. J., Reinhart, K., and Kissoon, N. (2018). The global burden of paediatric and neonatal sepsis: a systematic review. *The Lancet Respiratory Medicine*, 6(3):223–230.

Ghaemi, H., Thio, T., Grupp, D. e. a., Ebbesen, T. W., and Lezec, H. (1998). Surface plasmons enhance optical transmission through subwavelength holes. *Physical review B*, 58(11):6779.

Im, H., Sutherland, J. N., Maynard, J. A., and Oh, S.-H. (2012). Nanohole-based surface plasmon resonance instruments with improved spectral resolution quantify a broad range of antibody-ligand binding kinetics. *Analytical chemistry*, 84(4):1941–1947.

Joe, S.-F., Hsieh, L.-Z., Chang, L.-B., Hsu, C.-M., and Wu, C.-M. (2007). Kinetic analysis of antibody–antigen interactions using phase-detection-based surface plasmon resonance sensor system. *Japanese journal of applied physics*, 46(5R):3114.

Kundu, S., Tabassum, S., and Kumar, R. (2020). A perspective on sepsis pathogenesis, biomarkers and diagnosis: A concise survey. *Medical Devices & Sensors*, 3(4):e10089.

Linnér, A., Sundén-Cullberg, J., Johansson, L., Hjelmqvist, H., Norrby-Teglund, A., and Treutiger, C. J. (2013). Short-and long-term mortality in severe sepsis/septic shock in a setting with low antibiotic resistance: a prospective observational study in a swedish university hospital. *Frontiers in public health*, 1:51.

Macchia, E., Manoli, K., Holzer, B., Di Franco, C., Picca, R. A., Cioffi, N., Scamarcio, G., Palazzo, G., and Torsi, L. (2019). Selective single-molecule analytical detection of c-reactive protein in saliva with an organic transistor. *Analytical and bioanalytical chemistry*, 411(19):4899–4908.

Neugebauer, U., Trenkmann, S., Bocklitz, T., Schmerler, D., Kiehntopf, M., and Popp, J. (2014). Fast differentiation of sirs and sepsis from blood plasma of icu patients using raman spectroscopy. *Journal of biophotonics*, 7(3-4):232–240.

Nguyen, A. H., Shin, Y., and Sim, S. J. (2016). Development of sers substrate using phage-based magnetic template for triplex assay in sepsis diagnosis. *Biosensors and Bioelectronics*, 85:522–528.

Ohlsson, P., Petersson, K., Augustsson, P., and Laurell, T. (2018). Acoustic impedance matched buffers enable separation of bacteria from blood cells at high cell concentrations. *Scientific reports*, 8(1):1–11.

Raether, H. (1988). Surface plasmons (ser. springer-verlag tracts in modern physics), vol. 111.

Reinhart, K., Bauer, M., Riedemann, N. C., and Hartog, C. S. (2012). New approaches to sepsis: molecular diagnostics and biomarkers. *Clinical microbiology reviews*, 25(4):609–634.

Russell, C., Ward, A. C., Vezza, V., Hoskisson, P., Alcorn, D., Steenson, D. P., and Corrigan, D. K. (2019). Development of a needle shaped microelectrode for electrochemical detection of the sepsis biomarker interleukin-6 (il-6) in real time. *Biosensors and Bioelectronics*, 126:806–814.

Sarid, D. and Challener, W. A. (2010). *Modern Introduction to Surface Plasmons: Theory, Mathematica Modeling, and Applications*. Cambridge University Press.

Sener, G., Ozgur, E., Rad, A. Y., Uzun, L., Say, R., and Denizli, A. (2013). Rapid real-time detection of procalcitonin using a microcontact imprinted surface plasmon resonance biosensor. *Analyst*, 138(21):6422–6428.

Shenoy, S. (2019). Exosomal microrna as a sepsis biomarker: Assessing different volumes of plasma for possible quantification of exosomal microrna.

Sun, L. L., Leo, Y. S., Zhou, X., Ng, W., Wong, T. I., and Deng, J. (2020). Localized surface plasmon resonance based point-of-care system for sepsis diagnosis. *Materials Science for Energy Technologies*, 3:274–281.

Uddin, S. M. A., Chowdhury, S. S., and Kabir, E. (2017). A theoretical model for determination of optimum metal thickness in kretschmann configuration based surface plasmon resonance biosensors. In *2017 International Conference on Electrical, Computer and Communication Engineering (ECCE)*, pages 651–654. IEEE.

Usman, F., Dennis, J. O., Seong, K. C., Ahmed, A. Y., Ferrell, T. L., Fen, Y. W., Sadrolhosseini, A. R., Ayodele, O. B., Meriaudeau, F., and Saidu, A. (2019). Enhanced sensitivity of surface plasmon resonance biosensor functionalized with doped polyaniline composites for the detection of low-concentration acetone vapour. *Journal of Sensors*, 2019.

Yang, S., Ündar, A., and Zahn, J. D. (2006). A microfluidic device for continuous, real time blood plasma separation. *Lab on a Chip*, 6(7):871–880.

CHAPTER 4. PLASMONIC OPTICAL FIBER BASED CONTINUOUS IN-VIVO GLUCOSE MONITORING FOR ICU/CCU SETUP

Souvik Kundu[1], Shawana Tabassum[2], Ritwesh A. Kumar[1], E. Dale Abel[3], and Ratnesh Kumar[1]

[1] Department of Electrical and Computer Engineering, Iowa State University, Ames, IA, 50010, USA

[2] Department of Electrical Engineering, University of Texas, Tyler, TX 75799, USA

[3] Department of Medicine, The University of California, Los Angeles, CA, 90095, USA

Modified from a manuscript accepted in *IEEE Transactions on Nanobioscience*

4.1 Abstract

This paper reports a sensor architecture for continuous monitoring of biomarkers directly in the blood, especially for ICU/CCU patients requiring critical care and rapid biomarker measurement. The sensor is based on a simple optical fiber that can be inserted through a catheter into the bloodstream, wherein gold nanoparticles are attached at its far distal end as a plasmonic material for highly sensitive opto-chemical sensing of target biomolecules (glucose in our application) via the excitation of surface plasmon polaritons. For specificity, the nanoparticles are functionalized with a specific receptor enzyme that enables the localized surface plasmon resonance (LSPR)-based targeted bio-sensing. Further, a micro dialysis probe is introduced in the proposed architecture, which facilitates continuous monitoring for an extended period without fouling the sensor surface with cells and blood debris present in whole blood, leading to prolonged enhanced sensitivity and limit of detection, relative to existing state-of-the-art continuous monitoring devices that can conduct direct measurements in blood. To establish this proof-of-concept, we tested the sensor device to monitor glucose in-vivo involving an animal model, where continuous monitoring was done directly in the circulation of living rats. The

sensor's sensitivity to glucose was found to be 0.0354 a.u./mg.dl^{-1} with a detection limit of 50.89 mg/dl.

4.2 Introduction

There exists technological challenges in continuous biomarker monitoring in-vivo in whole blood. These include lack of stability of the sensors and limited re-usability, reduced sensitivity due to fouling from blood debris, real-time monitoring requirement, expensive manufacturing cost, are some examples of feasibility challenges needing viable solutions Zafar et al. (2022). In this paper, we establish a proof-of-concept of such a sensor architecture by targeting in-vivo continuous glucose monitoring (CGM), which is especially useful in ICUs/CCUs and where CGM becomes a critical aspect of treatment. In the case of hospitalized COVID-19 patients with pre-existing conditions of type-2 diabetes, the impact of unbalanced glucose levels is amplified, and the CGM need becomes even more given that patients with poorer blood glucose control showed an increased mortality rate relative to those with better glucose control Zhu et al. (2020).

Glycemia in critically ill ICU patients can range from hyperglycemia to hypoglycemia, where the former is not uncommon even among those patients who have not been previously diagnosed with diabetes Levetan et al. (1998). Those cases are clinically known as stress-induced hyperglycemia (SIH), or hospital-related hyperglycemia Palumbo (1981) Pomposelli et al. (1998) and are associated with increased ICU mortality. There is also a subtle relation between sepsis Kundu et al. (2020), one of the most common causes of death in ICUs Kundu et al. (2021), and glycemic status in ICU patients. In these patients, a hyper-metabolic state existsMcCowen et al. (2001), predominantly due to the intense hormonal and cytokine responses like TNF, IL-1, and IL-6, that important mediators of insulin resistance, resulting in hyperglycemiaMizock (2001). In the case of COVID-19 treatments, systemic glucocorticoids used for dampening the cytokine storm often raise blood glucose levels exponentially. This glycemic variability in the case of critically ill ICU patients is usually quantified via the standard deviation around the mean or coefficient of variation (CV), which equals standard deviation/mean Krinsley (2008). Greater

glycemic variability is associated with a significantly higher mortality rate: A blood glucose level standard deviation of $>$ 20 mg/dL was associated with a 9.6-fold increase in mortality compared with a blood glucose level standard deviation of $<$ 20 mg/dL. A study has also revealed that even a single episode of severe hypoglycemia or low glucose level is associated with an increased risk of mortalityKrinsley and Grover (2007). Some studies have found that glucose levels of 140-180mg/dL can be associated with the best risk-benefit ratioPreiser and Devos (2007), and based on that the American Association of Clinical Endocrinologists and the American Diabetes Association have adopted these levels as targets for ICU patients Kavanagh and McCowen (2010). Thus, continuous monitoring of glucose along with other critical ICU-relevant biomarkers is of utmost importance for the survival of critically ill ICU patients.

In this paper, we provide a sensor architecture for in-vivo continuous biomarker monitoring in blood and establish its proof-of-concept by detecting glucose. However, the approach applies to any other critical ICU/CCU biomarkers. Although there exist numerous glucose sensors (invasive, noninvasive, and minimally invasive), which can be broadly categorized as amperometric sensors, single-use with costly enzyme-based strips, or optical sensors (employing absorption spectroscopy, light scattering, or Raman spectroscopy), most of these cannot be used for continuous in-vivo monitoring in the blood due to fouling and interference caused by blood cells on the sensor surface, and the commonly used static sensor calibration is incapable of compensating for such fouling over time Vogler (2012). There exist low-fouling materials, e.g., poly(ethylene glycol) (PEG), but they also have only limited non-fouling capabilities in complex real-world media such as undiluted blood plasma and serum and its derivatives; are susceptible to oxidative damage over longer-term use; and are also difficult to directly functionalize with biomolecules for biosensing applications Li et al. (2007) Ostuni et al. (2001). Also, the wearable sensors integrated with bio-needles for measuring glucose continuously in sweat or other subcutaneous body fluids can lack a proper correlation with the immediate blood glucose concentration.

Fiber-optic sensors enjoy unique advantage for in-vivo monitoring in while blood, that those can be inserted through patient's catheter into the blood stream in ICU/CCU setting, and while

different types of gold nanoparticles coated optical fiber-based glucose sensors are reported in the literature Yang et al. (2020); Kumari et al. (2022), they are incapable of providing continuous in-vivo monitoring of glucose for a prolonged period due to fouling caused by the proteins, cells, and other interfering molecules present in the blood.

In contrast to these previous works that mainly focus on sensor design, our work advances the existing state-of-art in in-vivo glucose sensor design by integrating the fiber-tip sensor with a microdialysis probe for continuous glucose monitoring in whole blood for a prolonged period: In our sensing architecture, we have proposed the integration of a microdialysis (μD) probe with 20kDa membrane molecular weight cutoff (MWCO) to prevent the sensor from coming in direct contact with the larger blood molecules and thereby reduce its fouling. Integration of the microdialysis probe not only protects the sensor from fouling but also enables easy access to whole blood for continuous monitoring in an existing ICU/CCU setup: The functionalized opto-chemical fiber sensor can be inserted inside a microdialysis probe, and the entire assembly can be inserted through a patient's catheter that is already furnished in an ICU/CCU setup, thereby avoiding any extra logistic or overheads. We have established this proof-of-concept by doing live experiments in a live rat as narrated in the subsequent sections.

The main novelties of our work are:

- nano-sensing footprint of the fiber optic cable that makes it amenable for insertion into the bloodstream through a catheter for in-vivo monitoring in critical care setting without any extra logistics, and
- integration of the fiber-tip sensor with a microdialysis probe that allows continuous in-vivo monitoring in whole blood for a prolonged period. We have demonstrated a proof of concept by testing the integrated sensing system in a live rat, mimicking the ICU/CCU setup.

Summarily, the paper provides these contributions:

- Detailed fabrication process for the opto-chemical fiber optic sensor.

- Measurements exploiting localized surface plasmon resonance of the sensor and evaluation of sensitivity, LOD of the sensor.
- An integrated micro dialysis probe based *in-vivo* measurement for continuous glucose monitoring in living rats.
- Performance comparison of the proposed sensor against the continuous glucose monitoring sensors reported in the literature.

4.3 Plasmonic Sensor Working Principle

This section describes the working mechanism of the gold nanoparticle-coated optical fiber sensor probe. Given that an in-vivo detection requires a reflected (as opposed to transmitted) signal for measurement, the sensor is made on the far distal end of a fused bifurcated fiber (see Fig 4.1) that can be inserted through a catheter into the bloodstream. Gold nanoparticles (AuNP) are deposited as shown in Fig 4.1 (in the form of red dots) to provide for localized surface plasmon resonance (LSPR). Light guided through the optical fiber interacts with the AuNPs at the far distal end of the fiber and excites the surface plasmons (valence bonded electrons). At the LSPR wavelength, the incident light has maximum absorption (equivalently, minimum reflected intensity). The LSPR wavelength depends on the AuNP characteristics (material, size, shape, refractive index (RI)), and RI of the local surrounding medium—This is formalized below in Section 4.3.1. Accordingly, a change in local surrounding medium RI results in a shift in resonance wavelength and also a change in the absorption level (and so also the reflected intensity level) at the original resonance wavelength. We propose to measure intensity variations as opposed to resonance wavelength shifts because the sensors basd on localized surface plasmon have been reported to have reduced sensitivity in wavelength modulation configuration and hence the intensity modulation configuration is preferred Srivastava et al. (2012). For the specific detection of glucose molecules, the AuNP coated fiber is functionalized with glucose oxidase (GOx) enzyme (see the yellow Y's in Fig 4.1). During the glucose detection on the AuNP surface, the glucose

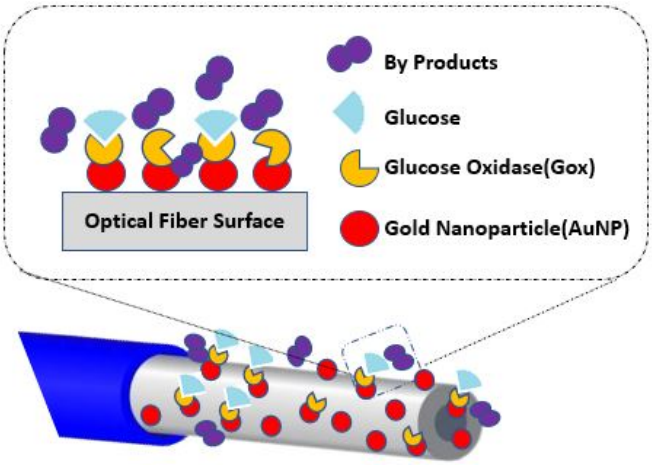

Figure 4.1 Fiber Optic LSPR based Glucose Sensing Principle.

trapped within the immobilized GOx enzyme gets oxidized by enzymatic reaction, producing gluconic acid and hydrogen peroxide as the products (see the dark and light blue dots in Fig 4.1) and changing the local surrounding medium RI. The effect of this on the refractive index change is then detected as an intensity change at the LSPR wavelength Yang et al. (2020).

4.3.1 Theoretical formulation of the sensing mechanism

The proposed fiber optic-based LSPR sensor system comprises three layers:

- Fiber core made up of silica (SiO_2) of refractive index, say η_0.
- Metallic (Au) nanoparticle layer, whose real part of dielectric constant ϵ_r is given by (4.1) Maier et al. (2007):

$$\epsilon_r = 1 - \frac{\lambda^2}{\lambda_p^2}, \tag{4.1}$$

  where λ_p is the plasma wavelength of the electrons in the metal nanoparticle layer, and λ is the wavelength of the incident light.
- Target sensing layer, whose dielectric constant and refractive index are denoted ϵ_s and η_s, respectively. (In this paper, the target sensing layer consists of GOx at its base that traps and oxidizes glucose.)

Fundamentally, surface plasmon resonance (SPR) is the oscillation resonance of the valence electrons in metal layers induced by incident radiation of an appropriate frequency. When this phenomenon is observed in nanoscale particles/layers, it is called localized surface plasmon resonance (LSPR). The mathematical formulation of the resonance condition and an expression for LSPR wavelength are presented next.

4.3.2 Resonance condition

The wave incident at the core and metallic nanoparticle layer interface can undergo extinction (E), transmission (T), and reflection (R). Since, in our optical fiber design, the light gets totally internally reflected at its far end, there is no transmission component, i.e., a part of the wave gets extinct due to the absorption and scattering by the nanoparticles, and the rest gets reflected for measurements. Thereby the reflected spectrum shows a dip at a wavelength where the extinction is maximum due to LSPR. For very small particles of diameters (d) less than wavelength of incident light, the scattered fields produced by a plane wave incident on a homogeneous conducting sphere (AuNPs in our case) results in the following extinction, scattering, and absorption components, given by (4.3), (4.2), and (4.4) respectively Bohren and Huffman (2008) Mayer and Hafner (2011):

$$E_{ext} = \frac{2\pi}{|k|^2} \sum_{L=1}^{+\infty} (2L+1)[Re(a_L + b_L)], \tag{4.2}$$

$$E_{sca} = \frac{2\pi}{|k|^2} \sum_{L=1}^{+\infty} (2L+1)[|a_L|^2 + |b_L|^2], \tag{4.3}$$

$$E_{abs} = E_{ext} - E_{sca}, \tag{4.4}$$

where k is the incident wave-vector, L values are integers representing the dipole, quadrupole, and higher multipoles of the scattering, and finally, a_L and b_L are composed of the Riccati-Bessel functions Mayer and Hafner (2011). In case of spherical AuNPs, $L = 1$, and the a_L and b_L values

for $L = 1$, as approximated from power series, are given by (4.5):

$$a_1 = \frac{(kd)^3}{12}\left(\frac{-i\epsilon_r^2 - i\epsilon_r\epsilon_s + 3\epsilon_i\epsilon_s - i\epsilon_i^2 + i2\epsilon_s^2}{(\epsilon_r + 2\epsilon_s)^2 + (\epsilon_i)^2}\right), b_1 \approx 0, \tag{4.5}$$

where $\epsilon = \epsilon_r + i\epsilon_i$, with ϵ_r being the real part and ϵ_i being the imaginary part of the metallic nanoparticle dielectric function, and ϵ_s is the dielectric constant of the surrounding medium. Substituting (4.5) into (4.2) and retaining only the $L = 1$ term yields (4.6):

$$E_{ext} = \frac{3\pi d^3 \epsilon_s^{\frac{3}{2}}}{2}\frac{\epsilon_i}{(\epsilon_r + 2\epsilon_s)^2 + \epsilon_i^2}. \tag{4.6}$$

Similarly, E_{sca} can be evaluated by substituting (4.5) into (4.3). The extinction in (4.6) is maximized when the denominator is minimized, and that condition is met when $\epsilon_r = -2\epsilon_s$ assuming ϵ_i is small or only weakly dependent on the wavelength of the incident light. This explains the dependence of the LSPR absorption peak on the surrounding environment. Substituting $\epsilon_r = -2\epsilon_s$ (resonance condition) and $\epsilon_s = \eta_s^2$ in (4.1), we obtain the expression for the LSPR wavelength (4.7):

$$\lambda_{\text{LSPR}} = \lambda_p\sqrt{2\eta_s^2 + 1}. \tag{4.7}$$

4.4 Sensor Fabrication and Functionalization

This section narrates the detailed steps to fabricate the fiber optic-based LSPR sensor probe. There are three basic steps to the fabrication as follows:

1. Preparation of ∼10 nm radius spherical gold nanoparticles.
2. Immobilization of the nanoparticles on the fiber surface.
3. Functionalization of glucose oxidase on the immobilized nanoparticles.

These steps are also depicted in Fig. 4.2. The integration of the sensor with a μD probe is discussed in Section 4.5.2.

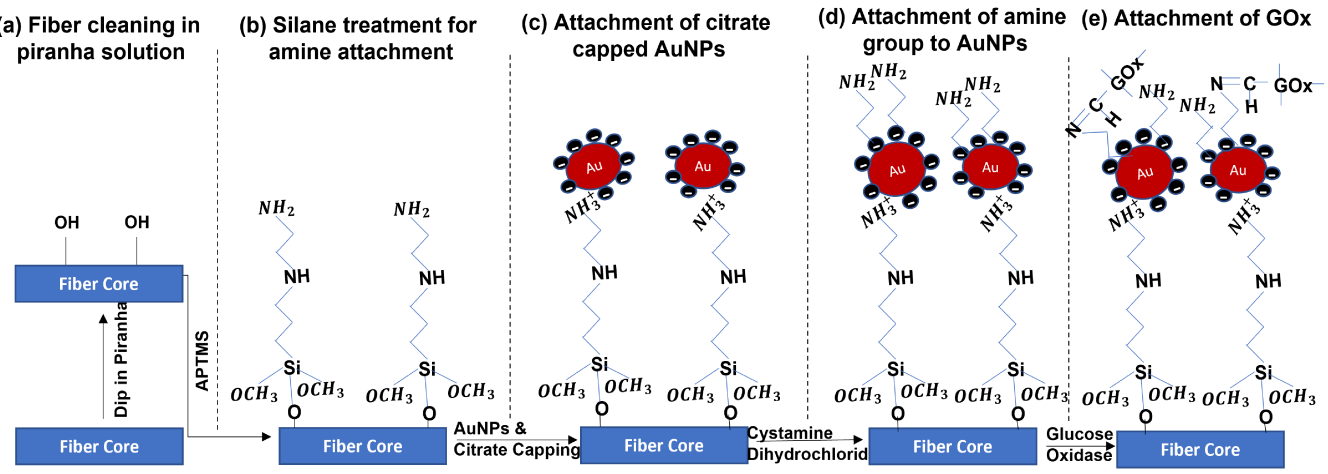

Figure 4.2 Sensor Fabrication Steps. (a)-(c) Illustrate the process of AuNP attachment on the sensor surface; (d)-(e) Illustrate the GOx functionalization on AuNPs by amine linker

4.4.0.1 Synthesis of ~10 nm radius gold nanoparticles

1 mM and 38.8 mM aqueous solutions of $HAuCl_4$ and trisodium citrate were prepared, respectively. 10 mg of $HAuCl_4.3H_2O$ was mixed in 50 ml of DI water, and 500 mg of Sodium Citrate was mixed in 50 ml of DI Water. 20 ml of aqueous solutions of $HAuCl_4$ was poured into a beaker at 200° C and constantly stirred at 500 rpm. As soon as the boiling started, trisodium citrate solution was added such that the volume ratio of the two solutions was $HAuCl_4$: citrate = 10 : 1. (The size of the gold nanoparticles can be modulated by changing the molar ratio of $HAuCl_4$ to trisodium citrate. Typically, AuNPs between 10 nm and 150 nm radii can be synthesized by adjusting the molar ratio, and the chosen ratio was to attain the desired 10 nm size.) A violet-colored liquid appeared quickly, transforming to a bright red after 30 minutes of boiling and stirring when $HAuCl_4$ was reduced by trisodium citrate. After that we stopped the boiling and stirred the solution until it was brought to room temperature (approximately 30 minutes) and gold nanoparticles thus formed was stored at room temperature until use. A detailed study has been presented in Dong et al. (2020), which is what we adopted.

4.4.0.2 Fabrication of the nanoparticle-coated sensor on the far distal end of the fiber

First, the external polymer jacket of the fiber at its tip was removed using a fiber optic stripper. Next, approximately 3-4 cm of the cladding of a multimode fiber was removed from its far distal end using an acetone-soaked Kimwipe by a multi-step stripping procedure dipping the fiber into acetone for 20 min. The cladding part starts to dissolve in acetone, making the stripping of the cladding easier. The distal end of a multi-mode fiber (with a core diameter of 200 μm) was cut with a fiber cutter to create a flat tip. The unclad sensing area was next cleaned and hydrolyzed with Piranha solution (volume ratio of $H_2SO_4 : H_2O_2 = 7 : 3$) for 30 min at 85° C, which provided –OH groups on the fiber surface as shown in Fig. 4.2(a). Next, the sensing region of the optical fiber was rinsed with DI water, blow-dried with N_2, and annealed in a vacuum oven for 30 min at 110° C then immersed in a 10% solution of 3-aminopropyl trimethoxysilane (APTMS) in methanol for 1 hr. at 40° C, which provided a monolayer of -NH_2 groups on the fiber surface as illustrated in Fig. 4.2(b). The fiber was next rinsed sequentially with ethanol and DI water to remove unbound APTMS, blow-dried with N_2, and again annealed in a vacuum oven for 30 min at 110° C. The sensing region was then incubated in a gold nanoparticle solution overnight. Afterwards, the fiber was washed with DI water to get rid of any unbound nanoparticles and dipped back in the nanoparticle solution for 12 hours to ensure effective attachment of the nanoparticles on the fiber surface, as seen in Fig. 4.2(c).

Note while ∼10 nm sized AuNPs predominately occur during the above-described synthesis process of Section 4.4.0.1, there may still exist AuNPs of smaller radii, which hardly contribute to LSPR. Hence, even after the AuNP attachment on the fiber surface, there is a possibility of improved LSPR signal by in-situ growth of the smaller AuNPs using, for example, a process described in Ziegler and Eychmuller (2011); Kim et al. (2019). In that case, the fiber needs to be immersed in 1 mM sodium citrate dehydrate aqueous solution for 5 min, where the citrate ions help accumulate the AuNPs, thereby facilitating the growth of the smaller radius AuNPs. Note

this is an optional step that can be employed in case the LSPR signal of the designed probe turns out to be low.

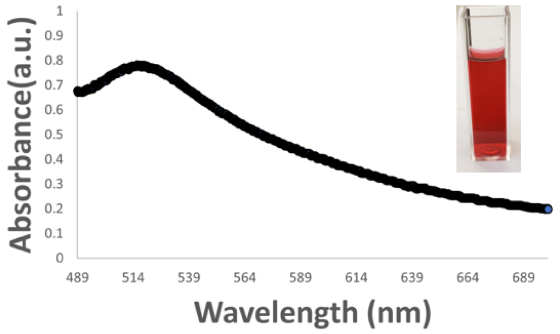

Figure 4.3 Absorbance Spectrum of AuNP of average diameter between 10 and 20 nm and maximum absorbance at 514 nm. Inset shows the corresponding gold nanoparticles

4.4.0.3 Sensor Functionalization

To attach the glucose oxidase enzyme to the sensor surface, first a 20 μM solution of glucose oxidase in 0.1 M sodium phosphate buffer (6.8 pH) was prepared and kept at 4° C. 30 mg sodium metaperiodate was added and mixed continuously for 1 hour in an ice bath made in a Styrofoam cup (rather than with a conventional immersion cooler system) to maintain the reaction temperature at 0° C. 6.97 μl of ethylene glycol was added to stop the reaction and it was followed by vigorous 30 minutes stirring. To attach the glucose oxidase enzyme to the sensor surface, the fiber optic sensor was first dipped in a 1 mM aqueous solution of cystamine dihydrochloride for 1 hr. This created a monolayer of amine groups on the nanoparticle-coated fiber as depicted in Fig. 4.2(d). The probe was then immersed in a glucose oxidase solution for 12 hrs, allowing the modified glucose oxidase to bind to the -NH_2 groups. After rinsing the fiber probes with DI water to discard any unbound species, they were incubated in the glucose oxidase solution for 12 hrs. This ensured effective binding of the glucose oxidase to the nanoparticles on the fiber probe as depicted by Fig. 4.2(e).

4.5 LSPR Characterization and Experimental Validation

After fabricating a gold nanoparticle (AuNP)-coated optical fiber sensor probe for in-vivo glucose detection in blood, the AuNPs were characterized using a UV-VIS spectrophotometer by observing the absorption spectrum as shown in Fig. 4.3. The peak absorption was observed at 514 nm, which confirms that the nanoparticles have an average diameter between 10 nm to 20 nm, in accordance with the fabrication process and the underlying theory Mondal et al. (2020). The scanning electron microscope image in the inset of Fig. 4.4(c) further confirms the successful attachment of AuNPs to the fiber surface (using (3-aminopropyl)trimethoxysilane linkers).

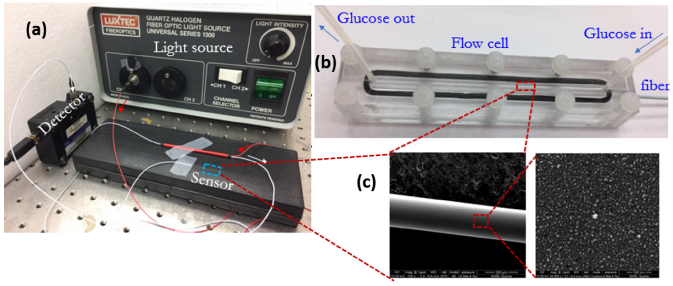

Figure 4.4 Experimental setup at ESSeNCE Lab, ISU. (a) Illustrates the light source and detector along with the fused fiber with the fabricated sensor at its far distal end. (b) Glucose measurement setup in flow cell. (c) Illustrates the SEM image of the gold nanoparticles after attaching them on the optical fiber surface.

4.5.1 Glucose monitoring validation in buffer solution

Fig. 4.4(a) depicts the optical sensor's experimental validation setup, consisting of a broadband white light source, an optical detector (range 400 nm to 750 nm), and a 2x1 fused optical fiber. The light source illuminates the sensing element of approximately 4 cm length toward the far distal end of the optical fiber. Light reflected off the element is detected by the detector, and its spectrum is recorded. The response of the sensor to glucose was independently validated before its in-vivo use by employing a flow cell around the sensing element (shown in Fig. 4.4(b)) through which distilled water-based solutions of various glucose concentrations

(within 0-250 mg/dL range) were passed, and the corresponding reflection spectra were recorded as shown in Fig. 4.5 (the plots of the figure are discussed in Section 4.6.1.)

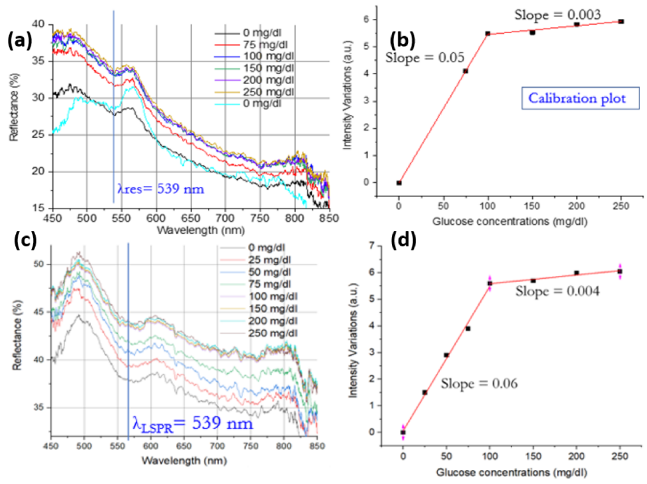

Figure 4.5 (a) Reflection spectrum in static glucose solution (b) Calibration curve in static glucose solution (c) Reflection spectrum in flow cell (d) Calibration curve in a flow cell.

4.5.2 Continuous Glucose Monitoring in Live Rats

Figure 4.6 shows the experimental setup for CGM in a live rat, along with the schematics of a bypass circuit to flow the blood through the sensor. To prevent the optical sensor from fouling secondary to sample deposition and coagulation, the sensor was inserted into a μD probe (MWCO 20kDa), chosen in accordance with and higher than the molecular weight of glucose. With the use of a μD probe with MWCO 20kDa, all bigger molecules having sizes higher than 20kDa get filtered, thereby preventing the fouling of the sensor probe and also reducing the non-specific bindings to a great extent, and eventually helping in enhancing the longevity, sensitivity, and specificity of the sensor.

There are seven main "points" of the by-pass circuit as labeled alphabetically in the schematic diagram of Figure 4.6. Point A depicts blood flow from the rat's right jugular vein into the surgically set bypass circuit. Point B is periodically opened and closed to sample blood from the bypass circuit to obtain the reference values of the blood glucose concentration from a commercial

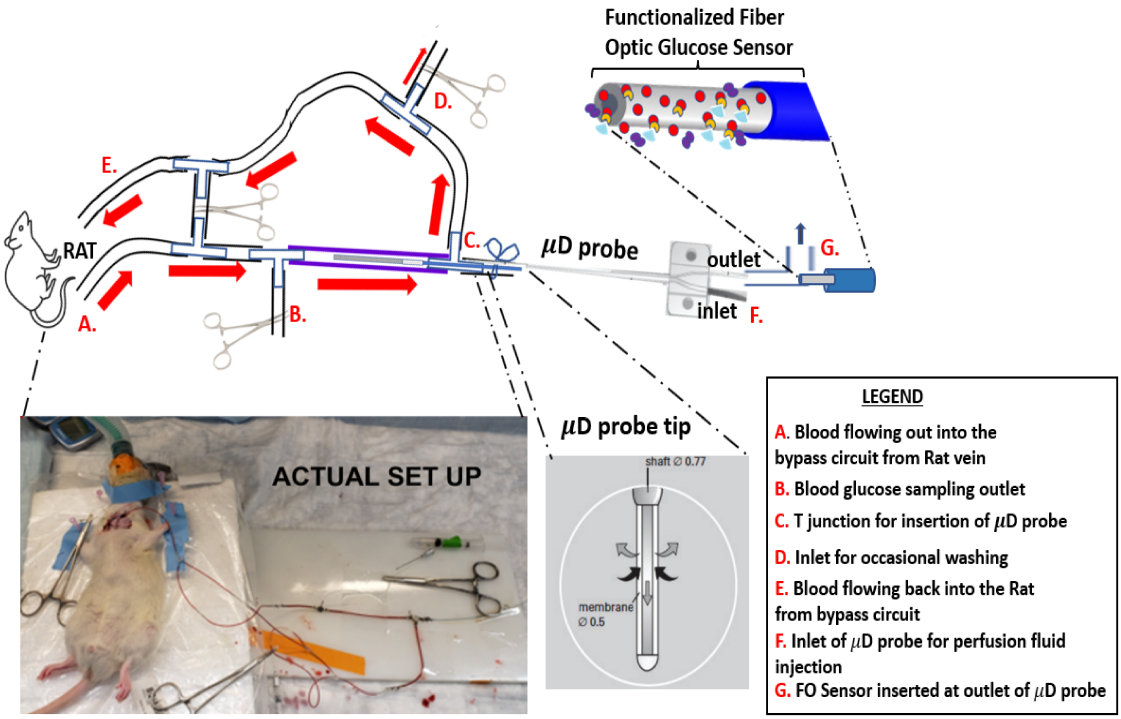

Figure 4.6 Experimental Setup for continuous glucose monitoring (CGM) on a live rat.

glucometer. At Point C, a 3-way T-junction is placed to reroute the blood back into the rat, and the μD probe is placed at this junction, as shown in the figure to allow only the blood components less than 20kDa to pass through the μD membrane while blocking the larger ones. Point D is an inlet made available for occasional washing of the external surface of the μD to remove any blood debris clinging onto the probe surface. At point E, the blood flows back into the jugular vein of the rat, thereby completing the bypass loop. The μD probe has one inlet (Point F) and one outlet (Point G). The inlet Point F is fed with heparin as a perfusion fluid, which prevents blood from clotting at the interface of the μD membrane, through which the glucose molecules percolate into the μD probe. The heparin solution, which has zero initial glucose concentration, creates a concentration gradient at the blood-micro dialysis membrane interface, which helps in the movement of glucose molecules from higher concentration (in the blood) to lower concentration (in heparin) across the membrane. Thus, the exiting heparin distillate contains glucose molecules which we detect at the outlet of the μD probe using our proposed optical fiber-based LSPR sensor.

During the measurement, the blood glucose level (BGL) was adjusted in the rat by managing the insulin and the glucose infusion rates via the right jugular catheter. For a normal rat with insulin flow at 2.5 mU/min/kg, we observed that a typical glucose infusion rate of about 55-60 mg/kg/min is needed to maintain the BGL steady at its initial value.

4.5.3 Instruments and Reagent Sources

For the measurements, a quartz halogen lamp which is a white light source of power 150-watt (Luxtec Fiber Optics, Plainsboro, NJ) was connected to 1x2 Multimode Fiber Optic Coupler, High OH, Ø200 µm Core, 0.39 NA, 50:50 Split, FC/PC. The reflected light from the fiber optic sensor tip was measured by a UV/VIS spectrometer (USB-4000, Ocean Optics) that is connected to the other end of the optical coupler. Syringe pumps were used to inject the glucose solution into the flow cell for experiments in buffer solution and for injecting the perfusion fluid through the inlets of the μD probe. $HAuCl_4$, tri-sodium citrate, 3-aminopropyl trimethoxysilane (APTMS), sodium metaperiodate, GOx and cystamine dihydrochloride were procured from Sigma-Aldrich. Sulfuric acid, hydrogen peroxide, methanol and DI water were obtained from Chemstore, ISU. Mouse blood was procured from Biochemmed, Winchester, VA.

4.6 Results and Discussions

To establish a proof-of-concept, we studied the behavior of the proposed sensor architecture for in-vitro (in flowing buffer solution) as well as in-vivo (in live rat) glucose detection. This section discusses the corresponding measurement results.

4.6.1 Sensor Characterization in Buffer Solution

The measurement results were obtained at the ESSeNCE Lab., ISU, where we tested the performance of the sensor in three different settings: (i) static glucose solution, (ii) in a flow cell with PBS buffered glucose solution, (iii) in mouse blood. A post-meal blood glucose level in a non-diabetic, should be < 180 mg/dl, and a pre-meal glucose level can range from 90 to

130 mg/dl. Hence, we tested for a concentration range of 0-250 mg/dl. The results in Figure 4.5(a)-(b) correspond to the measurements of dipping the sensing tip into still solutions of glucose. We observed sensitivity of 0.05 a.u./mg.dl^{-1} at glucose concentrations of 0 to 100 mg/dl, and 0.003 a.u./mg.dl^{-1} at glucose concentrations of 100 to 250 mg/dl.

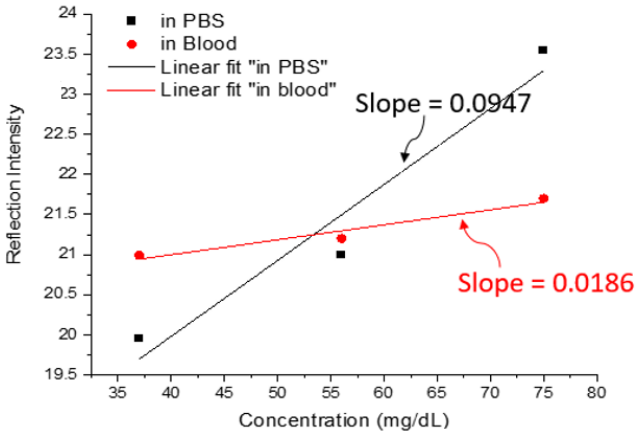

Figure 4.7 Sensor performance comparison in PBS buffer vs. mouse blood.

Fig. 4.4(b) illustrates a flow cell setup that we used to take readings of glucose in a flowing buffer solution. Fig. 4.5(c)-(d) depicts the performance of the fiber optic sensor in the flow cell, which shows nearly the same sensitivity both at lower and higher glucose concentrations. (Sensitivity of 0.06 a.u./mg.dl^{-1} was obtained at lower concentration of glucose between 0 to 100 mg/dl, and of 0.004 a.u./mg.dl^{-1} at higher concentration of glucose between 100 to 250 mg/dl.)

Since, in a real ICU/CCU scenario, glucose concentrations have to be measured in whole blood, we studied our sensor's sensitivity and LOD in mouse blood to imitate the behavior of the sensor's response in the presence of blood debris. Fig. 4.7 depicts that response, and although there is an expected reduction in sensitivity and LOD in blood solution compared to the case of PBS buffer solution, the sensor remains capable of detecting a very low glucose concentration in blood samples. The LOD of the sensor in the blood sample is 15.3 mg/dl, which, although higher

than the 2.59 mg/dl level of LOD in the PBS buffer solution, is still well below the normal lower limit of glucose concentration in a human being.

4.6.2 Sensor Characterization in Blood from Live Rats

The results obtained in the live rat model are reported in this section. The experimental environment is set by establishing a stable insulin infusion rate via a right jugular venous catheter, aiming to reach a steady state of plasma insulin. At the same time, to maintain stable blood glycemia at the desired level, we infused 50% glucose via the same catheter placed in the rat's right jugular vein at various variable flow rates. For a normal rat with insulin flow at 2.5 mU/min/kg, we typically needed glucose infusion rates of about 55-60 mg/kg/min. We performed this dyad of insulin and glucose infusion to regulate the blood glucose level of the rat to imitate the blood glucose range of 80 to 250 mg/dl as in the case of a human. This helped us to test our sensor in a similar setting which may prevail in an ICU. During the assay, we also manually collected blood for measuring glucose using a glucometer to independently obtain data for the sensor calibration. Fig. 4.8 depicts the entire response spectrum of the fiber optic sensor at different glucose concentrations.

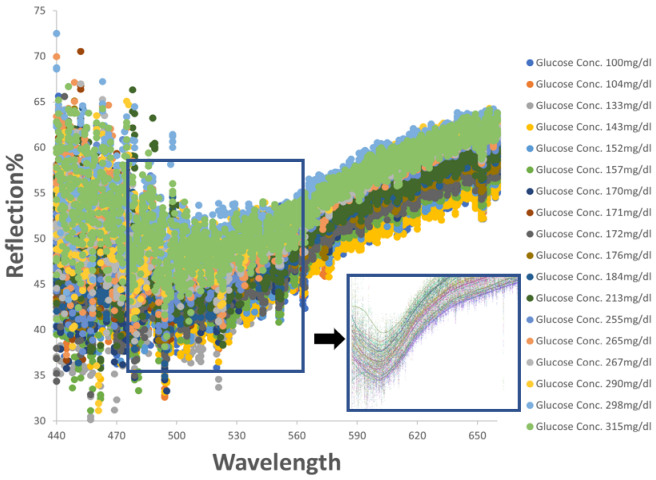

Figure 4.8 Raw reflection spectra for different glucose concentrations. Different colors depicts different glucose concentration spectrum across wavelengths.

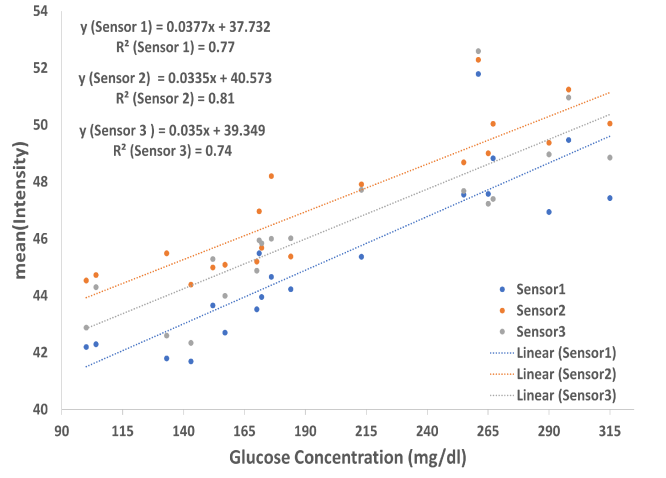

Figure 4.9 Stability and Repeatability Analysis.

For a stability and repeatability study, the measured spectra at different glucose concentrations (between 100 to 315 mg/dl) are illustrated in Fig. 4.9 for three different sensors. Based on the shift in intensity values at different glucose concentrations, calibration curves, chosen to be monotonically increasing functions (to guarantee 1-1 mapping essential for calibration), are fitted for all three sensors. The fitted curve for sensor1 is given by: $y = 37.73 + 0.03769x$ with $R^2 = 0.77$; for sensor2 it is given by $y = 40.57 + 0.03357x$ with $R^2 = 0.81$; and for sensor3 is given by: $y = 39.35 + 0.03497x$ with $R^2 = 0.74$. The sensitivities of all three sensors are comparable as it varies between 0.033 to 0.037. A combined calibration curve is derived from the three individual sensor curves as shown in Fig. 4.10 and is given by $y = 39.298 + 0.0354x$ with $R^2 = 0.7989$. This corresponds to an overall sensitivity of 0.0354 a.u./mg.dl^{-1}, using which, the limit-of-detection is determined to be, LOD $= \frac{3\times \text{SD}}{\text{sensitivity}} = \frac{3\times 0.600513}{0.0354} = 50.89$ mg/dl. The coefficient of variation (C.V.) at different glucose concentrations is given in Table 4.1, and found to be less than 2.5% on average.

Fig. 4.11 depicts the sensor response over 2 hrs when the glucose concentration was varied dynamically (red dots and the fitted red curve) and the resulting reflection% was captured (blue dots and the fitted blue curve). From the two curves, it is clear that the sensor responded linearly as expected from its linear calibration curve of Figure 4.10. The sensor response is nearly

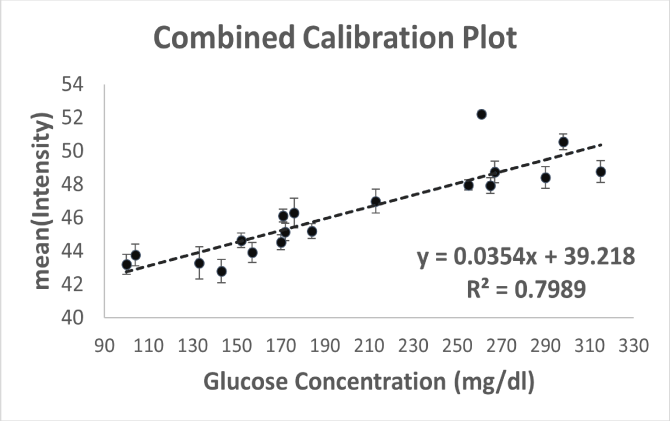

Figure 4.10 Combined Calibration Curve in whole rat blood.

Table 4.1 Coeff. of variance at each glucose concentration

Glucose Conc. (mg/dl)	100	104	133	143	152	157	170	171	172	176	184	213	255	261	265	267	290	298	315
Coeff. of Variance (CV)	2.78	2.95	4.48	3.28	1.94	2.71	1.99	1.63	2.31	3.86	2.01	3.01	1.29	0.77	1.97	2.71	2.68	1.88	2.68

real-time with a small delay of only about 2 min on average, as opposed to a lab test for certain biomarkers that can be time-consuming, making it non-real-time. The sensor delay is due to the time taken for the glucose to profuse through the microdialysis membrane and for its oxidation to occur. Through rigorous experiments, we observed that the sensor response delay can be reduced by pre-soaking the sensor in a buffered glucose solution prior to using it. Similarly, the delay incurred in profusion can be reduced by using a higher-quality microdialysis probe.

The R-squared value of the sensor in whole blood of 0.79 as depicted in Figure 4.10 lies within the 0.75-0.9 range, indicating that the sensor data is of good quality and is reliable Koo and Li (2016). Also, we only used simple-minded static calibration for this study, whereas with a more sophisticated dynamic calibration, the R-squared value is expected to be higher, and the development of dynamic calibration is part of our ongoing study Talukder et al. (2022). Indeed to validate that there is room for better fit through a more sophisticated calibration, we evaluated the sensor's nascent performance by fabricating and testing identical sensors, where the ICU setup circuit was mimicked by using a set of syringe pumps, and glucose spiked D.I. water of

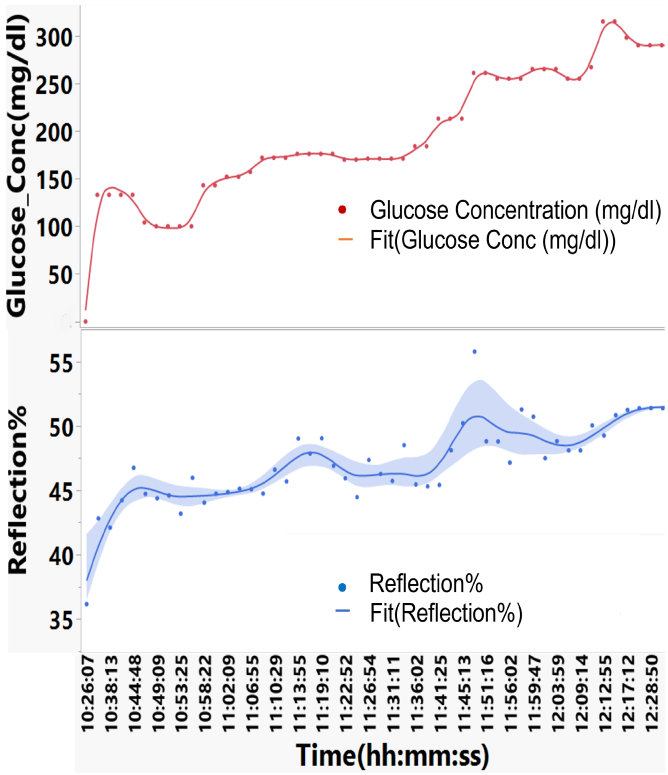

Figure 4.11 Sensor dynamics for in-vivo continuous glucose monitoring: glucose profile (top) vs. sensor response (bottom)

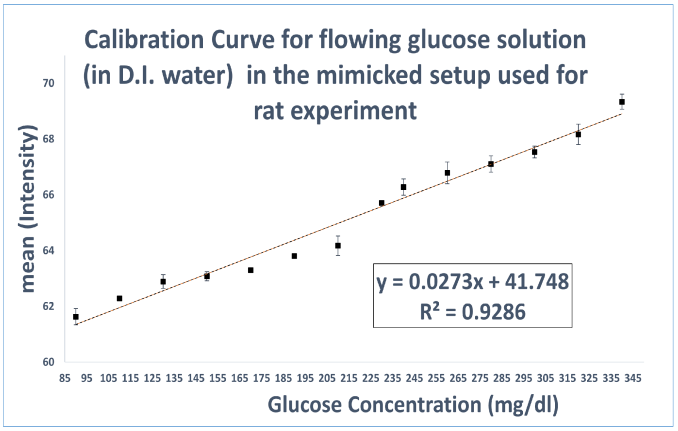

Figure 4.12 Sensor calibration curve when glucose spiked DI water was flown over the sensor in an ICU/CCU mimic setup

varying concentrations was flown over the sensor for measurements. The resulting calibration curve of Fig.4.12 depicts the R-squared value of 0.92, with low error bars. Also, another direction of sensor quality enhancement is by improving the quality of the microdialysis to filter out molecules with even lower molecular weights than the current 20kDa, which again is a topic of further study, inspired by the success of the proof-of-concept of the current design.

4.6.2.1 Sensor Calibration w.r.t. wavelength shift

Fig.4.13 depicts the sensor calibration by means of wavelength interrogation. Here the wavelengths corresponding to the minimum intensity for all glucose concentrations are plotted and fitted using a monotonically increasing function given by $y = 0.016x + 518.93$ with $R^2 = 0.76$. Here we see a slight drop in the R^2 value compared to the calibration done using intensity change where the R^2 was 0.79 at the resonant wavelength. From the calibration curve, we have calculated the sensitivity as 0.016 and L.O.D. $\frac{3\times0.473}{0.016} = 88.68$ mg/dl. This shows that the fabricated LSPR-based glucose sensor is more sensitive to intensity modulation than wavelength modulation. This finding is also in sync with the literature where LSPR-based sensors have been found to be less sensitive in wavelength modulation schemes Haes and Van Duyne (2004). Similarly, the work on LSPR-based U-shaped fiber optic biosensor for glucose reported in Srivastava et al. (2012), is also based on intensity modulation, and they have also observed a similar phenomenon where intensity change is more pronounced than wavelength change in LSPR sensors.

4.6.2.2 Combined Sensor Calibration w.r.t. wavelength shift and intensity

In this sub-section, the combined calibration curve for the sensor is provided with respect to both intensity and wavelength shift. The generalized equations of the individual calibration curves can be written as equation (4.8), where x is the intensity and y is the wavelength, and z_1, z_2 are glucose concentrations whose variances are given by σ_1^2 and σ_2^2 respectively.

$$x = f(z_1); y = g(z_2) \tag{4.8}$$

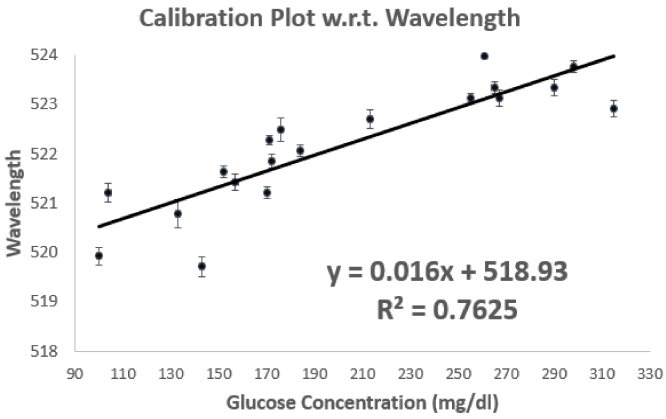

Figure 4.13 Sensor calibration curve w.r.t. wavelength shift

Again the equation (4.8) can be rearranged as equation (4.9), where $f^{'}$ and $g^{'}$ are the inverse function of f and g respectively.

$$z_1 = f'(x); z_2 = g'(y) \tag{4.9}$$

Now for combining the two independent calibration curves, we have assigned weights w_1 and w_2 to the calibration variables such that their overall variances are minimized at a given glucose concentration. Hence, the final combined calibration is given by equation (4.10), where $w_1 = \frac{\sigma_2^2}{\sigma_1^2+\sigma_2^2}$ and $w_2 = \frac{\sigma_1^2}{\sigma_1^2+\sigma_2^2}$.

$$Z = w_1 f'(x) + w_2 g'(y) \tag{4.10}$$

Therefore, overall variance is minimized, which helps in improving the measurement accuracy. The variance of the combined calibration curve can be obtained from equation (4.11)

$$\sigma^2 = \frac{\sigma_1^2 \sigma_2^2}{\sigma_1^2 + \sigma_2^2} \tag{4.11}$$

Hence, substituting the calibration values and calculated weights from intensity and wavelength interrogation in the generalized equation (4.10), we obtain the combined calibration curve of our proposed LSPR sensor, which is given by equation 4.12

$$Z = w_1 \frac{x - 39.218}{0.0354} + w_2 \frac{y - 518.93}{0.016} \tag{4.12}$$

The values of the weights were calculated based on the individual variances in intensity and wavelength data corresponding to each glucose concentration. Fig. 4.14 depicts a surface plot that shows both intensity (x) and wavelength (y) changes w.r.t. glucose concentration (Z), which corresponds to a combined calibration and thereby minimizes the overall variance in the final calibration.

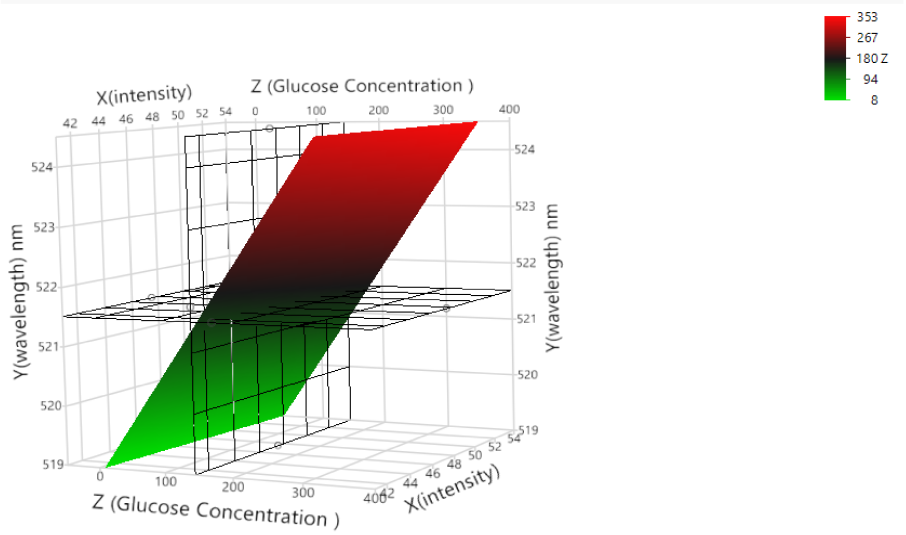

Figure 4.14 Combined calibration using both wavelength and intensity change

4.7 Performance Comparison

We compared the overall performance, merits, and complexity of the proposed sensor architecture with the existing state-of-the-art fiber optic glucose sensors, as shown in Table-4.2. The proposed sensor was tested for glucose concentrations ranging between 90 and 315 mg/dl in whole blood. The sensor's calculated limit-of-detection (LOD) is 50.89 mg/dl, meaning it can cover the glucose concentration range found in human blood (i.e., between 50 to 315 mg/dl), which bolsters the utility of the sensor for use in humans. There exist other sensors with larger range or higher sensitivity, but except for one, none are capable of in-vivo monitoring; plus, our sensor has an advantage over others due to the integration of μD probe, providing a prolonged period of in-vivo continuous measurement ($\sim$2 hrs.) without requiring any extra processing steps

Table 4.2 Performance Comparison

Sensor type	**Measurement range (mg/dl)**	**Sensitivity (a.u./mg.dl^{-1})**	**Measurement Type**	**Analyte**	**References**
MM Microfiber with APTES	0-300	0.0174	*In vitro*	SA buffer, horse, and calf serum	Li et al. (2018)
Graphene Oxide modified TFG	0-144	0.24	*In vitro*	DI Water	Jiang et al. (2018)
Nafion and Enzyme coated electrode	56.210-108.069	0.022	*In vivo*	Whole Blood	Turner et al. (1990)
Enzyme based needle electrode	70-420	3.10	*In vitro*	Interstitial Fluids, Fish blood	Yonemori et al. (2009)
Fiber Optic SPR with MEA	0-500	0.854	*In vitro*	SA buffer	Zheng et al. (2020)
Fiber Optic SPR and enzyme	0-400	3.10	*In vitro*	DI Water, Urine	Zhang et al. (2022)
Back-scattered MIR spectroscopy	80-160	not reported	*In vivo*	Skin interstitial fluid	Liakat et al. (2014)
Transmission MIR spectroscopy	75-600	not reported	*In vivo*	Trans-cutaneous	Vrancćicé et al. (2014)
LSPR with APTMS and Glucose Oxidase	50-315	0.0354	*In vitro, In vivo*	PBS Buffer and Whole Blood	This work

such as separation of plasma or serum, thereby reducing it's complexity. Most other continuous monitoring sensors reported in the literature do not measure glucose directly in blood and thus require extrapolation to correlate the blood glucose with that in the tissue fluid, making those not fully accurate or real-time. Further, in our design, the fabrication steps are relatively simpler, mostly involving standard chemical processing without the need for complex deposition techniques or equipment.

4.8 Conclusion

In summary, this paper presents an LSPR-based fiber optic opto-chemical sensor for continuous glucose monitoring in whole blood for 2 hrs. of unimpeded operation. The work reported a sensor architecture integrating a micro-dialysis probe for preventing the fouling of the sensor surface in the operational period, and minimizing non-specific signal output, thereby improving accuracy and offering better SNR. The designed sensor architecture was validated in buffer as well as in an animal model, producing a proof-of-concept for future development of fiber optic multiplexed sensors, targeting multiple biomarkers in whole blood for continuous monitoring in ICU/CCU settings. The good repeatability of the sensor demonstrates the robustness of the

proposed design for prolonged continuous biomolecular detection directly in whole blood. The proposed methodology involves the detection of variations in intensity in the visible light range, allowing integration of an inexpensive source and detector to make a portable, cost-effective point-of-care detector for biomarker continuous tracking in real-time, making the design amenable to scaling for mass production.

While the integration of μD probe prolongs the life of the sensor by blocking the deposition of larger blood-borne molecules on the sensor surface, smaller blood-borne molecules can still slowly deposit on the sensor probe, causing its response to drift slowly over time. To further prolong the sensor life for continuous monitoring applications, a sensor re-calibration will be required, that may interfere with the ability to do continuous monitoring Vettoretti et al. (2015); Guerra et al. (2012). This situation can be addressed by developing a generalized time-dependent calibration model capable of also correcting for any time drift in sensor response. We refer to such an approach as "dynamic calibration", where not just the current sensor response but also its historic readings are used for adjusting the calibration. The details of its mathematical formulation are reported in our paper Talukder et al. (2022), where we have proposed a Bayesian framework for dynamic calibration of sensors using the history of sensor measurements and the observed ground truth data.

4.9 References

Bohren, C. F. and Huffman, D. R. (2008). *Absorption and scattering of light by small particles*. John Wiley & Sons.

Dong, J., Carpinone, P. L., Pyrgiotakis, G., Demokritou, P., and Moudgil, B. M. (2020). Synthesis of precision gold nanoparticles using turkevich method. *KONA Powder and Particle Journal*, 37:224–232.

Guerra, S., Facchinetti, A., Sparacino, G., De Nicolao, G., and Cobelli, C. (2012). Enhancing the accuracy of subcutaneous glucose sensors: a real-time deconvolution-based approach. *IEEE Transactions on Biomedical Engineering*, 59(6):1658–1669.

Haes, A. J. and Van Duyne, R. P. (2004). A unified view of propagating and localized surface plasmon resonance biosensors. *Analytical and bioanalytical chemistry*, 379:920–930.

Jiang, B., Zhou, K., Wang, C., Sun, Q., Yin, G., Tai, Z., Wilson, K., Zhao, J., and Zhang, L. (2018). Label-free glucose biosensor based on enzymatic graphene oxide-functionalized tilted fiber grating. *Sensors and Actuators B: Chemical*, 254:1033–1039.

Kavanagh, B. P. and McCowen, K. C. (2010). Glycemic control in the icu. *New England Journal of Medicine*, 363(26):2540–2546.

Kim, H.-M., Jeong, D. H., Lee, H.-Y., Park, J.-H., and Lee, S.-K. (2019). Improved stability of gold nanoparticles on the optical fiber and their application to refractive index sensor based on localized surface plasmon resonance. *Optics & Laser Technology*, 114:171–178.

Koo, T. K. and Li, M. Y. (2016). A guideline of selecting and reporting intraclass correlation coefficients for reliability research. *Journal of chiropractic medicine*, 15(2):155–163.

Krinsley, J. S. (2008). Glycemic variability: a strong independent predictor of mortality in critically ill patients. *Critical care medicine*, 36(11):3008–3013.

Krinsley, J. S. and Grover, A. (2007). Severe hypoglycemia in critically ill patients: risk factors and outcomes. *Critical care medicine*, 35(10):2262–2267.

Kumari, A., Vyas, V., and Kumar, S. (2022). Synthesis, characterization, and applications of gold nanoparticles in development of plasmonic optical fiber-based sensors. *Nanotechnology*, 34(4):042001.

Kundu, S., Tabassum, S., and Kumar, R. (2020). A perspective on sepsis pathogenesis, biomarkers and diagnosis: A concise survey. *Medical Devices & Sensors*, 3(4):e10089.

Kundu, S., Tabassum, S., and Kumar, R. (2021). Plasmonic point-of-care device for sepsis biomarker detection. *IEEE Sensors Journal*, 21(17):18837–18846.

Levetan, C. S., Passaro, M., Jablonski, K., Kass, M., and Ratner, R. E. (1998). Unrecognized diabetes among hospitalized patients. *Diabetes care*, 21(2):246–249.

Li, L., Chen, S., and Jiang, S. (2007). Protein interactions with oligo (ethylene glycol)(oeg) self-assembled monolayers: Oeg stability, surface packing density and protein adsorption. *Journal of Biomaterials Science, Polymer Edition*, 18(11):1415–1427.

Li, Y., Ma, H., Gan, L., Liu, Q., Yan, Z., Liu, D., and Sun, Q. (2018). Immobilized optical fiber microprobe for selective and high sensitive glucose detection. *Sensors and Actuators B: Chemical*, 255:3004–3010.

Liakat, S., Bors, K. A., Xu, L., Woods, C. M., Doyle, J., and Gmachl, C. F. (2014). Noninvasive in vivo glucose sensing on human subjects using mid-infrared light. *Biomedical optics express*, 5(7):2397–2404.

Maier, S. A. et al. (2007). *Plasmonics: fundamentals and applications*, volume 1. Springer.

Mayer, K. M. and Hafner, J. H. (2011). Localized surface plasmon resonance sensors. *Chemical reviews*, 111(6):3828–3857.

McCowen, K. C., Malhotra, A., and Bistrian, B. R. (2001). Stress-induced hyperglycemia. *Critical care clinics*, 17(1):107–124.

Mizock, B. A. (2001). Alterations in fuel metabolism in critical illness: hyperglycaemia. *Best Practice & Research Clinical Endocrinology & Metabolism*, 15(4):533–551.

Mondal, P., Guo, C., and Yarger, J. L. (2020). Water soluble gold-polyaniline nanocomposite: A substrate for surface enhanced raman scattering and catalyst for dye degradation. *Arabian Journal of Chemistry*, 13(2):4009–4018.

Ostuni, E., Chapman, R. G., Holmlin, R. E., Takayama, S., and Whitesides, G. M. (2001). A survey of structure- property relationships of surfaces that resist the adsorption of protein. *Langmuir*, 17(18):5605–5620.

Palumbo, P. (1981). Blood glucose control during surgery. *The Journal of the American Society of Anesthesiologists*, 55(2):94–95.

Pomposelli, J. J., Baxter III, J. K., Babineau, T. J., Pomfret, E. A., Driscoll, D. F., Forse, R. A., and Bistrian, B. R. (1998). Early postoperative glucose control predicts nosocomial infection rate in diabetic patients. *Journal of Parenteral and Enteral Nutrition*, 22(2):77–81.

Preiser, J.-C. and Devos, P. (2007). Clinical experience with tight glucose control by intensive insulin therapy. *Critical care medicine*, 35(9):S503–S507.

Srivastava, S. K., Arora, V., Sapra, S., and Gupta, B. D. (2012). Localized surface plasmon resonance-based fiber optic u-shaped biosensor for the detection of blood glucose. *Plasmonics*, 7(2):261–268.

Talukder, S., Kundu, S., and Kumar, R. (2022). Dynamic calibration of nonlinear sensors with time-drifts and delays by bayesian inference.

Turner, R., Harrison, D., Rajotte, R., and Baltes, H. (1990). A biocompatible enzyme electrode for continuous in vivo glucose monitoring in whole blood. *Sensors and Actuators B: Chemical*, 1(1-6):561–564.

Vettoretti, M., Facchinetti, A., Del Favero, S., Sparacino, G., and Cobelli, C. (2015). Online calibration of glucose sensors from the measured current by a time-varying calibration function and bayesian priors. *IEEE Transactions on Biomedical Engineering*, 63(8):1631–1641.

Vogler, E. A. (2012). Protein adsorption in three dimensions. *Biomaterials*, 33(5):1201–1237.

Vrancćicé, C., Kroȯger, N., Gretz, N., Neudecker, S., Pucci, A., and Petrich, W. (2014). A quantitative look inside the body: minimally invasive infrared analysis in vivo. *Analytical chemistry*, 86(21):10511–10514.

Yang, Q., Zhang, X., Kumar, S., Singh, R., Zhang, B., Bai, C., and Pu, X. (2020). Development of glucose sensor using gold nanoparticles and glucose-oxidase functionalized tapered fiber structure. *Plasmonics*, 15(3):841–848.

Yonemori, Y., Takahashi, E., Ren, H., Hayashi, T., and Endo, H. (2009). Biosensor system for continuous glucose monitoring in fish. *Analytica chimica acta*, 633(1):90–96.

Zafar, H., Channa, A., Jeoti, V., and Stojanović, G. M. (2022). Comprehensive review on wearable sweat-glucose sensors for continuous glucose monitoring. *Sensors*, 22(2):638.

Zhang, J., Mai, X., Hong, X., Chen, Y., and Li, X. (2022). Optical fiber spr biosensor with a solid-phase enzymatic reaction device for glucose detection. *Sensors and Actuators B: Chemical*, 366:131984.

Zheng, W., Han, B., E, S., Sun, Y., Li, X., Cai, Y., and nan Zhang, Y. (2020). Highly-sensitive and reflective glucose sensor based on optical fiber surface plasmon resonance. *Microchemical Journal*, 157:105010.

Zhu, L., She, Z.-G., Cheng, X., Qin, J.-J., Zhang, X.-J., Cai, J., Lei, F., Wang, H., Xie, J., Wang, W., et al. (2020). Association of blood glucose control and outcomes in patients with covid-19 and pre-existing type 2 diabetes. *Cell metabolism*, 31(6):1068–1077.

Ziegler, C. and Eychmuller, A. (2011). Seeded growth synthesis of uniform gold nanoparticles with diameters of 15- 300 nm. *The Journal of Physical Chemistry C*, 115(11):4502–4506.

CHAPTER 5. APPLICATION OF ANALYTICS IN THE PREDICTION OF DISEASE AND EVALUATION OF FEATURES AND BIO-MARKERS FROM PATIENT DATA

Souvik Kundu[1], and Ratnesh Kumar[1]

[1] Department of Electrical and Computer Engineering, Iowa State University, Ames, IA, 50010, USA

Modified from a manuscript to be submitted in *IEEE Journal*

5.1 Abstract

The importance of label-free detection of essential biomarkers and their sensing principle was described in the previous three chapters, and in this chapter will discuss how patient data analytics can be used to forecast diseases by evaluating measured data. This has great potential to assist physicians in hospitals and clinics in making informed decisions and taking quick action based on patient data. Keeping in mind the flavor of the thesis, which examined optical sepsis-biomarker and glucose sensors, the developed data analytics technique is demonstrated below using sepsis patient data from the MIMIC III database, which is publicly available. Traditionally, physiological parameters are analyzed by clinicians to determine the sepsis state, and according to the most recent sepsis-3 definition, the quick SOFA (qSOFA) score is utilized to determine the sepsis condition. In this chapter, we compare the performance of qSOFA in ascertaining sepsis against that based on the proposed data analytics. This analysis is solely based on the laboratory data features (aka physio-bio-markers) present in the MIMIC-III database hence the selected feature list reported in this chapter is limited to that available in the database, but the significance of the data analytics approach developed is that it can be applied to other patient data in hospital databases and utilized in real-time.

5.2 Introduction

The majority of current research in post-injury sepsis is based on the 1991 and 2001 worldwide sepsis consensus criteria, sepsis-2, which are based on the existence of systemic inflammatory response syndrome (SIRS) Levy et al. (2003). Singer et al. (2016) issued new recommendations, sepsis-3, in 2016 with the goal of better distinguishing sepsis from other illnesses, where sepsis is now defined as a potentially fatal organ failure produced by a dysregulated host response to infection. Accordingly, SIRS was eliminated, and sepsis was clinically defined as a two-point or more increase in sequential (sepsis-related) organ failure assessment (SOFA) score in the presence of infection. Sepsis-3 also recommended a bedside assessment tool for sepsis screening in infected patients who were not admitted to intensive care units (ICUs), called the quick SOFA (qSOFA) score. It contains one point for each of these three criteria: (a) respiratory rate of 22 breaths per minute, (b) altered mental state, and (c) systolic blood pressure (SBP) of 100 mm Hg. A qSOFA score of >=2 is taken to indicate sepsis condition Seymour et al. (2016). Note since qSOFA score is solely based on physiological parameters, we do not have a detailed understanding of the disease dynamics; it's simply based on the corresponding response of the body with respect to the sepsis condition. Chapter-2, on the other hand, explored the etiology of sepsis and a subset of biomarkers associated with the condition, emphasizing the need of tracking related biomarkers in the blood. Thus, in this chapter, we will attempt to predict sepsis by analyzing appropriate biomarkers from a large pool of measured biomarkers available in the MIMIC-III sepsis database. To reduce the number of sensors required to predict sepsis without compromising the prediction accuracy by more than 5%, we used feature selection methods to reduce the number of features for training supervised machine learning models. The details of the dataset, inclusion criteria, analysis method, and performance are narrated in the subsequent sections.

5.3 MIMIC-III dataset and description

Medical Information Mart for Intensive Care (MIMIC) - III is freely accessible critical care database of its kind, and the dataset spans more than a decade, with detailed information about

Table 5.1 MIMIC-III database table description

Sl No	Table	Comments
1	admissions	Hospital admissions associated with an ICU stay.
2	callout	Record of when patients were ready for discharge (called out), and the actual time of their discharge (or more generally, their outcome).
3	caregivers	List of caregivers associated with an ICU stay.
4	chartevents	Events occuring on a patient chart. Physiological parameters, values and description
5	cptevents	Events recorded in Current Procedural Terminology.
6	d_cpt	High-level dictionary of the Current Procedural Terminology.
7	d_icd_diagnoses	Dictionary of the International Classification of Diseases (Diagnoses).
8	d_icd_procedures	Dictionary of the International Classification of Diseases (Procedures)
9	d_items	Dictionary of non-laboratory-related charted items.
10	d_labitems	Dictionary of laboratory-related items.
11	datetimeevents	Events relating to a datetime.
12	diagnoses_icd	Diagnoses relating to a hospital admission coded using the ICD9 system.
13	drgcodes	Hospital stays classified using the Diagnosis-Related Group system.
14	icustays	List of ICU admissions.
15	inputevents_cv	Events relating to fluid input for patients whose data was originally stored in the CareVue database.
16	inputevents_mv	Events relating to fluid input for patients whose data was originally stored in the MetaVision database.
17	labevents	Events relating to laboratory tests.
18	microbiologyevents	Events relating to microbiology tests.
19	noteevents	Notes associated with hospital stays.
20	outputevents	Outputs recorded during the ICU stay.
21	patients	Patients associated with an admission to the ICU.
22	prescriptions	Medicines prescribed.
23	procedureevents_mv	Procedure start and stop times recorded for MetaVision patients.
24	procedures_icd	Procedures relating to a hospital admission coded using the ICD9 system.
25	services	Hospital services that patients were under during their hospital stay.
26	transfers	Location of patients during their hospital stay.

individual patient care. MIMIC-III contains data associated with 53,423 distinct hospital admissions for adult patients (aged 16 years or above) admitted to critical care units between 2001 and 2012. The details of the complete database are narrated in Johnson et al. (2016). The database includes information such as demographics, vital sign measurements, laboratory test results, procedures, medications, caregiver notes, imaging reports, and mortality (including post-hospital discharge). The complete instruction for downloading the database, data description, and access methods are narrated in Pollard and Johnson III (2016). The access, copyright, usage notes, and version control are done by physionet Goldberger et al. (2000). The schema of the database is maintained at Sch, which contains 26 tables as described in Table 5.1. The database tables are connected by primary and foreign keys identified by the suffix "ID." To uniquely identify each patient, there is a *subject_id* in the patients table, and each hospital admission is tracked via hospital admission id (*hadm_id*) in the admissions table. As described in Table 5.1, to obtain the biomarker data for a given hospital admission, the tables lab events, *d_labitems*, and *d_items* can be joined and queried. In order to get the clinical diagnosis corresponding to a given hospital admission, the *diagnoses_icd* table is joined with the patient

information. Thus by joining the relevant tables, the clinical features (biomarkers results from blood work) can be obtained along with the physiological features like heart rate, oxygen levels, respiratory rates, etc. All other charted information corresponding to each patient can be queried by joining the chartevents table, which contains additional information on the procedures and sequence of operations in great detail, that can be explored in big data analytics for learning more features. There are other tables drugcodes, and prescriptions that detail the drugs prescribed by the physician, which can be utilized in some data analytics related to studies on medicines and dosages. In our case, since we worked mainly on the laboratory results, the additional data in the chartevents table were not relevant.

5.4 Methodology

In this section, we have described how the analysis was done, it's steps, and related programs used to achieve the results. We have first procured the data from MIMIC-III database by following the steps narrated in mim, where a Python environment was setup using Anaconda platform and following the instructions, directed in the repository mentioned in *README.md* file, which includes running the python files preprocess.py and sepsis_cohort.py in sequence on the MIMIC-III database (PostgreSQL database was installed for dumping the MIMIC-III database - instructions available at Pollard and Johnson III (2016)). To get the ground truth of true sepsis patients from the pool of all patients, we first obtained "icd9_code" from the "d_icd_diagnoses" table, which contained the diagnosis details of all patients for each hospital admission. Next, the table was joined with the "diagnosis_icd" table to obtain the "subject_id" and the hospital admission id ("hadm_id") of all the patients where physicians explicitly mentioned that the patient is suffering from sepsis. We found 1163 hospital admissions out of 52,423 that satisfied the above criteria, and they were split into 840 ($\tilde{7}0\%$) for the training set and 323 ($\tilde{3}0\%$) for the test set. Next, we randomly selected 1000 additional hospital admissions from the rest of the data not marked as sepsis cases and divided them in a 70:30 ratio into the training and test dataset. With

this, our total training set data was $840 + 700 = 1540$, and the test set data contained $323 + 300 = 623$ hospital admissions, as depicted in Fig. 5.1.

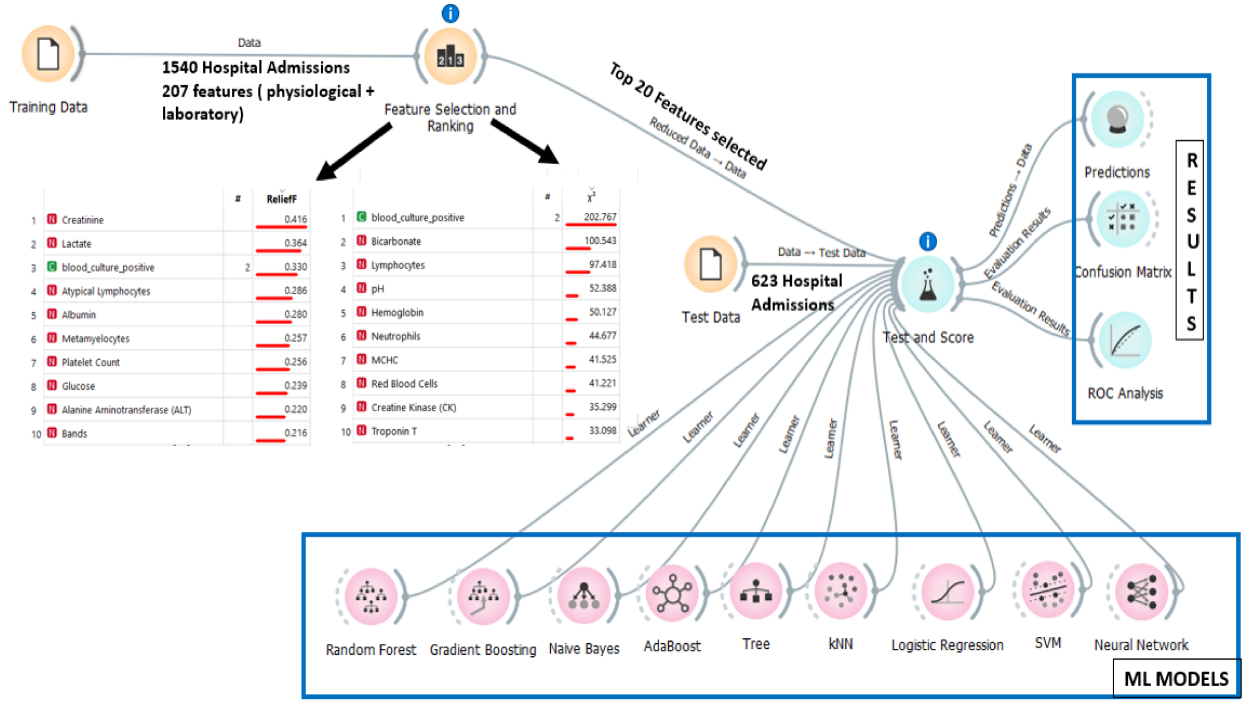

Figure 5.1 Block Diagram of the Methodology

5.4.1 The analytics

The goal of the analysis described in this section is to predict sepsis conditions by analyzing the laboratory results from the blood tests where several disease biomarkers are present. In particular, we constructed a binary classification of sepsis and non-sepsis cases from the training dataset, and compared it with the classification based on simple qSOFA scores, which is the traditional recommendation as per sepsis-3 definition Singer et al. (2016). We also identify dominant features based on feature selection algorithms available in the Orange data-mining application Demšar et al. (2013). With the reduced set of selected high-ranked features, we have trained 8 machine learning models viz. Random Forest, Gradient Boosting, Native Bayes,

AdaBoost, Tree, kNN, Logistic Regression, SVM, and Neural Network. Based on the learning, we have ranked all the models by comparing them based on the accuracy. From these 8 sets of ML models, we have chosen the model with the highest accuracy, and then we have compared our proposed model and feature selection method with the performance of the traditional qSOFA prediction. We compare our binary classification (determine only sepsis and non-sepsis cases) with the sepsis ground truth from MIMIC III data, as well as with the calculated qSOFA where all the qSOFA scores of $>= 2$ are labeled as sepsis and < 2 as non-sepsis cases. The performance metrics that were computed for comparing the traditional and proposed methodology are Accuracy (ability to measure the true predictions in the dataset), Sensitivity (how good a model is at detecting the positives), Specificity (how good a model is at avoiding false alarms/negatives), and Precision (how many of the positively classified by the model were relevant), as reported in the results section. Table 5.2 depicts the formula for calculating these parameters, where TP, TN, FP, FN are true positive, true negative, false positive, and false negative, respectively.

Table 5.2 Performance Metrics

Measure	**Implication**	**Formula**
Accuracy	Total accurate predictions	(TP+TN) / (P+N)
Sensitivity	True Positive Rate	TP/(TP+FN)
Specificity	True Negative Rate	TN/(TN+FP)
Precision	Positive Predictive Value	TP/(TP+FP)

5.4.2 Feature Selection

There is a total 207 relevant features being monitored in the MIMIC-III data table, after removing the features which were missing data. Two feature selection algorithms available in the Orange machine learning tool were applied to the 207 features, and the features were ranked, and the top 10 features from each feature selection algorithm output were selected for training the data. It is worth mentioning here that although using all 207 features the model can be more accurate, in real-world scenarios, measuring all 207 parameters using separate or multiplexed sensors may be infeasible or could be expensive. Hence one may have a accuracy reduction of say

about 4% in favor a reduced set of features to monitor. In the result section, we have described in detail how using 20 features gave an accuracy of 85.9% compared to 89.9% using all 207 features.

The first feature selection method that was applied is **Relief** Wikipedia (2023b) - which is a feature selection algorithm that uses a filter-method approach that is highly sensitive to feature interactions. It is used for binary classification with discrete or numerical features, as is the case with our dataset. Relief assigns a feature score to each feature, which is then used to rank and select the highest-scoring features for feature selection. This algorithm works on datasets with n instances and p features that belong to two known classes (binary classification). The algorithm is repeated m times. Start with a p-long weight vector (W) of zeros. At each iteration, the feature vector (X) belonging to one random instance and the feature vectors of the instance closest to X (measured using Manhattan(L1) norm Wikipedia (2023c)) from each class is processed. Then update the weight vector such that $W_i = W_i - (x_i - nearHit_i)^2 + (x_i + nearMiss_i)^2$. where the closest same-class instance is called 'near-hit,' and the closest different-class instance is called 'near-miss.' Thus the weight of any given feature decreases if it differs from that feature in nearby instances of the same class more than nearby instances of the other class and increases in the reverse case. After m iterations, each element of the weight vector is divided by m. This becomes the relevance vector. Features are selected if their relevance is greater than a threshold, by using Chebyshev's nequality Wikipedia (2023a). This algorithm was applied using the defined function available in Orange tool (for which we did not have any control over the internal parameters like the iterations, weights and thresholds). This can be a part to explore in the future using different tools or by physically coding the algorithm. Based on the Relief feature selection method, the 10 top features selected are illustrated in Fig.5.2(a).

The second feature selection method that was applied is **chi-square** χ^2 feature selection method. For each two variables, we can get observed value O and expected value E, and Chi-Square measures how E and O deviates from each other. The relationship between the independent category feature (predictor) and the dependent category feature (response) must be determined during feature selection. The goal of feature selection is to select characteristics that

are strongly dependent on the response. The formula for χ^2 is given by $\chi_c^2 = \sum \frac{((O_i - E_i)^2}{E_i}$. where c is degrees of freedom. The higher the Chi-Square value, the feature is more dependent on the response, and it can be selected for model training. Based on the **chi-square** feature selection method, the features selected are illustrated in Fig.5.2(b). We observed that except for the

		#	ReliefF
1	Creatinine		0.416
2	Lactate		0.364
3	blood_culture_positive	2	0.330
4	Atypical Lymphocytes		0.286
5	Albumin		0.280
6	Metamyelocytes		0.257
7	Platelet Count		0.256
8	Glucose		0.239
9	Alanine Aminotransferase (ALT)		0.220
10	Bands		0.216

(a)

		#	χ^2
1	blood_culture_positive	2	202.767
2	Bicarbonate		100.543
3	Lymphocytes		97.418
4	pH		52.388
5	Hemoglobin		50.127
6	Neutrophils		44.677
7	MCHC		41.525
8	Red Blood Cells		41.221
9	Creatine Kinase (CK)		35.299
10	Troponin T		33.098

(b)

Figure 5.2 Selected Features (a) Relief (b) χ^2

categorical variable of blood_culture_positive (where the infectious microbes were found in blood), all other top 10 features selected by the two feature selection algorithms are disjoint. Hence total of 19 top-ranked features was selected for machine-learning based model learning.

5.4.3 Correlation between top-ranked features and sepsis in real-world medical aspect

The top-ranked features thus reported by the feature selection method were explored to see if there exists any correlation between the selected features with sepsis in the medical literature for confirmation. Interestingly we have found evidence from the publications that all the features selected correlate to sepsis as corresponding research confirm the facts and relationships between them and sepsis: In Legrand and Kellum (2018), serum creatinine levels have been found correlating with the critically ill patient with sepsis suffering from co-morbid kidney diseases. Blood lactate concentrations reflect the balance between lactate production and clearance Kang

and Park (2016). Elevated serum levels of the intracellular enzyme Lactate Dehydrogenase (LDH) in sepsis might result from various mechanisms, including cellular injury related to bacterial toxins, ischemia and cytotoxic-reactive oxygen species generated during reperfusion. In Zein et al. (2004) it has been hypothesized that increased LDH in patients with severe sepsis and septic shock would reflect the extent of tissue injury and be associated with a worse prognosis. Hence lactate biomarker can be useful sepsis feature. Again, the 3rd feature positive blood culture is a good initial signature and has been ranked high by the feature selection algorithm. Hypoalbuminemia is common in the intensive care unit in patients with sepsis and may be due to decreased synthesis by the liver and/or to increased losses or increased proteolysis and clearance Tamion (2010). Hence lower levels of albumin correlate well with sepsis. de Pablo et al. (2014) narrates the correlation between lymphocytes in blood and sepsis, and atypical lymphocytes have a direct correlation with acute bacterial and viral infections. High levels of metamyelocytes and band cells have been found to be increased mortality in sepsis Mare et al. (2015). Levels of myelocytes and metamyelocytes were higher in patients with definite sepsis than in healthy controls. Platelets are involved in both hemostasis and immune response. These mechanisms work together in a complex and synchronous manner, making the contribution of platelets of major importance in sepsis Vardon-Bounes et al. (2019). Critical illness, and particularly severe sepsis, induces profound changes in the function of the normal liver. The balance of hepatic metabolic activity may be shifted rapidly in response to systemic inflammation with an "acute phase reaction (APR)." This results in a series of phenomena that includes complex changes in circulating and functional levels of immunological, transport, and coagulation proteins. Hence the levels of aspartate aminotransferase (AST) Bernal (2016) in the liver is also a good indicator of severe sepsis. Hyperglycemia in severe sepsis Wernly et al. (2016) is also common as that is the body's way of protecting human cells when a person is critically ill. Hemodynamic instability in critically ill patients with sepsis can induce multiple organ compromises, including renal dysfunction and tissue hypoperfusion, both of which are widely believed to cause decreased serum bicarbonate levels Paudel et al. (2022). Further, this is also related to metabolic acidosis, which is

frequently found in patients with severe sepsis Ganesh et al. (2016). Hence pH and bicarbonate levels are also great feature selectors as sepsis indicators. Several mechanisms contribute to an acute reduction in hemoglobin levels in the setting of sepsis, including reduced production of red blood cells induced by the systemic inflammatory response, as well as increased destruction of red cells due to hemolysis and bleeding Muady et al. (2016). Hence low levels of hemoglobin in hospitals are a potential indicator biomarker in sepsis. Hence, this proves that the ranked feature selection was not arbitrary but bears a fair correlation with real-world medical data.

5.5 Results

As depicted in Fig. 5.1, the selected top 10 ranked features from both the feature selection algorithm outputs were applied to 8 different ML models viz. Random Forest, Gradient Boosting, Native Bayes, AdaBoost, Tree, kNN, Logistic Regression, SVM, and Neural Network with their default settings, and it was observed that the Random Forest model was found to be most accurate in classifying sepsis and non-sepsis cases as it had an accuracy of 85.9%. However, we have also applied all 207 features to the Random Forest model and have achieved an accuracy of 89.9%. Hence we have a 4% reduction in prediction accuracy once we scale the feature size down from 207 to 20 (a $> 90\%$ feature reduction for $< 4\%$ loss in accuracy). Based on the 19 domiant features and random forest model, we tested on the test set and compared the performance of our trained model performance with qSOFA-based prediction. Fig.5.3 depicts the results obtained after the comparison. It reports the qSOFA performance for all 2163 data, which comprise both training and test data cumulatively. It was observed that the model with 20 selected features outperforms the qSOFA based approach in terms of sensitivity, specificity, precsion, accuracy (marked in green).

Again, the goal of this analysis was not to propose the absolute list of biomarkers for sepsis treatment but to present a methodology of selecting and for classifying physio-bio data to try to predict sepsis rather than rely solely on physiological parameters.

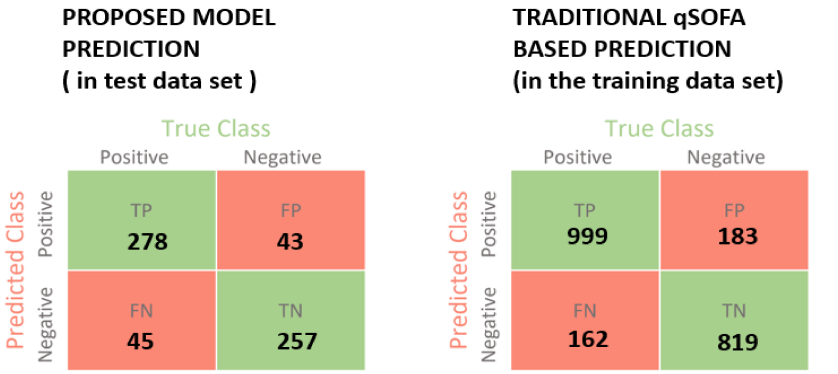

Measure	Formula	Propose Model (in test data set)	qSOFA (in all 2163 data)
Sensitivity	TPR = TP / (TP + FN)	**0.8607**	0.8605
Specificity	TNR = TN / (FP + TN)	**0.8567**	0.8174
Precision	PPV = TP / (TP + FP)	**0.8660**	0.8452
Accuracy	ACC = (TP + TN) / (P + N)	**0.8587**	0.8405

Figure 5.3 Comparison of traditional qSOFA and proposed prediction model

5.6 Conclusion

In this study, we examined how data analytics can be used to help doctors make more precise decisions based on physio-bio parameters rather than just the traditional physiological parameters as recommended by the qSOFA score of sepsis-3 definition. This analysis was demonstrated on a data from the mimic database with a focus on the biomarkers measured in blood tests and sepsis condition as the target variable. This research opens the door for more powerful AI-based decision-making based on more information and traits and can be applied to other diseases. Also while the models investigated in this work depended on the Orange software's model availability and capability, the approach can be expanded to other models of supervised/unsupervised learning. More sophisticated feature selection methods can also be explored in the future where an ensemble feature selection can be thought of based on fusing multiple feature selection algorithms with appropriate weights. Also while the performance of the current model was based on the default model choices, it is possible to tweak these values through to find their optimal

setting, which can also assist in increasing the accuracy of the existing models. Finally, apart from relying on one database and limited biomarkers available, other publicly available databases can also be explored, like eICU Research Institute (eRI) Pollard et al. (2018) database, which may have another diverse set of patient data along with additional biomarkers.

5.7 References

Bernal, W. (2016). The liver in systemic disease: Sepsis and critical illness. *Clinical Liver Disease*, 7(4):88.

de Pablo, R., Monserrat, J., Prieto, A., Alvarez-Mon, M., et al. (2014). Role of circulating lymphocytes in patients with sepsis. *BioMed research international*, 2014.

Demšar, J., Curk, T., Erjavec, A., Črt Gorup, Hočevar, T., Milutinovič, M., Možina, M., Polajnar, M., Toplak, M., Starič, A., Štajdohar, M., Umek, L., Žagar, L., Žbontar, J., Žitnik, M., and Zupan, B. (2013). Orange: Data mining toolbox in python. *Journal of Machine Learning Research*, 14:2349–2353.

Ganesh, K., Sharma, R., Varghese, J., and Pillai, M. (2016). A profile of metabolic acidosis in patients with sepsis in an intensive care unit setting. *International journal of critical illness and injury science*, 6(4):178.

Goldberger, A. L., Amaral, L. A., Glass, L., Hausdorff, J. M., Ivanov, P. C., Mark, R. G., Mietus, J. E., Moody, G. B., Peng, C.-K., and Stanley, H. E. (2000). Physiobank, physiotoolkit, and physionet: components of a new research resource for complex physiologic signals. *circulation*, 101(23):e215–e220.

Johnson, A. E., Pollard, T. J., Shen, L., Lehman, L.-w. H., Feng, M., Ghassemi, M., Moody, B., Szolovits, P., Anthony Celi, L., and Mark, R. G. (2016). Mimic-iii, a freely accessible critical care database. *Scientific data*, 3(1):1–9.

Kang, H. E. and Park, D. W. (2016). Lactate as a biomarker for sepsis prognosis? *Infection & chemotherapy*, 48(3):252–253.

Legrand, M. and Kellum, J. A. (2018). Serum creatinine in the critically ill patient with sepsis. *Jama*, 320(22):2369–2370.

Levy, M. M., Fink, M. P., Marshall, J. C., Abraham, E., Angus, D., Cook, D., Cohen, J., Opal, S. M., Vincent, J.-L., Ramsay, G., et al. (2003). 2001 sccm/esicm/accp/ats/sis international sepsis definitions conference. *Intensive care medicine*, 29:530–538.

Mare, T. A., Treacher, D. F., Shankar-Hari, M., Beale, R., Lewis, S. M., Chambers, D. J., and Brown, K. A. (2015). The diagnostic and prognostic significance of monitoring blood levels of immature neutrophils in patients with systemic inflammation. *Critical Care*, 19:1–11.

Muady, G. F., Bitterman, H., Laor, A., Vardi, M., Urin, V., and Ghanem-Zoubi, N. (2016). Hemoglobin levels and blood transfusion in patients with sepsis in internal medicine departments. *BMC Infectious Diseases*, 16(1):1–8.

Paudel, R., Bissell, B., Dogra, P., Morris, P. E., Chaaban, S., and Bissell, B. D. (2022). Serum bicarbonate: Reconsidering the importance of a neglected biomarker in predicting clinical outcomes in sepsis. *Cureus*, 14(4).

Pollard, T. J., Johnson, A. E. W., Raffa, J. D., Celi, L. A., Mark, R. G., and Badawi, O. (2018). The eICU Collaborative Research Database, a freely available multi-center database for critical care research. *Scientific data*, 5(1):1–13.

Pollard, T. J. and Johnson III, A. (2016). The mimic iii clinical database, version 1.4. *The MIMIC-III Clinical Database. PhysioNet*.

Seymour, C. W., Liu, V. X., Iwashyna, T. J., Brunkhorst, F. M., Rea, T. D., Scherag, A., Rubenfeld, G., Kahn, J. M., Shankar-Hari, M., Singer, M., et al. (2016). Assessment of clinical criteria for sepsis: for the third international consensus definitions for sepsis and septic shock (sepsis-3). *Jama*, 315(8):762–774.

Singer, M., Deutschman, C. S., Seymour, C. W., Shankar-Hari, M., Annane, D., Bauer, M., Bellomo, R., Bernard, G. R., Chiche, J.-D., Coopersmith, C. M., et al. (2016). The third international consensus definitions for sepsis and septic shock (sepsis-3). *Jama*, 315(8):801–810.

Tamion, F. (2010). Albumin in sepsis. In *Annales francaises d'anesthesie et de reanimation*, volume 29, pages 629–634.

Vardon-Bounes, F., Ruiz, S., Gratacap, M.-P., Garcia, C., Payrastre, B., and Minville, V. (2019). Platelets are critical key players in sepsis. *International journal of molecular sciences*, 20(14):3494.

Wernly, B., Lichtenauer, M., Hoppe, U. C., and Jung, C. (2016). Hyperglycemia in septic patients: an essential stress survival response in all, a robust marker for risk stratification in some, to be messed with in none. *Journal of thoracic disease*, 8(7):E621.

Wikipedia (2023a). Chebyshev's inequality — Wikipedia, the free encyclopedia. http://en.wikipedia.org/w/index.php?title=Chebyshev's%20inequality&oldid=1149053088. [Online; accessed 30-June-2023].

Wikipedia (2023b). Relief (feature selection) — Wikipedia, the free encyclopedia. http://en.wikipedia.org/w/index.php?title=Relief%20(feature%20selection)&oldid=1146206106. [Online; accessed 30-June-2023].

Wikipedia (2023c). Taxicab geometry — Wikipedia, the free encyclopedia. http://en.wikipedia.org/w/index.php?title=Taxicab%20geometry&oldid=1160519294. [Online; accessed 30-June-2023].

Zein, J. G., Lee, G. L., Tawk, M., Dabaja, M., and Kinasewitz, G. T. (2004). Prognostic significance of elevated serum lactate dehydrogenase (ldh) in patients with severe sepsis. *Chest*, 126(4):873S.

CHAPTER 6. GENERAL CONCLUSION

This thesis contributes towards the development of novel optical bio-sensors which has a great amount of potential for being used in point-of-care setting, as the sensors proposed for sepsis and glucose detection are portable, light weight, affordable, and can be used for rapid detection of biomarkers related to sepsis and glycemia. It is worth mentioning that similar techniques can be employed for measuring other biomarkers in blood. One such setting could be multiplexed detection of multiple biomarkers simultaneously in whole blood. The sensing probes can be made insertable through catheters in ICU/CCU patients for continuous measurement: The fiber-optic sensor bundle can be first embedded inside a microdialysis probe and then through the catheter. An integrated system can be developed with all the optics, electronics, and data logging packaged into a portable system. Figure 6.1 demonstrates the schematic of the integrated sensing platform. This integrated system will allow one to conduct an animal study of septic/glycemic shock and resuscitation to determine if combined set of biomarkers can be monitored simultaneously which can guide successful prognostics.

Another aspect of future work could be on the dynamic calibration of biosensors. As discussed in Chapter 4, sensor drift is caused by biofouling that clogs the probe surface. As a result, frequent re-calibration is typically required to correct such sensor drifts, thus affecting continuous monitoring. One can develop a generalized data-driven 'dynamic calibration' Bayesian framework

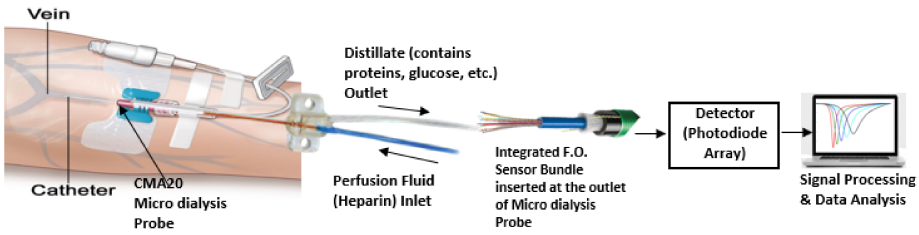

Figure 6.1 Fiber Optic Multiplexed Sensing Set up

to help correct the sensor drift, allowing continuous monitoring and extending its lifetime. The real-time sensor data can help in building the historic data dictionary, which can further help in making the calibration more accurate and robust.

Following Chapter 5, effective machine learning models with reliable feature selection techniques can be investigated to improve prediction accuracy, assist doctors in making more precise choices, and ultimately save lives by acting when it matters most and administering the proper life-saving medications to the patients. The AI-based processes provide insights into the patient's state, allowing for the initiation of early therapy. The combination of developments in the sensing regime and the analytics regime will ultimately pave the way for a better treatment and help in reducing mortality.